A CORRELATION BASED THEORY FOR PHONON TRANSPORT

A Dissertation
Presented to
The Academic Faculty

by

Wei Lv

In Partial Fulfillment
of the Requirements for the Degree
Doctor of Philosophy in the
George W. Woodruff School of Mechanical Engineering

Georgia Institute of Technology
May 2017

A CORRELATION BASED THEORY FOR PHONON TRANSPORT

Approved by:

Dr. Asegun Henry, Advisor
George W. Woodruff School of
Mechanical Engineering
Georgia Institute of Technology

Dr. Martin Maldovan
School of Physics
Georgia Institute of Technology

Dr. Baratunde A. Cola
George W. Woodruff School of
Mechanical Engineering
Georgia Institute of Technology

Dr. Samuel Graham
George W. Woodruff School of
Mechanical Engineering
Georgia Institute of Technology

Dr. Shannon Yee
George W. Woodruff School of
Mechanical Engineering
Georgia Institute of Technology

Date Approved: 11/10/2016

ACKNOWLEDGEMENTS

First and foremost, I would like to express my sincere thanks to my advisor and mentor Dr. Asegun Henry for his guidance and encouragement throughout my Ph. D. studies. Looking back, I am very grateful for his offering me the opportunity of joining in the Atomistic Simulation and Energy Lab four years ago. At that time, I was totally unfamiliar with phonon transport and it was Dr. Henry who brought me to this very interesting field without whom this dissertation would have never become reality. I benefited tremendously from the inspiring discussions with him, and the confidence and courage he gave me to face the challenges. I would also like to thank my Committee members: Dr. Shannon Yee, Dr. Baratunde Cola, Dr. Samuel Graham and Dr. Martin Maldovan for their valuable suggestions.

My sincere appreciation also goes to my current group members and friends at Gatech. It is a really wonderful thing to discuss and collaborate with them during my Ph. D. study. I would also like to thank Kiarash Gordiz, Colby Jarrett, Diane England, Freddy DeAngelis, Gregory Wilk, Cansheng Yuan, Sanzida Sultana, Hamid Seyf and Andrew Rohskopf for fruitful collaborations and interactions.

In addition, I would also like to thank the Intel corporation for partially supporting the work in this dissertation.

Finally, I am greatly indebted to my gradparents, parents and my wife for their love and encouragement through all these years. I also want to thank numerous friends for their company and support.

TABLE OF CONTENTS

LIST OF FIGURES

LIST OF SYMBOLS

Variables

C	volumetric specific heat J/m³K
h	Planck constant divided by 2π, 1.055×10^{-34} J s
$\mathbf{p}$	velocity vector
$\mathbf{q}$	displacement vector
$\mathbf{k}$	wavevector, m^{-1}
k_B	Boltzmann constant, 1.381×10^{-23} J K^{-1}
$\boldsymbol{Q}$	heat flux, W m^{-2}
V	volume, m^3
υ	frequency, THz
$\mathbf{r}$	displacement vector, m
T	Temperature, K
$\mathbf{v}$	velocity, m/s
m	mass, kg
$\mathbf{x}$	atom displacement, m
$\dot{\mathbf{x}}$	atom velocity, m/s
X	phonon mode amplitude from displacement
$\dot{X}$	phonon mode amplitude from velocity
n	mode number
N	number of atoms
e	eigenvector
E	energy of atom (potential and kinetic energy)
H	hamiltonian operator
$\mathbf{S}$	heat flux operator
p	polarization index

u displacement, m

r distance between atoms, m

F force, N

D thermal diffusivity $m^2 s^{-1}$

G reciprocal lattice vector

Greek symbols

Φ potential energy

λ wavelength in vacuum, m

κ thermal conductivity, $W m^{-1}K^{-1}$

ω angular frequency, rad s^{-1}

τ phonon relaxation time s^{-1}

Subscripts

j atom number

ij from atom i to atom j

1 material 1

2 material 2

x, y, z direction of coordinates

total total heat flux

$\alpha\beta$ directions

q quantum specific heat

m classic specific heat

Q the ratio of the quantum to the classic specific heat

κ frequency dependent thermal conductivity from GKMA

optical all optical phonon branches

pr propagons

LIST OF ABBREVIATIONS

1D	one-dimensional
2D	two-dimensional
3D	three-dimensional
PGM	phonon gas model
GKMA	Green-Kubo modal analysis
FPU	Fermi, Pasta, and Ulam
DOS	density of states
TC	thermal conductivity
NMA	Normal Mode Analysis
A-F	Allen-Feldman method
BTE	Boltzmann Transport Equation method
SED	Spectral energy decomposition method
MFP	Mean Free Path
PBE	Peierls-Boltzmann equation
LD	lattice dynamics
a-Si	amorphous silicon
a-SiO_2	amorphous silica
a-C	amorphous carbon
MD	molecular dynamics
EMD	equilibrium molecular dynamics
NEMD	nonequilibrium molecular dynamics
a-C	amorphous carbon
HAMR	heat-assisted magnetic recording
SW	Stillinger-Weber potential
EDIP	Environment-Dependent Interatomic potential

IPA	Inverse participation ratio
SCLD	Supercell lattice dynamics
ucs	unit cells

SUMMARY

The phonon gas model is the idea that the quantized collective vibrations of atoms, termed phonons, can be treated as a gas of particles that exchange energy through scattering events. The PGM is originated from the behaviors observed and rationalized in homogenous crystalline solids. It has exhibited remarkable success in describing the behavior of a wide variety of solids, microstructures, nanostructures and molecules. Given its success, it has become the primary lens with which phonon transport is viewed. However, for amorphous materials, or other structurally/compositionally-disordered systems, due to the lack of periodicity, one cannot clearly define the phonon velocity. Since the PGM hinges on knowledge of the phonon velocities, the application of the PGM to amorphous materials has been highly questionable.

Here, we developed a new method for direct calculation of the modal contributions to thermal conductivity, which is termed the Green-Kubo modal analysis (GKMA). The GKMA method combines the lattice dynamics formalism with the Green-Kubo formula for thermal conductivity, such that the thermal conductivity becomes a direct summation of modal contributions, where one does not need to define a phonon velocity. The predicted temperature dependent thermal conductivity of several amorphous materials shows the best agreement with experiments to date.

Furthermore, we demonstate a few cases that the PGM fails. We first exhibit the violations of the PGM in case studies of the amorphous materials and single polymer chains. PGM based methods fail to explain the experimental results of the thermal conductivity of the amorphous solids. Then we utilize GKMA to calculate and explain the results. It further proves the deficiency of the PGM based methods on predicting the thermal properties on non-crystaline solids.

CHAPTER 1

INTRODUCTION :

THE THEORY OF PHONON TRANSPORT

1.1 The origin and utility of the Phonon Gas Model

In all phases of matter, heat is transported due to the vibration of individual atoms. While electrically conducting solids can transport heat through electrons, in dielectric solids and polymers, which are the focus of this thesis, heat is transported almost entirely by the vibration of atoms. In well-ordered materials, fundamental quantized lattice vibrations are called phonons, which exist as an excited state in the quantized modes of vibrations in elastic structures of interacting atoms. Quantum mechanics dictates that the energy of each phonon is discrete and must be a multiple of $\hbar\omega$, where ω is the angular frequency of the phonon, and $\hbar$ is the reduced Planck constant.

The name phonon comes from the Greek word φωνή (phonē), which translates to sound or voice because long-wavelength phonons give rise to sound. The concept of a phonon was first introduced for the crystalline materials, whereby it describes spatially periodic lattice vibrations with distinct wavelengths, polarization vectors, and phonon group velocities. When examining the motion of atoms due to phonon excitation in a crystalline material, the atoms trace out a sinusoidal wave. The phonon wavelength is the spatial period of the wave, i.e. the distance over which the wave's shape repeats. The polarization vector of each phonon is an eigenvector, which describes the direction and magnitude of vibration of atoms for a given phonon. One can interpret it as the atomistic

vibrational direction and magnitude of each atom for a phonon. Polarization vectors will be discussed in further detail in Chapter 2. The group velocity of a phonon is the velocity at which the wave propagates through the lattice.

A phonon at a specific frequency and wavelength is a lattice wave extends through the entire crystal. A wave packet is the finite set of phonons of different wavelength with phases and amplitudes such that they interfere constructively over a small region of space, and destructively elsewhere. It can be viewed as an envelop of a localized wave. It can also be considered as particles as long as they are significantly smaller than the crystal size. Using this phonon particle picture, these wave packets propagate in the materials, transport heat from one location (high temperature) to another location (low temperature). Heat in a dielectric crystal is conducted by such a phonon gas similar to that in a box of gas molecules. The collision of phonon particles is due to the interactions of phonon waves. This phonon particle view is called phonon gas model (PGM). It originates from the behaviors observed and rationalized in homogenous crystalline solids.

Under the PGM, each phonon with a polarization vector (momentum) $\mathbf{k}$ and polarization index p carries energy of $\hbar\omega$. It travels at a group velocity $\mathbf{v}$, until it is scattered by anharmonic phonon-phonon scattering, lattice imperfections, impurities, boundaries, interfaces etc. Similar to the gas flux in the kinetic theory of gases, the heat current in dielectric crystals is described by the sum of the contributions from each individual phonon,

$$\mathbf{Q} = \frac{1}{V}\sum_{\mathbf{k}}\sum_{p}\hbar\omega_{\mathbf{k}}\mathbf{v}_{\mathbf{k}p}\delta n_{\mathbf{k}} \tag{1.1}$$

where V is the volume of the sample and $\delta n_{\mathbf{k}}$ is the perturbed phonon populations of mode $\mathbf{k}$. Equation (1.1) describes the essence of the PGM and it is at the heart of virtually every expression for phonon transport, because the derivation of almost all expressions begin with such a statement [1,2].

Using Fourier's law, one can derive an expression for thermal conductivity using Eq. (1.1). Fourier's law states that the heat current $\mathbf{Q}$ is proportional to the temperature gradient ∇T, $\mathbf{Q} = -\kappa\nabla T$, where the tensor κ is the thermal conductivity. Assuming a small uniform temperature gradient, the distribution function to a first order approximation is

$$n_{\mathbf{k}} = n_{\mathbf{k}0} + (\partial n_{\mathbf{k}} / \partial T)\phi_{\mathbf{k}} \cdot \nabla T \tag{1.2}$$

where $n_{\mathbf{k}0}$ is the equilibrium Bose Einstein distribution $(\exp(\hbar\omega_{\mathbf{k}} / k_B T) - 1)^{-1}$. From Eq. (1.2) one can obtain $\delta n_{\mathbf{k}} = (\partial n_{\mathbf{k}} / \partial T)\phi_{\mathbf{k}} \cdot \nabla T$. Equation (1.2) defines the vector function $\phi_{\mathbf{k}}$. One can define the phonon relaxation time as $\tau_{\mathbf{k}p} = \phi_{\mathbf{k}} \cdot \mathbf{v}_{\mathbf{k}p} / \mathbf{v}_{\mathbf{k}p}^2$ [3]. The phonon relaxation time is the time that a phonon takes to return to equilibrium in a perturbed system. Substituting $\tau_{\mathbf{k}p}$ and Eq. (1.2) into Eq. (1.1), gives thermal conductivity as

$$\kappa = \frac{1}{3}\sum_{\mathbf{k}p} C_{\mathbf{k}}\mathbf{v}_{\mathbf{k}p} \cdot \mathbf{v}_{\mathbf{k}p}\tau_{\mathbf{k}p} \tag{1.3}$$

where $C_{\mathbf{k}}$ is the specific heat per phonon, which equals to $\hbar\omega_{\mathbf{k}}(\partial n_{\mathbf{k}}/\partial T)/V$ (or k_B/V in the classical limit). Based on the Eq. (1.3), phonon thermal conductivity depends on the individual phonon heat capacities (C), phonon group velocities ($\mathbf{v}$), and phonon relaxation times (τ). Hence, based on PGM, the phonon thermal conductivity contribution is represented by these three parameters.

Specific heat and relaxation time are the two universal properties of all types of phonons. The group velocity is valid and well defined only in homogenous crystalline solids. Because in homogenous crystalline solids have both compositional and structural periodicity, all of the phonon eigenvectors correspond to plane wave modulated vibrations (i.e., propagating waves). The eigenvectors represent the phonon vibrational shape. Plane wave modulated vibrations exhibit a well-defined group velocity, because each wave has a clearly defined wavevector and dispersion relation. A dispersion relation describes the relationship between the wavelength and frequency. These phonons then transport heat as they propagate, with a well-defined velocity, which is consistent with the PGM based description of their transport. In the PGM, each phonon carries energy $\hbar\omega$ with a group velocity $d\omega/d\mathbf{k}$, and mean free path (MFP) Λ, which is the product of the velocity and the time between energy exchanges between phonons (e.g., scattering events). Group velocity here is defined as $d\omega/d\mathbf{k}$, which is based on the phonon dispersion relation.

Due to the how the PGM is derived, it successfully describes the thermal conductivity of virtually any solid homogenous crystal. Furthermore, it allows corresponding nanostructures to be computed from first principles [4–10]. Given its

success, it has become the primary lens through which phonon transport is viewed. However, applying the PGM to materials that do not have a well-defined phonon dispersion relation (and therefore do not have well-defined group velocities) becomes problematic, particularly because the group velocity is a critical quantity in Eq. (1.1), since it determines the rate at which its energy is transported through the material. Amorphous solids and single molecules are two specific types of materials that do not follow the PGM and will be the focus of this thesis.

1.2 Shortcomings of the Phonon Gas Model

In non-crystalline materials, in which long-range order does not exist, the eigenvectors/phonon shape is not necessarily described by a plane wave. Hence there is no well-defined wavevector or wavelength for these phonons. As a result, the group velocity cannot be well defined; thus, usage of the PGM to describe such materials is at best questionable. For systems that lack periodicity, such as amorphous materials, random alloys, or single molecules, using the PGM to describe their phonon transport is inconsistent with the actual atomic vibrations in the material. This issue is critical, because these classes of materials are used in countless applications involving heat transfer.

1.2.1 Amorphous Materials

One class of materials that is poorly defined by the with PGM based arguments is amorphous materials. Several existing theories [11–14] have worked towards understanding thermal transport in amorphous solids, but they are all based on the PGM. However in amorphous solids, the majority of modes are non-propagating based on their

phonon shapes [15,16]. Phonons in crystalline materials can be treated as propagating waves with a well-defined wavevector. However in amorphous materials, not all the phonons are propagating and most of the modes do not have a well-defined wavevector.

Based on the phonon shapes/eigenvectors, Allen & Feldman [15] first introduced a different nomenclature to distinguish the phonons in amorphous solids, delineating three different classes of thermal vibrations.. The first class of modes is termed "propagons", which are illustrated in the Fig. 1.1, with eigenvectors are represented as the blue arrows in amorphous silicon. The wavelength can be clearly recognized as the distance over which the wave's shape (defined by the eigenvectors) repeats, ranging from hundreds to tens of interatomic spacing. For the propagating modes, they can travel the speed of sound over distances of at least two or three interatomic spacing before scattering with other phonons over distance [17]. The average distance of propagation of a mode is the mode's MFP. For non-propagating modes, the diffusive vibration occurs over any meaningful distance, and the concepts of wavevector lose usefulness.

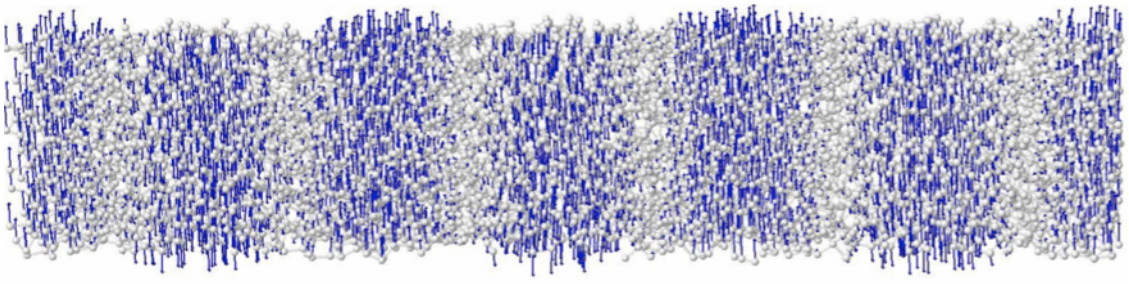

Figure 1.1 Eigenvectors of a propagon in amorphous silicon (a-Si). The arrows represent eigenvector magnitude and direction.

As shown in the Fig. 1.2, the eigenvectors of a diffusive mode are not spatially periodic and vibration directions are much more random. Hence one cannot define an

effective wavevector for this type of vibrations. The modes are called “diffusons” by Allen & Feldman [15]. Most of the atoms in the system are involved in the vibration in a diffuson. However these vibrations are not spatially periodic as with propagons.

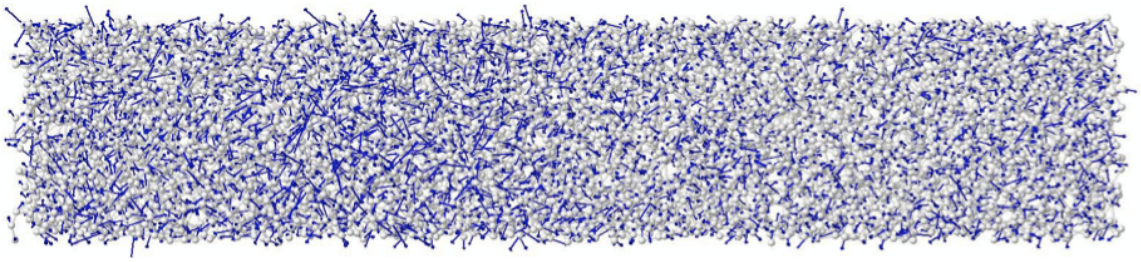

Figure 1.2 Eigenvectors of a diffuson in a-Si. The arrows represent eigenvector magnitude and direction on the atoms.

Fig. 1.3 shows the third category of the phonon mode termed “locons”. In locons, a localized region, similar to the diffusons, the eigenvectors are random and not spatially periodic. But unlike diffusons and propagons that are extended modes, these modes are spatially localized and constrained in a particular region of the solid.

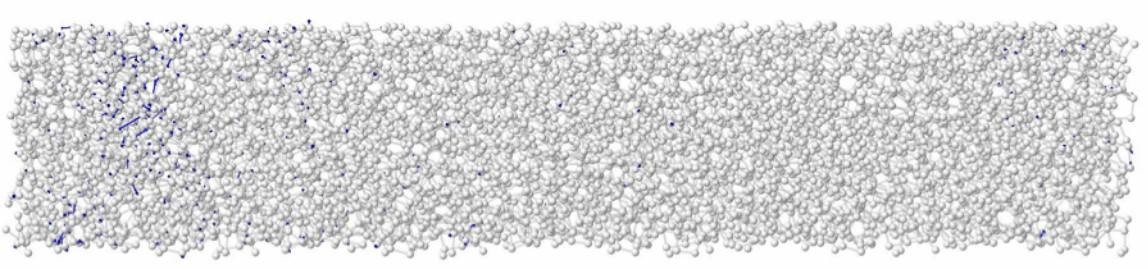

Figure 1.3 Eigenvectors of a locon in a-Si. The arrows represent eigenvector magnitude and direction on the atoms.

Harmonic normal modes of vibration can be divided into extended and localized modes. Both propagons and diffusons are extended modes and the locons are localized modes. There are sharp boundaries between extended modes and localized modes, known as the mobility edge [18]. One can use the mode participation ratio [19] to quantitatively distinguish the extended modes and localized modes. However the boundary between

propagons and diffusons, which is called “Ioffe-Regel limit”, is not as distinct [20]. This boundary separates the phonon spectrum into a propagating region where the wavevector is well defined and a region with only diffusive modes where the wavevector is ill-defined but the modes are still extended.

Allen and Feldman have not only created a new terminology for phonons in amorphous solids but also introduced a new method for calculating thermal conductivity amorphous silicon based on a supercell structure [21]. In doing so, they developed a model for thermal conductivity (termed the A-F model) that, for the first time, was based on the actual modes of vibration in an amorphous material by using the Kubo formula to compute thermal conductivity and to calculate the contributions of different modes, assuming that the interactions between atoms were harmonic [18,21]. A detailed formulation of A-F model will be discussed in Chapter 2.

The A-F model exhibits better agreement with experimental data than previous PGM based work. As a result, researchers concluded that anharmonicity is unlikely to significantly affect thermal conductivity. Michalski [22], on the other hand, argued that anharmonicity is in fact significant, and a more recent study showed that the A-F method does not accurately describe many amorphous materials other than a-Si [23]. For example, the A-F model results for amorphous silica and amorphous polystyrene are inaccurate. This discrepancy raises questions and concerns that led us to propose a more accurate model to calculate and understand phonon properties in non-crystalline solids and polymers.

MD simulations offer an ideal platform for analyzing the interactions for amorphous materials, allowing us to improve our understanding of phonon transport in amorphous materials [24–27]. The critical challenge of the MD simulation is to include modal analysis in the equilibrium MD (EMD) framework based on the Green-Kubo (GK) formulation. Here, EMD is preferred for thermal conductivity calculations, since for systems where periodic boundary conditions are applied, finite size effects only affect phonon wavelengths and not their MFPs [28]. In this thesis, we present a new formalism, termed the Green-Kubo modal analysis (GKMA), which combines GK and modal analysis methods.

1.2.2 Single Molecules

Another class of materials whose thermal conductivity cannot be explained by PGM is single molecules, particularly single polymer chains. In 1955 Fermi, Pasta, and Ulam (FPU) [29] conducted a numerical experiment with a one-dimensional chain of anharmonic oscillators by introducing, a small, but non-zero cubic term to a harmonic potential. The expected result was that any degree of anharmonicity would cause interactions between the normal modes of vibration, leading to attenuation and an eventual equipartition of the mode energy, which would confirm that the system behaves ergodically, according to the PGM. The resulting effect of the interactions between modes would then translate to finite thermal conductivity. This, however, was not the case. FPU observed that even though a small amount of anharmonicity did result in mode interactions, it did not lead to equipartition, and the system trajectory was periodic, indicating non-ergodic behavior in contrast to the PGM. In the PGM, one of the most important assumptions is that phonon scattering events are random and ergodic [30,31].

When the non-ergodic phonon interactions happen, FPU found that even an anharmonic system could exhibit infinite thermal conductivity [29].

The class of materials that most closely resembles the 1D chains that have been studied previously [31–34] are polymers, specifically individual polymer molecules. Henry and Chen [28] discovered that even in a realistic model for the interactions between atoms in a polyethylene (PE) chain, thermal superconductivity is possible. This evidence arises from direct calculation of the thermal conductivity via EMD simulations, which include anharmonicity to full order. In this thesis, we use EMD to study another single polymer chain, namely polythiophene in which we observe similar divergent behavior. Furthermore, we use the GKMA to determine which mode is responsible for the divergent thermal conductivity.

It is expected that boundaries (i.e., the end of polymer chains) or other perturbative stimuli, such as phonon-photon scattering, can disrupt the persistent correlation and cause finite thermal conductivity. However, it remains to be proven whether or not such perturbative interactions are sufficiently strong to disrupt the non-ergodic behavior in all cases. In single polythiophene chains, we observed similar abnormal thermal conductivity even for a finite length chain, indicating that thermal superconductivity can overcome boundary scattering. Even more interesting, we find the finite chain thermal conductivity at certain lengths is larger than the maximum thermal conductivity calculated by the PGM for that chain.

PGM explains the divergence of the infinite chain by infinite relaxation time of modes. However we find the divergent mode has finite relaxation time. Hence it is not

the cause of the divergence. Thus, it is not clear what causes the divergent thermal conductivity phenomenon observed in polymers. In Chapter 4, we will answer this question using EMD, GKMA and sonification techniques.

1.3 Outline

This thesis describes a new paradigm that is universally applicable for analyzing the phonon mode properties for any arbitrary system of atoms that vibrate about stable equilibrium sites. Amorphous materials and single molecules are studied using this new correlation-based theory and emerging computational tools at the atomistic level.

In Chapter 2, we introduce the GKMA method, which utilizes a combination of molecular dynamics (MD) and lattice dynamics (LD). Meanwhile, the other modal analysis methods are briefly discussed and compared, namely normal mode analysis (NMA) using MD, solution of the Boltzmann transport equation (BTE) using Fermi's Golden rule to determine scattering rates, and the Allen and Feldman (A-F) method. The other two possible decomposition formulations of GKMA are also included.

In Chapter 3, the application of GKMA to materials including crystalline silicon, amorphous silicon, amorphous silica, amorphous carbon and single polythiophene chains are discussed. The mode level comparison between GKMA and other modal analysis method is made for crystalline silicon. The GKMA results of a few amorphous solids are also compared with experimental results.

In Chapter 4, a series of case studies have been conducted using accurate phonon mode properties obtained by GKMA. We show that the relaxation time becomes an

incorrect descriptor for mode thermal conductivity above room temperature for amorphous materials. We show the first numerical evidence that (1) locons can contribute to thermal conductivity; (2) anharmonicity increases thermal conductivity in amorphous materials; (3) diffusons exhibit size effects, and (4) individual modes cause the total thermal conductivity of single polythiophene chains to diverge. Finally, Chapter 5 lists potential future work and gives some concluding remarks.

CHAPTER 2

A NEW PARADIGM BASED ON CORRELATION INSTEAD OF SCATTERING

In this chapter we introduce the formulation of a new numerical model, termed GKMA, which can be used to investigate the mode thermal conductivity of solids and polymers. As discussed in Chapter 1, GKMA is different from existing modal analysis methods which are based on PGM. GKMA is grounded on fluctuation-dissipation theory or Green Kubo (GK) formula. Although using GK formula and combining with MD simulations, one can study the thermal conductivity of a wide variety of materials including solids, fluids and polymers, it lacks mode level information on the individual phonon. In order to obtain mode level information of phonon, GKMA combines Green Kubo formula and LD. In this chapter we introduce the theory of GKMD after we present GK formula and LD theory. Then we discuss the differences between GKMA and other modal analysis methods.

2.1 Green-Kubo (GK) formulation

To understand GKMA, one needs to start with the GK formula. It is developed by Green and Kubo [1] from the linearized Liouville equation. Firstly, we define N particle distribution function $f^{(N)}$ with particle coordinate $\mathbf{r}$ and momentum $\mathbf{p}$. It represents the probability density of finding a particular system at a specific state defined by N particle coordinates $\mathbf{r}$ and momentum $\mathbf{p}$. By solving the linearized Liouville equation for the N particle distribution function, one can use this distribution to determine the response

when a system is subjected to a thermal disturbance as a temperature perturbation. At last, one can identify the portion of the result that is proportional to the temperature gradient which is the thermal conductivity. The derivation is briefly discussed here [1].

We start with N particles and Hamiltonian equations of motion [1], which comes from a basic conservation relation $Df / Dt = 0$, meaning there is no change in number states in a finite volume of phase space corresponding to a given macrostate.

$$\frac{\partial f^{(N)}}{\partial t} = \left\{ H, f^{(N)} \right\} \tag{2.1}$$

where $f^{(N)}$ is the N particle distribution and the Poisson bracket $\{\_,\_\}$ is defined as

$$\left\{ A, B \right\} \equiv \sum_{i=1}^{N} \left(\frac{\partial A}{\partial \mathbf{q}_i} \cdot \frac{\partial B}{\partial \mathbf{p}_i} - \frac{\partial A}{\partial \mathbf{p}_i} \cdot \frac{\partial B}{\partial \mathbf{q}_i} \right) \tag{2.2}$$

with A and B as arbitrary functions of the phase space variables, $\mathbf{p}$ is velocity vector and $\mathbf{q}$ is the displacement vector. We then define the Liouville operator Γ as

$$\Gamma \equiv i \cdot \left\{ H, \_ \right\} \tag{2.3}$$

Such that

$$\frac{\partial f^{(N)}}{\partial t} = -i \cdot \Gamma f^{(N)} \tag{2.4}$$

where $i = \sqrt{-1}$. In linear response theory, the Liouville operator is assumed to not have explicit time dependence. If this is valid, one can solve the Liouville equation (2.4),

$$f^{(N)}(\mathbf{q},\mathbf{p},t) = \exp(-i \cdot t \cdot \Gamma) f^{(N)}(\mathbf{q},\mathbf{p},0) \tag{2.5}$$

Using this solution, one can derive an expression for the thermal conductivity by considering the linear response to a thermal disturbance.

Now considering a canonical ensemble, the system at equilibrium temperature T with a small temperature disturbance δT, the distribution function of the system is given by the Boltzmann distribution

$$f_0 = const \cdot \exp(-\frac{\varepsilon \cdot \Delta V}{k_B \cdot T}(1 - \frac{\delta T}{T})) \tag{2.6}$$

where ε is the local energy density and ΔV is the local volume. Taking the second term in the exponent as the perturbation energy we write the perturbed Hamiltonian H' as

$$H'(t) = -\int \varepsilon(\mathbf{q}(t)) \frac{\delta T(\mathbf{q}(t))}{T} dV \tag{2.7}$$

Now we rearrange the Liouville equation as,

$$\frac{\partial f^{(N)}}{\partial t} = \left\{ H_0, f^{(N)} \right\} + \left\{ H', f_0^{(N)} \right\} \tag{2.8}$$

where H_0 is the energy of the unperturbed system with $H_0 = H - H'$. By substituting Eq. (2.7) into Eq. (2.8), we arrive at

$$\frac{\partial f^{(N)}}{\partial t} = -i \cdot \Gamma_0 f^{(N)} - (\frac{f_0^{(N)}}{k_B \cdot T^2}) \cdot \int \frac{\partial \varepsilon(\mathbf{q}(t))}{\partial t} \cdot \delta T(\mathbf{q}(t)) dV \tag{2.9}$$

Using energy conservation

$$\frac{\partial \varepsilon}{\partial t} + \nabla \cdot \mathbf{Q} = 0 \tag{2.10}$$

where ε is the local energy and $\mathbf{Q}$ is the local heat current, we then substitute into (2.9)

$$\frac{\partial f^{(N)}}{\partial t} = -i \cdot \Gamma_0 f^{(N)} - \left(\frac{f_0^{(N)}}{k_B \cdot T^2}\right) \cdot \int \begin{bmatrix} -\nabla \cdot (\mathbf{Q}(\mathbf{q}(t)) \cdot \delta T(\mathbf{q}(t))) \\ +(\mathbf{Q}(\mathbf{q}(t)) \cdot \nabla \cdot \delta T(\mathbf{q}(t))) \end{bmatrix} dV \tag{2.11}$$

The first term in the integral is negligible, which allows us to focus on integrating the second term, resulting in

$$\frac{\partial f^{(N)}}{\partial t} = -i \cdot \Gamma_0 f^{(N)} - \left(\frac{f_0^{(N)}}{k_B \cdot T^2}\right) \cdot \nabla \cdot \delta T \cdot \mathbf{Q}_{total} \tag{2.12}$$

where $\mathbf{Q}_{total}$ is now the net heat current in the system. The first term inside the integral of Eq. (2.12) is small assuming $\mathbf{Q}(\mathbf{q}(t))$ and the disturbance $\delta T(\mathbf{q}(t))$ itself independent, resulting in a smaller volumetric integral by comparison to the second term.

One can continue solving Eq. (2.12) for the phase space density,

$$f^{(N)}(\mathbf{q},\mathbf{p},t) = \frac{-V}{k_B \cdot T^2} \cdot \nabla \cdot \delta T \cdot \int_{-\infty}^{t} \exp(-i \cdot (t - t') \cdot \Gamma_0) \mathbf{Q} \cdot dt' \tag{2.13}$$

then use the result to calculate the ensemble averaged heat current,

$$\left\langle \mathbf{Q}_{total}(t) \right\rangle = \iint \mathbf{Q}^{(N)}(\mathbf{q},\mathbf{p},t) \cdot f^{(N)}(\mathbf{q},\mathbf{p},t)\, d\mathbf{q}\, d\mathbf{p} \tag{2.14}$$

By substituting Eq. (2.13), we arrive at

$$\left\langle \mathbf{Q}_{total}(t) \right\rangle = \frac{-V}{k_B \cdot T^2} \int_{-\infty}^{t} \left\langle \mathbf{Q}(t) \cdot \mathbf{Q}(t-t') \right\rangle \cdot \nabla \cdot \delta T \cdot dt \tag{2.15}$$

We then extract the temperature gradient, resulting in an expression for the heat current, similar to heat current defined by Fourier's law $Q = -\kappa \cdot \nabla T$. Substituting Fourier's heat current equation, we now identify an expression for the thermal conductivity, using a Fourier transform to rewrite the integral to obtain:

$$\kappa_{\alpha\beta}(T,\omega) = \frac{V}{k_B \cdot T^2} \int_{0}^{\infty} \left\langle \mathbf{Q}_{\alpha}(0) \cdot \mathbf{Q}_{\beta}(\tau) \right\rangle \cdot \exp(-i\omega \cdot \tau) \cdot d\tau \tag{2.16}$$

$\kappa_{\alpha\beta}(T,\omega)$ is the temperature and frequency dependent thermal conductivity tensor, where ω is the perturbation frequency, the *ij* subscripts denote the directional components, V is the volume of the system, $\mathbf{Q}$ is the heat current of the system and τ the time separation. In macroscopic heat conduction, we most often encounter constant currents and therefore require the zero frequency limit of equation 2.16 [1].

$$\kappa_{ij}(T) = \frac{V}{k_B \cdot T^2} \int_{0}^{\infty} \left\langle \mathbf{Q}_{i}(0) \cdot \mathbf{Q}_{j}(\tau) \right\rangle \cdot d\tau \tag{2.17}$$

where $\kappa(T)$ is now the thermal conductivity most often required in macroscopic analysis, and where the time scale of the system perturbations are orders of magnitude slower than atomic scale fluctuations. However for high frequency inputs of similar time scales as the atomic fluctuations, the frequency dependent thermal conductivity can deviate from the static value by orders of magnitude.

The next step is to calculate the volume averaged heat current for the system in terms of the microscopic variables that can extract from an MD simulation. Hardy[55]

derived the heat current operator that is generalized for any phase of matter and can be applied to any empirical form of potential energy, provided the energy is expressed as a sum of individual atom energies – which is in practice always the case. Hardy used a generic form for the Hamiltonian operator in order to express the heat current operator in terms of the microscopic variables available in a MD simulation. He then defined a local energy density operator in terms of a spatially dependent weighting function that incorporates contributions to the heat current from the local environment. Then he obtained the microscopic heat current operator.

Starting from energy conservation,

$$\dot{H}(x) + \nabla \cdot \mathbf{s}(x) = 0 \tag{2.18}$$

where $\mathbf{s}(x)$ is now a local heat current operator and $\dot{H}(x)$ is related to the energy density operator H by,

$$\dot{H}(x) = \frac{1}{i \cdot \hbar}\left\{H(x), H\right\} \tag{2.19}$$

Combining these two expressions gives

$$\nabla \mathbf{s}(x) = \frac{1}{i \cdot \hbar}\left\{H(x), H\right\} \tag{2.20}$$

in order to express the heat current operator in terms of the microscopic variables available in a MD simulation, then we assume a generic form for the Hamiltonian operator,

$$H = \sum_{i=1}^{N}\left(\frac{\mathbf{p}_i^2}{2 \cdot m_i} + \Phi_i\right) \tag{2.21}$$

where Φ is potential energy. Hardy defined a local energy density operator in terms of a spatially dependent weighting function that incorporates contributions to the heat current from the local environment [35],

$$H = \frac{1}{2}\sum_{i=1}^{N}\left\{\Delta(\mathbf{x}-\mathbf{q}_i)\left(\frac{\mathbf{p}_i^2}{2\cdot m_i}+\Phi_i\right)+H.c.\right\} \tag{2.22}$$

where H.c. is the Hermitian conjugate and $\Delta(\mathbf{x}-\mathbf{q}_i)$ is a spatial weighting function normalized to unity,

$$\int \Delta(\mathbf{x}-\mathbf{q}_i)\,dV = 1 \tag{2.23}$$

Taking

$$\Delta(\mathbf{x}-\mathbf{q}_i) = \left(\frac{1}{I\cdot\sqrt{\pi}}\right)^3 \cdot \exp\left(-\left(\frac{\left|\mathbf{x}-\mathbf{q}_i\right|}{I}\right)^2\right) \tag{2.24}$$

and using the commutation relations for the position and momentum operators, along with a Taylor expansion of the spatial weighting function, allows simplification of Eq. (2.20) to

$$\frac{i}{\hbar}\left\{H(x),H\right\} = \sum_{\alpha}\frac{\partial \mathbf{s}_\alpha}{\partial \mathbf{x}_\alpha} \tag{2.25}$$

Here α denotes a vector component and the spatially dependent heat current is given by

$$\mathbf{s}(\mathbf{x}) = \frac{1}{2V}\left[\sum_{i=1}^{N}\left(\Delta(\mathbf{x}-\mathbf{q}_i)\frac{\mathbf{p}_i}{2m_i}+\frac{\mathbf{p}_i}{2m_i}\Delta(\mathbf{x}-\mathbf{q}_i)\right)\left(\frac{\mathbf{p}_i^{\,2}}{2m_i}+\Phi_i\right)+\ldots\right.$$
$$\left.\sum_{ij}^{N}\left(\left(1+\frac{1}{2!}\sum_b(\mathbf{q}_i^b-\mathbf{q}_i^b)\right)\Delta(\mathbf{x}-\mathbf{q}_i)\right)\cdot(\mathbf{q}_i-\mathbf{q}_j)\cdot\frac{1}{i\hbar}\left\{\frac{\mathbf{p}_i^{\,2}}{2m_i}+\Phi_i\right\}+H.c.\right. \tag{2.26}$$

now average the local heat current operator $\mathbf{s}(\mathbf{x})$, to yield an expression suitable for implementation in a MD simulation,

$$\mathbf{s} = \frac{1}{V}\sum_{i=1}^{N}\left[(\frac{\mathbf{p}_i^2}{2\cdot m_i} + \Phi_i)\cdot\frac{\mathbf{p}_i}{m_i} + \sum_{\substack{j=1 \\ j\neq i}}^{N}(\frac{\partial\Phi_j}{\partial\mathbf{q}_i}\cdot\frac{\mathbf{p}_i}{m_i})\cdot(\mathbf{q}_i - \mathbf{q}_j)\right] \tag{2.27}$$

where $\mathbf{s}$ is now a volume averaged heat current operator, $\mathbf{p}$ is momentum vector, $\mathbf{q}$ is the displacement vector, ij denotes the atom indices, m is the mass, and Φ is the potential energy.

Converting Eq. (2.27) to a familiar form which has been widely used as,

$$\mathbf{Q}(t) = \frac{1}{V}\sum_{i}\left[E_i\dot{\mathbf{x}}_i + \sum_{j}(-\nabla_{\mathbf{r_i}}\Phi_j\cdot\dot{\mathbf{x}}_i)\mathbf{r}_{ij}\right] \tag{2.28}$$

Where V is volume of the super cell, E_i is the kinetic and potential energy of atom i, Φ_j denotes potential energy of atom j, $\dot{\mathbf{x}}_i$ is the velocity of atom i and $\mathbf{r}_{ij}$ is distance between atom i and j. Equation (2.28) has two physically meaningful terms that correspond to the two mechanisms that carry heat in all phases of matter. The first term, often called the convective or diffusion term, dominates in liquids and gases where energy is transported through the kinetic energy of the constituent molecules [36]. In solids the second term dominates, because the forces are large and atoms are constrained to their local environment – i.e. the time between interactions is of the same order as the time of the interaction itself.

The GK formula offers a way of calculating the transport properties other than the PGM. GK is based on linear response theory and fluctuation-dissipation theory. The

PGM treats phonons as particles. All phonon interactions are considered to be scattering events. Here we focus on two types of phonon-phonon scattering: momentum-conserved scattering and momentum-destroying scattering . The second type, which is also known as umklapp scattering, gives rise to thermal resistance. The more often these umklapp scattering events happen, the higher the thermal resistance, and hence lower the thermal conductivity. The GK formula on the other hand is derived from the Liouville equation and describes the response of the system to small external disturbances from equilibrium. This approach leads to general results for the system response functions and transport coefficients, like thermal conductivity. As shown in Eq. (2.17), the thermal conductivity is proportional to the total heat current autocorrelation under the GK formula. Based on the GK perspective or correlation paradigm, we consider any form of patterned or correlated motion in the system's trajectory as a contribution to thermal conductivity. Using Eq. (2.28), one can measure the total heat current, which is valid for any phase of matter. The duration over which the heat current function remains correlated with itself is proportional to the thermal conductivity. Thus, in a material with a high thermal conductivity, the correlation will be long lasting (i.e., fluctuations from equilibrium dissipate slowly). For a material with a low thermal conductivity, the correlation will be short-lived. In liquids and gases, the first term in the heat current equation, which is known as convective term in Eq. (2.28), is important since there is diffusion/convection. Teng et al. have shown in fluids, the convective term correlation is the dominant contributor to the thermal conductivity [37]. However in solids, the second term, which is called conductive term is more important, since there is little or no convection. For instance, McGaughey et al. has shown the conductive term dominates when calculating

the total heat current in solid crystalline argon [24]. This thesis focuses on solids and polymers, in which the heat current is derived primarily from the 2nd term in Eq. (2.28), which depends on inter-atomic forces, distance, and velocities of atoms.

In GK calculation, the heat current is calculated using Eq. (2.28) in real time. The heat current includes the information of atomic interactions in the time domain. It also includes all phonon mode interactions.

Here we wish to emphasize the two important differences between GK and PGM paradigm. First, in the GK calculation, all the mode interactions are captured in time domain. In PGM, scattering processes are considered as the only interactions between phonons, hence phonon modes are nearly always independent, except when scattering events happen. However in the GK paradigm, the phonon interactions are evaluated at all times using Eq. (2.28). The second term in Eq. (2.28) describes the interatomic forces, distances and atomic velocities, including all the phonon interaction information for solids. The correlation of the heat current function is essentially calculating how similar/correlated of the heat current at time t and $t+\tau$, as shown in Eq. (2.18). The more correlated the heat current is, the higher the thermal conductivity. At a modal level, all the mode interactions are included in the heat current. These interactions' effect on the thermal conductivity is reflected by the heat current correlation function. Compared to the PGM, the GK paradigm includes the missing phonon interaction information that occurs before scattering events happen. After all, one single phonon cannot generate a temperature gradient in material; the phonon has to interact with other phonons to generate a temperature gradient. Secondly, the GK formula does not need to predefine wavevectors for phonons while the PGM does. In the PGM, a well-defined wavevector is

essential for every phonon, since the group velocity is defined by the derivative of frequency over the wavelength of a phonon. This pre-requirement limits the application of the PGM to non-periodic structures. Since the GK method does not have this limitation, it can be applied to non-crystalline solids and even fluids or gases. In sum, the GK paradigm offers a different method of calculating and understanding the phonon thermal conductivity for all phases of materials.

Although GK can be applied to more materials and structures than PGM based methods, it is not able to shed light upon individual phonon contributions, which the PGM based methods are able to offer. In the next two sections, we will discuss a new modal decomposition method, GKMA, derived from the GK formula and extended so that one can obtain the mode level details similar to PGM based methods. The GKMA method is also more generalized than the PGM based method, since it does not require a well-defined wavevector for each individual phonon. The GKMA method is derived from GK and LD methods. In order to understand the GKMA derivation, we first introduce the general form of the LD formulation.

2.2 Lattice dynamics formulation

Consider an arbitrary collection of N atoms that collectively form a stable rigid body, whereby each atom vibrates around a stable equilibrium site. This group of atoms can have any internally inhomogeneous structure and/or composition and need not be periodic in any sense whatsoever. For such a system, there will in general exist 3N collective modes of vibration that can be determined using the LD formalism in the harmonic limit. The most general form of the LD formalism does not require

wavevectors. Instead the formalism can be applied to any arbitrary group of atoms that oscillate around stable equilibrium sites, even without periodic boundary conditions. What results are 3N solutions to the equations of motion described in terms of polarization vectors for each individual atom, which describe the direction and relative amplitude of displacement for each solution (e.g., eigen/normal mode). The use of a wave vector is merely a generalization and simplification of the resulting solutions that occur for periodic systems, which are a special case.

In periodic systems, only the atoms within an individual unit cell are distinguishable, while all others are repetitions that have the same solutions modulated by different plane waves whose wavelength and direction are described by the corresponding wave vector. The formulations are listed below as [38]

$$\omega^2(\mathbf{k},p)\cdot\mathbf{e}(\mathbf{k},p)=\mathbf{D}(\mathbf{k})\cdot\mathbf{e}(\mathbf{k},p) \tag{2.29}$$

where $\mathbf{e}(\mathbf{k},p)$ is a complex polarization vector, which represents the mode shape, p represents different branch, and $\mathbf{k}$ is the wavevector. The $\mathbf{D}(\mathbf{k})$ is the dynamics matrix containing the mass and stiffness information. The $\mathbf{D}(\mathbf{k})$ matrix is calculated by

$$\mathbf{D}_{\alpha\beta}(jj',\mathbf{k})=\frac{1}{(m_j\cdot m_{j'})^{1/2}}\cdot\sum_{l'}\phi_{\alpha\beta}(jj',0l')\cdot\exp(i\cdot\mathbf{k}\cdot\left[r(j'l')-r(j0)\right]) \tag{2.30}$$

$$\phi_{\alpha\beta}(jj',0l')=\frac{\partial^2\Phi}{\partial u_\alpha(jl)\partial u_\beta(j'l')} \tag{2.31}$$

The indices j and j' represent individual atoms, l identifies the unit cell where the atom j is located. The dynamics matrix is symmetric and Hermitian, guaranteeing real eigenvalues, which are also related to the harmonic frequencies of the

atoms. The eigenvector can be complex which represent the coefficient of a polarized wave.

If one were to then use a suitable description of the interatomic forces, one can conduct an EMD simulation to obtain the time history of the positions and velocities of all the atoms, which would contain all degrees of the anharmonicity. The LD eigenmodes, however, can still be used to understand the interactions between modes as McGaughey and Kaviany were the first to show that by projecting the MD trajectory onto the LD mode shapes, one can obtain each mode's amplitude as a function of time [39]. With this approach, one can calculate the relaxation time of any mode, regardless of whether it is a propagon, diffuson or locon[40]. However, without a clear definition for the phonon velocity, one cannot complete the calculation of thermal conductivity.

Here, we treat the system more generally in the sense that we do not attempt to describe the solutions in terms of plane waves and wave vectors since in general they will greatly deviate from that description when the structure or composition is disordered. In terms of the more common terminology, it is equivalent to treating the entire simulation cell as though it is a single, possibly complicated unit cell on a cubic lattice, such that all of the LD calculations are carried out at the gamma point ($\mathbf{k} = 0$). Substitute $\mathbf{k} = 0$ in Eq. (2.29-2.30), one will obtain the most general form of the LD formula. Then j and j' represent any atom in the simulation domain instead of only atoms in a unit cell. In this supercell LD approach (SCLD), one effectively treats the entire super cell calculation domain as one unit cell. This approach then allows us to generalize the GKMA formalism for any type of material that simply satisfies the most basic requirement that atoms

vibrate around stable equilibrium sites. This would then apply to systems with any degree of order or disorder or lack of periodicity, such as crystals, random alloys, amorphous materials and individual molecules. Using SCLD, we can obtain the mode shape/eigenvectors of the phonons. The next step is to input the mode information into GK and heat current formula such that one can calculate mode level information from MD simulation that include anharmonicity.

2.3 Green-Kubo modal analysis method formulation

After we obtain the eigenvectors from LD, we need another formula to combine the eigenvectors with the heat current operator and GK formula. Then, we introduce the GKMA method, as it is a combination of Green-Kubo and the normal mode analysis method based on LD. The main idea is to decompose the heat current into mode heat current. And then calculate mode heat current correlation with total heat current, which is the mode thermal conductivity. By inspecting the heat current in Eq. (2.28), there are several ways to decompose the heat current, such as decomposition based on velocity, displacement, and force. Using velocity is an obvious choice, since velocity appears in each term and thus the entire heat current expression is proportional to it. This is the only choice of variable decomposition that allows one to decompose both terms in the heat current operator and therefore allows the entire heat current to become proportional to a summation over modes. Velocity is therefore a simple, obvious and straightforward way of performing the decomposition. However, it has been shown that the first term in the heat current is not very important for solids [24] and thus we should also consider that one might need to also focus on the term that contains the forces and displacements. Therefore, in the following section, we will first discuss the formulism and feasibility of

the other two possible decomposition methods. And we prove that these two decompositions are either theoretically incorrect or impossible to implement.

After we prove that the velocity decomposition is rigorously correct and feasible, we will briefly discuss the implementation of GKMA. GKMA is implemented in the MD simulation since MD includes all degree of anharmonic interactions. Once obtaining the mode thermal conductivity from GKMA, one needs to apply the quantum correction due to the classic nature of MD. At last, we will discuss one calculation scheme we used to reduce the computational cost, which is partial summation of modes.

2.3.1 Heat current decomposition based on velocity

First, we start with velocity decomposition. We derive the GKMA formulation of partitioning heat current by decomposing velocity into mode level coordinates. Here, we utilize the same concept of projecting the MD trajectory onto the mode shapes obtained from LD, but instead of using the mode amplitudes to calculate relaxation times we conduct a direct modal decomposition of the heat current. Towards this end, we first examine the meaning of the reverse transformation from normal mode coordinates back to individual atom coordinates, where the normal mode amplitudes are calculated from,

$$X(n) = \sum_j \sqrt{m_j}\,\mathbf{e}_j^*(\mathrm{n}) \cdot \left(\mathbf{x}_j - \mathbf{x}_{j0}\right) \tag{2.32}$$

and

$$\dot{X}(n) = \sum_j \sqrt{m_j}\,\mathbf{e}_j^*(\mathrm{n}) \cdot \mathbf{v}_j \tag{2.33}$$

whereby the displacement and velocity of each atom and can be obtained from the normal mode coordinates via,

$$\mathbf{x}_j = \frac{1}{m_j^{1/2}} \sum_n \mathbf{e}_j(\mathrm{n}) X(\mathrm{n}) \tag{2.34}$$

$$\dot{\mathbf{x}}_j = \frac{1}{m_j^{1/2}} \sum_n \mathbf{e}_j(\mathrm{n}) \dot{X}(\mathrm{n}) \tag{2.35}$$

In Eqs. (2.32- 2.35) n denotes the mode (e.g., the n$^{\text{th}}$ solution to the equations of motion), m_j is the mass of the j$^{\text{th}}$ atom, and $\mathbf{e}_j(\mathrm{n})$ is the polarization vector which gives the relative magnitude and direction of motion for atom j in mode n. Equations (2.32- 2.35) are not new and are well established within the context of the LD formalism [38].

Here, we postulate that Eqs. (2.32) and (2.33) essentially state that at every instant, each atom's position and velocity are composed of their respective contributions from the different collective vibrations in the system. Thus, every atom's position and velocity are dictated by the respective magnitudes of each normal mode's amplitude $\mathbf{x}_j(n)$ and its time derivative $\dot{\mathbf{x}}_j(n)$. By thinking of each atom's position and velocity as being composed of an exact sum of modal contributions at every instant, it was then postulated that if an individual mode's contribution to the displacement or velocity of an atom is used in an expression for the calculation of any other property that depends on that atom's position and/or velocity, one would subsequently obtain that mode's contribution to that property. For example, one can calculate each mode's contribution to the temperature of the system via, $T(\mathrm{n}) = \frac{1}{3N_t k_B} \sum_i^{N_t} \left| \mathbf{e}_i(\mathrm{n}) \dot{X}(\mathrm{n}) \right|^2$. Similarly, towards the calculation of thermal conductivity, the modal contributions to the velocity of each atom

can be substituted into the heat current operator derived by Hardy [35], to obtain each mode's contribution to the volume averaged heat current at each time step in a EMD simulation,

$$\mathbf{Q} = \sum_{n}^{3N} \mathbf{Q}(n) = \sum_{n}^{3N} \frac{1}{V} \sum_{i} \left[E_i \mathbf{v}_i(n) + \sum_{j} (-\nabla_{r_i} \Phi_j \cdot \mathbf{v}_i(n)) \mathbf{r}_{ij} \right] \tag{2.36}$$

where $\mathbf{v}_i(n) = \frac{1}{m_i^{1/2}} \mathbf{e}_i(n) \dot{X}(n)$, E_i is the sum of potential and kinetic energy of atom i, V is the volume of the supercell, Φ_j is the potential energy of atom j, and $\mathbf{r}_{ij}$ is the distance between atom i and atom j.

We can then take this expression and substitute it directly into the Green-Kubo expression, Eq. (2.17), for thermal conductivity, to obtain an equation that expresses the thermal conductivity as a direct summation over individual mode contributions,

$$\kappa(n) = \frac{V}{k_B T^2} \int_0^{\infty} \left\langle \mathbf{Q}(\mathrm{n},t) \cdot \mathbf{Q}(0) \right\rangle dt \tag{2.37}$$

Furthermore, one can also substitute the summation of modal contributions to the heat current in both places of the heat current autocorrelation to obtain the thermal conductivity as a double summation over individual mode-mode heat current correlation functions,

$$\kappa = \frac{V}{k_B T^2} \int_0^{\infty} \left\langle \sum_{n} \mathbf{Q}(n,t) \cdot \sum_{n'} \mathbf{Q}(n',0) \right\rangle dt = \frac{V}{k_B T^2} \sum_{\mathrm{n,n'}} \int_0^{\infty} \left\langle \mathbf{Q}(\mathrm{n},t) \cdot \mathbf{Q}(\mathrm{n}',0) \right\rangle dt \tag{2.38}$$

Equations (2.32) to (2.38) are generally applicable to any system where the atoms vibrate around equilibrium positions. However for crystalline materials, one can

exploit the structural symmetry, using wavevectors to describe the spatial periodicity. GKMA can also work for these systems, providing the detail information of phonons behaviors on different phonon branches as described in the following.

Similar to Eq. (2.32) and (2.35), using the LD formalism, for a pure, homogenous crystalline material we can use the eigenmode coordinates to write the velocity of every individual atom as,

$$\dot{x}(j) = \frac{1}{(Nm_j)^{1/2}} \sum_{\mathbf{k}} \sum_{p} \mathbf{e}(j,\mathbf{k},p) \cdot \exp(i \cdot \mathbf{k} \cdot \mathbf{r}(j)) \cdot \dot{X}(\mathbf{k},p) \tag{2.39}$$

where

$$\dot{X}(\mathbf{k},p) = \frac{1}{N^{1/2}} \sum_{j} \sqrt{m_j}\, \mathbf{e}(j,\mathbf{k},p) \cdot \exp(-i \cdot \mathbf{k} \cdot \mathbf{r}(j)) \cdot \mathbf{v}(j) \tag{2.40}$$

where j denotes the atom, m_j is its mass, N is the number of unit cells in the system, $\mathbf{k}$ denotes the wavevector, p is the phonon branch, and $\mathbf{e}(j,\mathbf{k},p)$ is the polarization vector which gives the direction in which each atom moves. Equations (2.32) and (2.33) represent a transformation to and from the normal mode coordinates. Equation (2.32) gives the modal contributions to every individual atom's velocity. From Eqs. (2.32) and (2.33) one can describe the modal contributions to any quantity that is a direct function of the atomic displacements or velocities. To study thermal conductivity, we substitute the modal velocity into the heat current operator [35], to obtain the modal heat current

$$\mathbf{Q}(\mathbf{k},p) = \frac{1}{V} \sum_{j} \left[E_i \mathbf{v}(\mathbf{k},p) + \sum_{j} (-\nabla_{r_i} \Phi_j \mathbf{v}(\mathbf{k},p)) \cdot \mathbf{r}_{ij} \right] \tag{2.41}$$

where $\mathbf{v}(\mathbf{k},p)=\frac{\mathbf{e}(j,\mathbf{k},p)\exp(i\cdot\mathbf{k}\cdot\mathbf{r}(j))\dot{X}(\mathbf{k},p)}{(Nm_j)^{1/2}}$. We can then take this expression for the heat current and substitute it directly into the GK expression for modal thermal conductivity,

$$\kappa(\mathbf{k},p)=\frac{V}{k_bT^2}\int_0^\infty\left\langle\mathbf{Q}(\mathbf{k},p,t)\mathbf{Q}(0)\right\rangle dt \tag{2.42}$$

resulting in,

$$\kappa(\mathbf{k},p)=\frac{V}{k_bT^2}\int_0^\infty\left\langle\mathbf{Q}(\mathbf{k},p,t)\sum_{\mathbf{k}'}\sum_{p'}Q(\mathbf{k}',p',0)\right\rangle dt \tag{2.43}$$

With this method, we are able to calculate each mode's contribution to thermal conductivity for crystalline materials.

Equations (2.32-2.38) are the general form of the GKMA formula that can be applied to any systems that the atoms vibrate at the equilibrium positions. Equations (2.39-2.43) are applicable to crystalline materials that have well defined wavevectors. In the following chapters, the comparison between GKMA and other modal analysis method based on Eqs. (2.39-2.43) will be illustrated.

Equations (2.36-2.37) and (2.41-2.42) are the primary results termed the GKMA method, which empowers us to obtain each mode's contribution to the total thermal conductivity. We are guaranteed by Eqs. (2.36) and (2.41) that the summation in Eqs (2.37) and (2.42) will exactly recover the total GK thermal conductivity. Also Eqs. (2.37) allows one to examine how the correlation between pairs of modes contributes to thermal conductivity.

Aside from these benefits, the main power of the GKMA method (e.g., Eqs. (2.9-2.10)) is that it now allows for calculation of the eigenmode contributions to thermal conductivity without the need to define a phonon velocity. This is a critical issue for situations where the PGM becomes questionable, such as for disordered materials. With the GKMA method, however, it is now possible to calculate the thermal conductivity contributions of individual modes for any arbitrary collection of atoms, as long as they vibrate around stable equilibrium sites.

So far, we completed the discussion on the GKMA formulation using velocity decomposition. As we mentioned earlier, two alternative choices to decompose heat current are to (1) decompose the portion of the heat current that has the force vectors $-\nabla_{\mathbf{r}_i}\Phi_j$ or (2) the heat current based on the position vectors $\mathbf{r}_{ij}$. The subsequent analysis shows that decomposing force cannot be evaluated for systems employing periodic boundary conditions, as is customary in simulations that approach the limiting behavior of a bulk material. Secondly we show that decomposing based on position would be qualitatively incorrect via a simple thought experiment.

2.3.2 GKMA with force decomposition

Following a similar procedure to velocity, to decompose the heat current based on force, we first write the force term as scalar modal force amplitude:

$$F_i(n) = \sum_j \sqrt{m_j}\,\mathbf{e}_j^*(\mathrm{n}) \cdot (-\nabla_{\mathbf{r}_i}\Phi_j) \tag{2.44}$$

Similar to velocity, the force vector needed in the heat current should then obtained by summation of the modal force amplitudes, multiplied by each atom's polarization vector,

$$-\nabla_{\mathbf{r}_i}\Phi_j = \sum_n \frac{1}{m_j^{1/2}}\mathbf{e}_j(\mathrm{n})\cdot F_i(n) \tag{2.45}$$

$$-\nabla_{\mathbf{r}_i}\Phi_j = \sum_n \mathbf{f}(n) = \sum_n \left[\frac{1}{m^{1/2}}\mathbf{e}_j(n)\cdot\sum_j \sqrt{m_j}\,\mathbf{e}_j^*(n)\cdot(-\nabla_{\mathbf{r}_i}\Phi_j)\right] \tag{2.46}$$

$$\mathbf{Q} = \sum_n^{3N}\mathbf{Q}(n) = \sum_n^{3N}\frac{1}{V}\sum_i\left[\sum_j(\mathbf{f}(n)\cdot\dot{\mathbf{x}}_i)\mathbf{r}_{ij}\right] \tag{2.47}$$

$$\mathbf{Q} = \sum_n^{3N}\mathbf{Q}(\mathrm{n}) = \sum_n^{3N}\frac{1}{V}\sum_i\left\{\sum_j\left[\frac{1}{m_j^{1/2}}\mathbf{e}_j(\mathrm{n})\left(\sum_{j'}\sqrt{m_{j'}}\,\mathbf{e}_{j'}^*(\mathrm{n})\cdot(-\nabla_{\mathbf{r}_i}\Phi_{j'})\right)\cdot\dot{\mathbf{x}}_i\right]\mathbf{r}_{ij}\right\} \tag{2.48}$$

Inspection of Eq. (2.44) shows that there is an issue that would make the implementation of such an expression much more computationally expensive as compared to a decomposition based on velocity, namely: In order to decompose $-\nabla_{\mathbf{r}_i}\Phi_j$ (the force on atom i due to atom j), instead of velocity $\dot{\mathbf{x}}_i$, one must decompose $-\nabla_{\mathbf{r}_i}\Phi_j$ for every atom i, which means one has to conduct the decomposition n times (number of atoms in the system) instead of decomposing $\dot{\mathbf{x}}_i$ one time at every time step. However, even if one disregards the much larger computational expense, there is a more problematic issue encountered.

Upon attempting to implement this decomposition in a much less computationally expensive potential such as LJ in order to test it, we noticed the following problem. The force term in Eq. (2.45) is the summation of the force from atom j and all the other atoms in the system, which includes periodic images of other atoms when one applies periodic boundary conditions. The problem with periodic images is the fact that the corresponding $\mathbf{r}_{ij}$ that must be used for each term in the decomposition is different for an atom in the

cell and a periodic image. The problem then arises from the fact that the periodic image of an atom has exactly the same polarization vector. Therefore, when one multiplies the modal force amplitude in Eq. (2.45) by the atom's polarization vector, one does not obtain the force between atom i and j, but instead the sum of force terms between i and j, including all periodic images of j. This then becomes problematic, because one cannot obtain the force terms for each individual instance/image of j (i.e., in the supercell vs. periodic image(s)) and therefore one cannot multiply each term by the appropriate $\mathbf{r}_{ij}$ for each respective instance/image. As a result, if there is a periodic image of an atom, one cannot obtain the correct total heat current (2nd term only) via the summation in Eq. (2.48).

This issue essentially shows that force decomposition would rely on every atom in the system having a different polarization vector, so that one can properly map the force contributions to the corresponding values of $\mathbf{r}_{ij}$. Thus, the central problem with using force as a basis for decomposition is the inability to properly map the force components to the correct atoms, since the summation in Eq. (2.48) simply returns the sum of all forces between atom i and all atoms with the polarization vector $\mathbf{e}_j$. Clearly this is problematic for periodic boundary conditions and also structures where the eigenvectors themselves are periodic, which is generally the case for sinusoidally modulated/propagating modes. Thus, it cannot be implemented in general. Furthermore, one can easily see how the same issue arises if one were to even analyze a crystal, even without periodic boundary conditions. In a crystal, the eigenvectors would be repeated for every instance of the unit cell. Therefore, when Eq. (2.48) is evaluated, one would not be

able to properly separate interactions between individual atoms and periodic instances of the same basis atom in different unit cells. Thus, although we identified the issue in the context of assessing periodic boundary conditions, the issue is more general and is associated with periodicity in the polarization vectors, which cannot be applied to crystalline systems altogether. Thus, the decomposition of heat current based on force is incorrect.

2.3.3 GKMA with displacement decomposition

Decomposing the heat current based on position by projecting $\mathbf{r}_{ij}$ onto the polarization vectors will be incorrect based on the following simple thought experiment. Consider the system at the following state, which is a common initial condition, used in many MD simulations, whereby all atoms are at their equilibrium sites, but have initial velocities. In this state, the heat current would be non-zero because the velocities are non-zero and can be asymmetric. However, if one were to have decomposed the heat current based on the displacements, in this state, all modal contributions will become equal to zero because the displacements are zero. This is because when one expands the difference in atom positions, there are two components to the vector ($\mathbf{r}_{ij} = \mathbf{r}_{i0} + \mathbf{u}_i - (\mathbf{r}_{j0} + \mathbf{u}_j) = \mathbf{r}_{i0} - \mathbf{r}_{j0} + \mathbf{u}_i - \mathbf{u}_j$). The modal decomposition would arise from each atom's relative displacement from equilibrium (e.g., the $\mathbf{u}_i - \mathbf{u}_j$ term) and in the aforementioned state, all modal contributions would be zero since every atom would be located at its equilibrium position $\mathbf{r}_{i0}$. As a result, the entire heat current would arise from the term associated with $\mathbf{r}_{i0} - \mathbf{r}_{j0}$, which is static and only gains time dependence through

its multiplication with the force and velocity terms. Therefore the problem with such a modal decomposition is the fact that no matter what modes are excited at the proposed initial state, decomposing based on position would yield the same modal contributions (e.g., all zero), which is clearly incorrect. Thus, by inspection of Eq. (2.41), one can see that a decomposition of the heat current based on position cannot be correct at the state described and therefore cannot be correct in general. Sun and Allen have used a power series of the relative displacements to decompose heat current [3]. However from second to highest order terms, all the terms are multiplied by $\mathbf{r}_{i0} - \mathbf{r}_{j0}$ in the end. Hence the same issue arises as long as the atoms are at equilibrium locations, the decomposition of displacement will give zero modal heat current for any order terms. Therefore decomposing heat current on displacement is not correct.

In conclusion, the decomposition based on velocity is both rigorous and correct. Furthermore, the most obvious alternative decompositions are incorrect/problematic.

2.3.4 Quantum correction on the specific heat

Since the GKMA method allows us to determine the thermal conductivity contributions with respect to each mode and the LD provides the mode frequencies, we can then apply a quantum correction to the classical MD GKMA results. The underlying assumption in doing so is that, only the quantum effect on the specific heat must be accounted for in this case. Turney and McGaughey [41] have clearly shown that for crystalline materials, quantum corrections are ill-founded because there are two quantum effects, one on the heat capacity, and the other one on the scattering rate due to incorrect mode-mode occupations. This second effect is both important and intuitive, as one can

envision that in the limit that only a single mode is excited in the system, the time it takes to couple with other modes and relax towards equipartition is a strong function of the amplitudes of other modes. Thus, when other modes are simultaneously excited, it affects the rate at which mode-mode interactions occur. Turney and McGaughey [41] have clearly shown that for crystalline materials this effect is crucial, and because classical MD trajectories do not yield the correct quantum mode amplitudes observed at low temperatures, MD incorrectly predicts higher scattering rates. However, even though this issue is critical for bulk homogenous crystalline materials, one can envision other situations where another scattering mechanism dominates the phonon relaxation times, such as boundary [42], impurity [43] or structural scattering [12]. In such situations, where the phonon-phonon scattering processes (e.g., umklapp scattering) are not the primary mechanism governing the low frequency mode thermal conductivity contributions, one would imagine that the error associated with incorrect mode-mode occupations at low temperatures can become negligible. Hence in the amorphous solids that we studied here, the second effect is neglected. The quantum heat capacity and a few other temperature dependent corrections are included in the GKMA analysis.

Using GKMA one can calculate the thermal conductivity of individual modes. However a few temperature dependent corrections are needed to accurately predict the thermal conductivity. Due to the classic nature, MD results in a constant heat capacity with respect to temperature, since every mode is equally excited at all temperatures. However, once each individual mode's thermal conductivity is obtained, one can easily apply a quantum specific heat correction, which extends the MD based predictions to

essentially any temperature. To obtain the more accurate temperature dependence, one can then use the following expression,

$$\kappa(T) = \sum_n f_Q\left(\omega(n,T),T\right)\cdot f_\kappa(n,T) \tag{2.49}$$

which includes three explicit functions of temperature, namely f_Q, f_κ and ω . In Eq. (2.49) the function f_Q represents the ratio of the quantum to classical specific heat for mode n, which has frequency ω at temperature T and is unit-less. The function f_κ represents the GKMA derived mode thermal conductivity contributions (e.g., it has the units of thermal conductivity), obtained from MD simulations at discrete values of T, where the MD simulations are performed. The function ω represents the phonon frequency of mode n, which itself also exhibits some temperature dependence. In the next three paragraphs, the three temperature dependences are explained explicitly. In Chapter 3, we demonstrate how thermal conductivity prediction improves as each aspect of the temperature dependence is included in amorphous silica, which will henceforth be referred to using the subscripts Q, κ, and ω. It should also be noted that thus far in testing the GKMA method, we have only applied Eq. (2.49) to amorphous materials thus far and have yet to apply it to a crystalline material.

The first and most important source of temperature dependence is in the quantum to classical specific heat ratio f_Q, which is what causes the thermal conductivity to decrease to zero as $T \rightarrow 0$K for amorphous materials. Furthermore, it restricts the contributions of the high frequency modes at low temperatures and modulates the MD derived thermal conductivity contributions determined from the GKMA method. The

specific heat is calculated using analytical function. The quantum expression of volumetric specific heat, based on Bose-Einstein statistics is given by [44],

$$C_q(\omega) = \frac{k_B x^2}{V} \frac{\exp(x)}{\left[\exp(x)-1\right]^2}; x = \frac{h\omega}{k_B T} \tag{2.50}$$

and the classical volumetric specific heat is given by $C_m(\omega) = \frac{k_B}{V}$. Thus, the quantum heat capacity correction factor is the ratio,

$$C_q(\omega) / C_m(\omega) = \frac{x^2 \exp(x)}{\left[\exp(x)-1\right]^2} \tag{2.51}$$

where $f_Q(\omega) = C_q(\omega) / C_m(\omega)$.

The second important source of temperature dependence enters through the GKMA derived thermal conductivity contributions f_κ. As temperature changes, the modal interactions change and the contributions of different modes are inherently temperature dependent via the anharmonic nature of the interactions. However, unlike the quantum specific heat correction, which is a continuous function of temperature, MD simulations are run at discrete temperatures. To then generate a piece-wise continuous function for thermal conductivity vs. temperature, one can interpolate the data for f_κ at discrete values of temperature. Here, one can use the data at a few initial temperatures and determine by inspection, what temperature ranges may require additional simulations to improve the resolution of the temperature dependence, in temperature ranges where the contributions change more rapidly. This is because it is advantageous to minimize the number of temperatures needed for f_κ to minimize computational expense. Let us

assume we calculated the frequency dependent thermal conductivity at 3 temperatures for a material. For the intermediate temperatures, one can linearly interpolate the mode diffusivity using the three temperatures GKMA results for each individual mode diffusivity and then multiplied by the specific heat at the temperature of interest. For example, for $T_1 < T < T_2$, $D_T(n) = \frac{D_{T_1}(n)(T_2 - T) + D_{T_2}(n)(T - T_1)}{(T_2 - T_1)}$. In this expression, $D_{T_1}(n)$ and $D_{T_2}(n)$ are the mode diffusivity at T_1 and T_2 respectively. Due to the classical nature of MD simulations, all of the modes are excited. Hence we can determine the mode diffusivity from the mode thermal conductivity by dividing by the classical specific heat. After interpolation, one obtains the mode diffusivity and multiplies by the quantum corrected specific heat using Bose-Einstein statistics to yield the thermal conductivity at a given temperature.

Lastly, the phonon frequencies (ω) can slightly change with temperature, due to anharmonicity (e.g., frequency softening) and thermal expansion [45]. All of the simulations are performed using constant volume, hence thermal expansion does not play a role, but anharmonic effects can still cause the mode frequencies to change. The extent of the frequency shift as a function of temperature can be easily determined by interpolation of the data at discrete temperatures, using the peak frequency obtained from a Fourier transform of the mode amplitudes.

Using GKMA and temperature dependence corrections, one can calculate the temperature dependent thermal conductivity accurately. Furthermore GKMA can provide mode details from correlation maps. The mode-mode correlations are computed from,

$$\kappa(n,n')|_T = \frac{V}{k_B T^2}\int_0^\infty \left\langle \left(\mathbf{Q}(n,t)\sqrt{\frac{C_q(\omega(n),T)}{C_m}} \right) \cdot \left(\mathbf{Q}(n',0)\sqrt{\frac{C_q(\omega(n'),T)}{C_m}} \right) \right\rangle dt \qquad (2.52)$$

where n and n' represent two modes, k_B is Boltzmann constant, T is the temperature and V is volume, $\mathbf{Q}$ is heat current for a mode, C_q is quantum specific heat from Bose-Einstein statistics[44], and C_m is classic specific heat, and ω is frequency of the mode. Partitioning the specific heat ratio C_q / C_m from Eq. (2.51) into $\sqrt{C_q / C_m}$ for each mode heat current is mathematically correct. However it makes Eq. (2.52) offer a slightly different result as Eq. (2.49). In Eq. (2.49), the quantum effect is included once for every individual mode. After calculating one mode correlations with all other modes, then correct the specific heat once for this mode. Using this method, we consider that whether one mode is activated or not at a specific temperature based upon its specific heat ratio. However this equation does not consider whether the other modes, which it correlates with, are excited from ground state or not at the specific temperature. In order to consider this quantum effect, in Eq. (2.52), one can include the quantum heat correction in the correlating pair of two modes in the correlation function, which will make the quantum heat correction more rigorous. To understand Eq. (2.52), one needs to rationalize why heat current $\mathbf{Q}$ is proportional to $\sqrt{C_q / C_m}$. In order to prove $\mathbf{Q}$ is proportional to $\sqrt{C_q / C_m}$, we start with a special case, under PGM assumption, heat current is expressed as $\mathbf{Q} = \frac{1}{V}\sum_{\mathbf{k}}\sum_{p} \hbar\omega_{\mathbf{k}} \mathbf{v}_{\mathbf{k}p} \delta n_{\mathbf{k}}$, as shown in Eq. (1.1). Since $\left\langle \delta n^2 \right\rangle = \frac{e^x}{(e^x - 1)^2}$ [31], hence δn is proportional to $\frac{e^{x/2}}{e^x - 1}$, where $x = \frac{\hbar\omega}{k_B T}$. Substitute $\delta n = \frac{e^{x/2}}{e^x - 1}$ and $\hbar\omega = k_B T x$ into Eq.

1.1, one will obtain $\mathbf{Q} = \frac{1}{V}\sum_{\mathbf{k}}\sum_{p}\sqrt{k_B}T\mathbf{v}_{\mathbf{k}p}\sqrt{\frac{x^2e^x}{(e^x-1)^2}}$. Substitute specific heat ratio, which is defined in Eq. (2.51), $\mathbf{Q}$ then becomes $\frac{1}{V}\sum_{\mathbf{k}}\sum_{p}\sqrt{k_B}T\mathbf{v}_{\mathbf{k}p}\sqrt{C_q / C_m}$. Therefore the mode heat current is proportional to the square root of the mode specific heat ratio, which can be calculated based on the frequency of the mode. Using the summation of all correlation functions between pairs of modes $\sum_{n}^{3N}\sum_{n'}^{3N}\kappa(n,n')$, the resulting sum yields the Green-Kubo thermal conductivity at the simulated temperature, which represents the total integrated volume of the 3D map.

The introductions of the GKMA formulation and quantum correction are completed. Then we briefly discuss the implementation of GKMA and focus on the partial summation scheme, which can significantly reduce the computational cost.

2.3.5 Partial summation to reduce the computational cost

Modal analysis methods typically are computational demanding. In order to reduce the computational cost of GKMA, we proposed a scheme that combines any desired group of modes together to calculate the summed contribution of their combined heat current at one time. In Eq. (2.38) individual mode level detail is retained, but we can sum as many modes as desired to obtain their net contribution at one time, which mitigates the need to separately output and store the heat current associated with each mode.

As an example of how one can reduce the computation by grouping modes together, one can sum the contributions of all optical modes in crystalline material and calculate their thermal conductivity contribution all at once via,

$$\kappa_{optical} = \frac{V}{k_B T^2} \int_0^{\infty} \left[\sum_{n}^{optical} \mathbf{Q}(n,t) \cdot \mathbf{Q}(n,0) \right] dt \tag{2.53}$$

Such a simplification is useful, because very often there may be a group of modes that are of primary interest, and individual mode level detail can be targeted on such groups, while other modes such as optical modes, which are known to have minimal contributions to the thermal conductivity [46], can be separately computed. This is somewhat of an advantage to other formalisms [8,39], whereby every mode's contribution has to be recorded separately. Methods, such as the spectral energy decomposition (SED) have been developed to reduce this computational load [45]. However, it has been shown that although SED predicts accurate phonon frequencies, the phonon lifetimes are inaccurate, because the information about the phonon eigenvectors is discarded [45].

Thus far we have completed the discussion on the GKMA formulation and implementation. In the next chapter, we will demonstrate the results calculated using GKMA and compare with other modal analysis methods. In the following section, we will briefly discuss several other modal analysis methods' theories/formulations and their limitations.

2.4 Other mode level descriptions

2.4.1 Other modal analysis methods (NMA & BTE & A-F)

There are several modal analysis methods existing in the literature. Most of the methods are only applicable to pure crystalline materials or alloys because these methods are based on PGM. As discussed in Chapter 1, under PGM, the lattice heat conduction is described in terms of specific heat, phonon relaxation time, and group velocity. The phonon velocity is defined as $d\omega / dk$. ω is the phonon frequency and k is the phonon wavevector. PGM works well on crystalline solids. Next we discuss the formulations of two well-known PGM methods which are anharmonic force constant method and normal mode analysis method briefly.

We have discussed the calculation of specific heat and phonon group velocity earlier. The other important parameter is phonon relaxation time. Calculating of the phonon relaxation time is challenging, since anharmonicity needs to be considered. In order to calculate the phonon relaxation times, the anharmonic force constant methods use second and third order force constants and Fermi's golden rule; the normal mode method uses the anharmonic vibrations from MD to determine the time dependence of the normal mode coordinates.

In the anharmonic force constant method, the phonon lifetimes are obtained based on Fermi's golden rule. The total lattice thermal conductivity is determined under the relaxation time approximation by summing up the contribution from each mode in first

Brillouin zone. By applying Fermi's golden rule to the cubic Hamiltonian [4,7,47,48], the phonon lifetimes $\tau_{\mathbf{k}p}$ due to the three-phonon scattering processes can be expressed as

$$\frac{1}{\tau_{\mathbf{k}p}} = 2\Gamma_{\mathbf{k}p} = \pi \sum_{\mathbf{k}'p'} \sum_{p''} \left|V_3(\mathbf{k}p, \mathbf{k}'p', \mathbf{k}''p')\right|^2 \times \Big[2(n_{\mathbf{k}'p'} - n_{\mathbf{k}''p'})\delta(\omega(\mathbf{k}p) + \omega(\mathbf{k}'p') - \omega(\mathbf{k}''p')) + (1 + n_{\mathbf{k}'p'} + n_{\mathbf{k}''p'})\delta(\omega(\mathbf{k}p) - \omega(\mathbf{k}'p') - \omega(\mathbf{k}''p')) \Big] \tag{2.54}$$

where V_3 is the cubic interatomic force constants are needed to compute the three-phonon scattering matrix elements, which measure the strength of the scattering events. And $n_{\mathbf{k}p}$ is the equilibrium Bose-Einstein distribution function. The conservation of momentum requires $\mathbf{k} + \mathbf{k}' + \mathbf{k}'' = G$, where G is a reciprocal lattice vector, for which G =0 results in the normal processes and $G \neq 0$ relates to the umklapp processes. The choices of $\mathbf{k}''$ are limited by the choices of $\mathbf{k}$ and $\mathbf{k}'$, and thus the summation involves only $\mathbf{k}'$. Then one can compute the lattice thermal conductivity based on the relaxation time approximation using the PGM formula.

$$k = \frac{1}{3VN_0} \sum_{\mathbf{k}p} \mathbf{v}_{\mathbf{k}p}^2 \tau_{\mathbf{k}p} \hbar\omega_{\mathbf{k}p} \frac{\partial n_{\mathbf{k}p}}{\partial T} \tag{2.55}$$

where $\mathbf{v}_{\mathbf{k}p}$ is the amplitude of the group velocity. Recently there are several commercial packages[49,50] have been developed to apply the anharmonic force constant method to crystalline materials.

NMA, in short, uses the MD trajectory that is transformed to normal mode coordinates via LD calculations. Similar to GKMA, one needs to calculate the mode amplitude from displacement and velocity. Using Eq. (2.33), one can obtain the mode

amplitude from velocity. Similarly one can calculate the mode amplitude from atom displacement as

$$X(\mathbf{k},p)=\frac{1}{N^{1/2}}\sum_{j}\sqrt{m_j}\,\mathbf{e}(j,\mathbf{k},p)\cdot\exp(-i\cdot\mathbf{k}\cdot\mathbf{r}(j))\cdot\mathbf{r}(j) \tag{2.56}$$

The quantity $X(\mathbf{k},p)$ is also time dependent and represents the instantaneous amplitude of a specific mode, which can then be used compute the mode's total energy,

$$E(\mathbf{k},p)=\frac{1}{2}\omega^2 X^*\cdot X+\frac{1}{2}\dot{X}^*\cdot\dot{X} \tag{2.57}$$

The phonon lifetimes are then determined by [8,39,51]

$$\tau(\mathbf{k},p)=\int_0^\infty\frac{\langle\delta E(t)\delta E(0)\rangle}{\langle\delta E(0)\delta E(0)\rangle}dt \tag{2.58}$$

where $\delta E(t)=E(t)-\langle E(t)\rangle$.

The above two methods have been widely applied to many crystalline materials including Si [4,5,8] , Ge [4], Diamond [52], GaAs [53], half-heusler [54], PbTe [55], PbSe [7], CNT [56], graphene [57], to name a few. However the application of the two methods is limited to crystalline materials. The limitation with the usage of the above two methods is because they are based on PGM that needs a well-defined wavevector for each phonon in order to calculate the dispersion relation and group velocity. The lack of a clearly defined velocity is critical, because the PGM hinges on the velocity being defined in order to properly describe a mode's contribution to thermal transport. For systems that lack periodicity or compositional homogeneity, the normal modes do not in general correspond to plane wave modulated vibrations with clearly identifiable wavelengths, and

therefore one cannot define the phonon dispersion or velocity. Thus, for systems that lack periodicity, such as amorphous materials, or small molecules, using the PGM to describe their phonon transport is inconsistent with the atomic level vibrations. This issue is critical, because these classes of materials represent a major fraction of the materials used in various applications that involve heat transfer.

For the amorphous materials, the application of PGM is questionable. However, most studies on amorphous solids are still based on PGM [58–60]. The major exception has been the A-F method, proposed by Allen and Feldman [15,18,40], who made an important step forward by conducting LD calculations on supercell of amorphous Si [18,21,61]. In doing so, they developed a model for thermal conductivity that was based on the actual modes of vibration in an amorphous material.

Using the A-F method, first calculate the overlap of two eigenmode as

$$V_{ij} = \frac{i}{2\sqrt{\omega_j \omega_{j'}}} \sum_{\alpha,\beta} \sum_{k,k'} e_\alpha(k,j) D_{\beta\alpha}^{kk'} e_\beta(k',j') \tag{2.59}$$

where e is the eigenvector, α,β represents dimensions, j,j' are the atom number, and k,k' are mode numbers .This is then multiplied by the average mode energy $\hbar\omega$ of two modes,

$$S_{ij} = \frac{\hbar}{2V} V_{ij}(\omega_i + \omega_j) \tag{2.60}$$

One can then calculate the mode thermal diffusivity as

$$D_{AF}(\omega_i) = \frac{\pi V^2}{\hbar^2 \omega_i^2} \sum_{j \neq i} \left|S_{ij}\right|^2 \delta(\omega_i - \omega_j) \tag{2.61}$$

$\delta(\omega_i - \omega_j)$ indicates that the frequency of two modes have to close in order to contribute to the thermal diffusivity. In effect, it can be noticed that the delta function is substituted by a Lorentzian function of width. Typically the width is chosen to be of the order of energy spacing in the density of states (DOS) so that the latter is a smooth function of the frequency and does not display any oscillations with sharp peaks, which would appear if the width is too small. The diffusivity times the specific heat gives back the thermal conductivity as

$$\kappa_{AF} = \frac{1}{V} \sum_{i,\omega_i > \omega_{pr}} C(\omega_i) D_{AF}(\omega_i) \tag{2.62}$$

Their model exhibited better agreement with experimental data than previous work and it is based on harmonic approximation in LD. As a result they concluded that anharmonicity was not likely to be important. Michalski [22], on the other hand, argued that anharmonicity is important and a more recent study showed that the A-F method exhibits less agreement with experiments for amorphous materials other than a-Si [23]. This leads one to question if anharmonicity is the critical feature that has been missing from the previous model. It should also be emphasized here that correspondence with experimental data for thermal conductivity is the ultimate test for a model, and to date a model that exhibits excellent quantitative and qualitative agreement across multiple amorphous materials has yet to emerge. In Chapter 3, we will discuss the results calculated from the three modal analysis methods and compare with GKMA.

2.5 Phonon Transport – a correlation-based perspective

In order to compare the PGM and GKMA paradigms, we start from the wave packet concept. A wave packet is a finite set of phonons of different wavelength with phases and amplitudes such that they interfere constructively over a small region of space, and destructively elsewhere. A wave packet can be viewed as an envelop of a localized wave. From the PGM perspective, when a wave packet scatters with other phonons, defects, or boundaries, it gives rise to thermal resistance; thus all PGM based methods essentially predict the frequency and probability of the scattering events between phonons. These scattering events create and eliminate phonons [1]. However, these methods disregard the phonon interactions that occur between the phonon generation and its annihilation. In fact, in one single wave packet, all the phonons in this wave packet oscillate and remain together. The continuous interactions between these phonons allow the wave packet to contribute to the heat flow. In the extreme case, a single phonon cannot generate a temperature gradient, because the amplitude of a single phonon is identical everywhere in a material and the amplitude is proportional to the local temperature. In the GK paradigm, how long the phonon stays or correlates together is proportional to the thermal conductivity. The longer they correlate, the more they contribute to the heat flow. When the wave packet dies down, the correlation abates. GKMA allows us to extract the mode level information out of the total heat current and correlations. Using GKMA, researchers can obtain the mode heat current correlations which illustrate how the two phonons interact with each other. The correlation function between two mode heat currents describe how these two heat current functions resemble at time t and $t+\tau$, as shown in Eq. (2.38). Assuming two phonons are in a wave packet,

when the wave packet moves in space, these two phonons will oscillate together. Hence these two phonons behave similarly (i.e. oscillate in phase), and the correlation between them will be large. On the contrary, when the wave packet fades away, the correlation between these two phonon heat currents will be reduced. In summary, the PGM treats phonons as particles and includes the scattering processes between phonons. The correlation paradigm incorporates information from not only scattering events but also correlating events.

CHAPTER 3

A FEW EXAMPLES OF GKMA APPLICATIONS

In the preceding chapter, the GKMA formulation is introduced and discussed. In this chapter we will demonstrate the applications of GKMA to several amorphous solids and a single polymer chain. GKMA generates accurate thermal conductivity results for all the amorphous solids that we have tested. And we have observed an interesting divergent thermal conductivity on single polythiophene chains and apply GKMA to understand which phonon branch is responsible for the divergence.

To start our investigation, we began with the comparison of GKMA with other existing modal analysis methods based on PGM on the crystalline silicon (c-Si). After we confirmed that the GKMA and PGM based methods agreed well on mode level details for c-Si, we start to apply GKMA on the amorphous silicon (a-Si). The GKMA results on a-Si agree well with experiments, which produce better agreement than A-F method. It validates the feasibility and accuracy of GKMA on disordered materials. As discussed in the previous chapter, for the disordered materials, the PGM based methods are not applicable. Although A-F method is applicable, the GKMA produces better results comparing to the experiments than A-F method, since GKMA includes the anharmonic effects which are not included in the A-F method. To test all temperature dependent functions in GKMA, we apply GKMA on amorphous silica. After we exam the GKMA on amorphous silicon and silica, we apply GKMA on amorphous carbon in which the majority of the modes are not excited at room temperature. As GK with classic MD is not able to eliminate the unexcited modes contributions to the thermal conductivity, the MD

result on amorphous carbon is significantly different from experiments. The good agreement with experiments using GKMA proves that the quantum specific heat correction is accurate enough for the amorphous solids thermal conductivity prediction. In the last section, we show the divergent thermal conductivity that we find in a polymer chain, polythiophene (Pth) and utilize GKMA to identify that two transverse acoustic phonon branches that are responsible for the divergence.

3.1 Crystalline silicon

3.1.1 Mode level comparison with existing modal analysis methods

Before applying GKMA to non-crystalline materials, it is first important to test whether the fundamental postulate the GKMA method is based on, is in fact correct; specifically, to test whether it is true that the individual terms of the sum in Eq. (2.42) correspond to the actual modal contributions to thermal conductivity. To assess this, we compare the interpretation of the GKMA results with other well established methods discussed in Chapter 2 for a crystalline material, namely silicon, since it has been studied extensively [4,5,8]. The MD simulation procedures are described here briefly next. The Tersoff potential [62], as implemented in the Large-scale Atomic/Molecular Massively Parallel Simulator (LAMMPS) [63], was used for all simulations discussed herein and the force routine was modified to include the modal decomposition for GKMA. For crystalline silicon, we used an 8x8x8 supercell (4096 atoms) as a first test and the lattice constant was $5.432\,\mathring{A}$. Using a larger supercell would provide higher resolution and lower frequency phonons, but several studies have shown that a supercell as small as 4096 atoms exhibits similar thermal conductivity to larger supercell [8]. The simulations

employ periodic boundary conditions in all directions and use a 0.5 femtosecond time step. Each simulation begins with equilibration under temperature control using velocity-rescaling (NPT and NVT) method for 100 ps at 300K and 1 atm. After an initial equilibration period, the modal heat current and other modal information are computed at equilibrium in the NVE (microcanonical) ensemble for 10 ns, without temperature control.

Figure 3.1(a) shows the thermal conductivity accumulation for silicon using Eq. (2.42) via the Tersoff potential. The first comparison is the correspondence it exhibits with respect to the accumulation computed from the NMA method using the same potential. The shapes of both the NMA and GKMA accumulations, when using the same potential are almost identical and exhibit the same features. The main difference between the GKMA and NMA accumulations is the contributions from the transverse optical (TO) modes. In the PGM it is impossible for a mode to exhibit a negative contribution to thermal conductivity, and thus the concept of negative thermal conductivity contributions is undefined in the context of the PGM. In the context of GKMA, however, there is nothing that requires the contributions of a given mode to be positive as it is possible for a mode's heat flow to remain correlated with the total heat flow, but be out of phase giving rise to a net negative contribution. Nonetheless, in practice the total thermal conductivity is always positive, as is required by the second law. It is interesting to note though, that for other methods, the TO mode contributions are effectively zero in the context of the PGM, while the GKMA approach ascribes a slightly negative value. Still, there is excellent correspondence between the NMA and GKMA accumulations and also the amount attributed to each polarization. This suggests that the fundamental postulate

of the GKMA formalism is correct as it yields similar modal contributions as the NMA method, which is defined and evaluated independently. It is also worth noting that the accumulation results in Fig. 3.1 are in general agreement with previous work [8] using the environment dependent interatomic potential (EDIP) [64]. It should also be noted that the values reported in Fig. 3.1 are normalized to unity by the total thermal conductivity predicted by each respective method and potential. It is both well known and appreciated that the total values of thermal conductivity predicted by different potentials vary greatly. Nonetheless, it is useful to compare the results of different potentials on a normalized basis, so that one can assess whether or not the relative contributions of different modes are the same. Qualitatively, Fig. 3.1 shows that all three sets of results indicate the same relative contributions, despite the significant disparity in total thermal conductivity. This correspondence serves as additional evidence that Eqs. (2.36) and (2.37) do in fact correspond to the thermal conductivity contributions associated with a given mode.

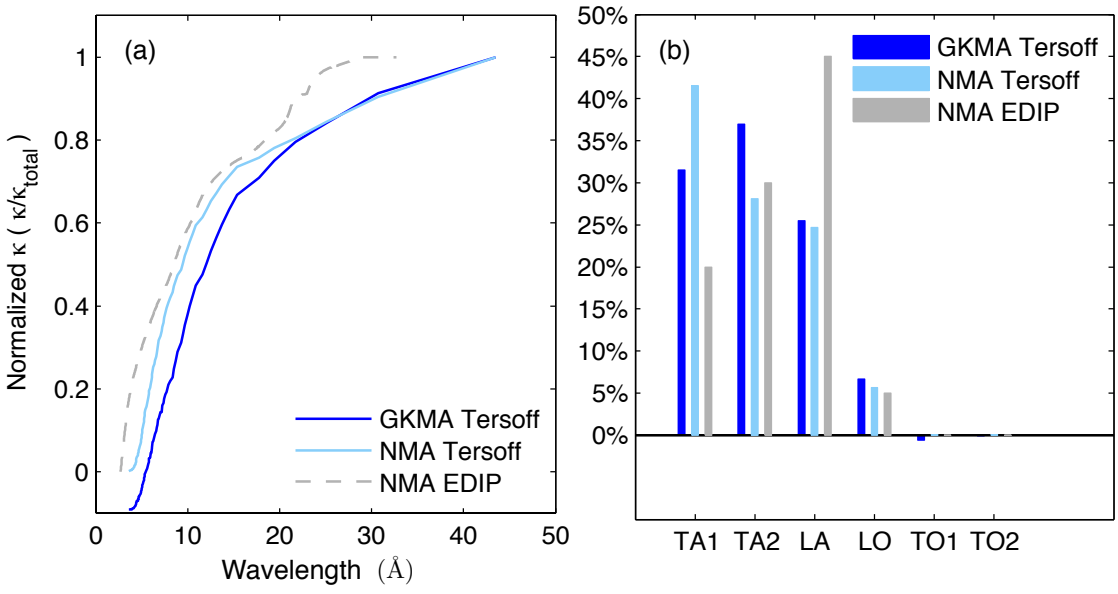

Figure 3.1 (a) Thermal conductivity of c-Si accumulation with wavelength. (b) Comparison of each phonon polarization's contribution to the thermal conductivity of c-Si. The six polarizations

are the transverse acoustic (TA), longitudinal acoustic (LA), transverse optical (TO) and longitudinal optical (LO).

The comparison of NMA and GKMA absolute values of thermal conductivity results are shown in Fig. 3.2. The absolute values calculated from NMA and GKMA using Tersoff potential differ by less than 10%, which is within the statistical variation between individual MD simulations. Furthermore, it should be emphasized that the results for each method only represent one individual trajectory. This comparison further validates the GKMA mode level agreement with NMA for crystalline silicon.

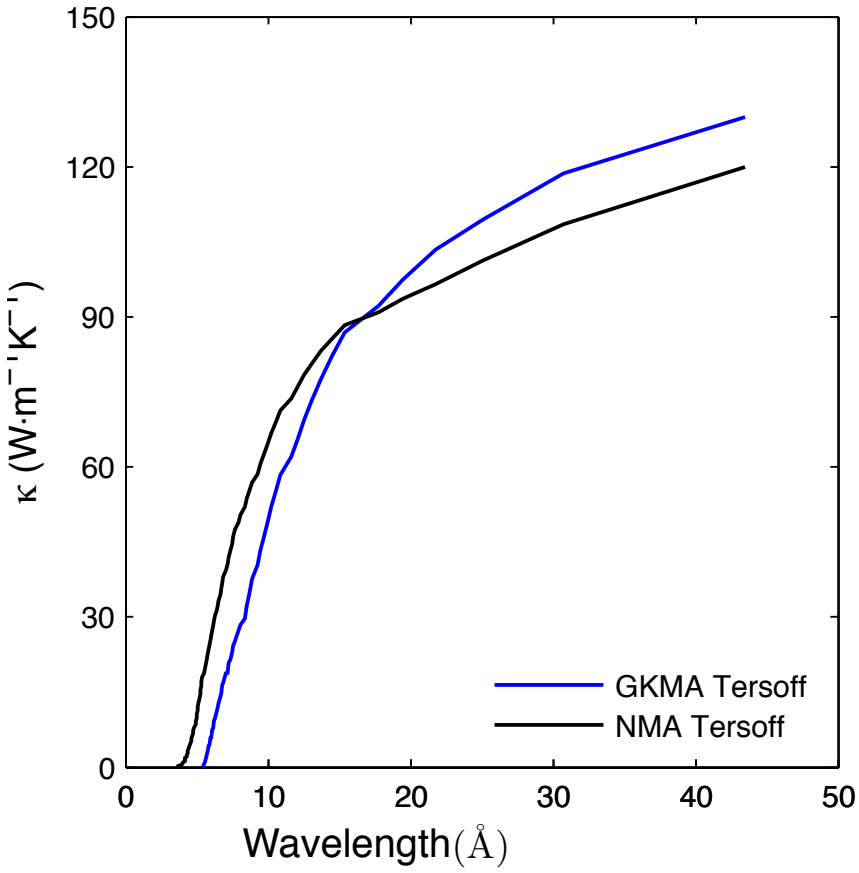

Figure 3.2 Thermal conductivity accumulations vs. wavelength using GKMA and NMA with Tersoff potential for crystalline silicon without normalization.

3.2 Amorphous silicon

After this initial validation, we applied the GKMA method to a-Si, which is a system that cannot be well described by NMA and anharmonic force constant methods. Our calculations used the Tersoff potential [65] with a 4096 atom WWW-generated a-Si structure [66]. The density of a-Si was 2.33 g/cm^3 in all simulations, which is equivalent to the crystalline silicon with lattice constant 5.432 $\mathring{A}$. The details of the a-Si structure generation are discussed in the references [9] and [10]. The inverse participation ratio (IPR) is defined by $\frac{1}{P_n} = \sum_j \left| e_j(n) e_j^*(n) \right|$, where P_n is participation ratio of mode n, j denotes each atom, while $e_j(n)$ is the polarization vector for mode n. Supercell with 4096 atoms, obtained from WWW methods [66] is employed. The initial structures were annealed at 1100K for 10 ns in order to avoid structural meta-stability [68]. The time step of the simulation was 0.25 fs and after 500 ps equilibration with NVT (constant number of atoms, volume and temperature), the modal heat currents were written every 1 fs for 6 ns at equilibrium in the microcanonical ensemble at 300K.

The IPR indicates the extent to which a mode is localized and does not involve all of the atoms in the system as a widespread collective vibration. Propagons and diffusons are delocalized and therefore have small IPR. Locons, on the other hand, are localized vibrations and therefore exhibit high IPR, which in Fig. 3.3(a) manifests at the higher frequencies.

We then applied the GKMA to analyze the modal contributions to thermal conductivity in a-Si for all modes where propagons, diffusons and locons are all treated

the same way via Eq. (2.37). The normalized thermal conductivity accumulation function vs. phonon frequency for a-Si is shown in Fig. 3.3 (c). For comparison, the accumulation from the A-F method is also shown, which was calculated using the implementation in the General Utility Lattice Program (GULP) [69].

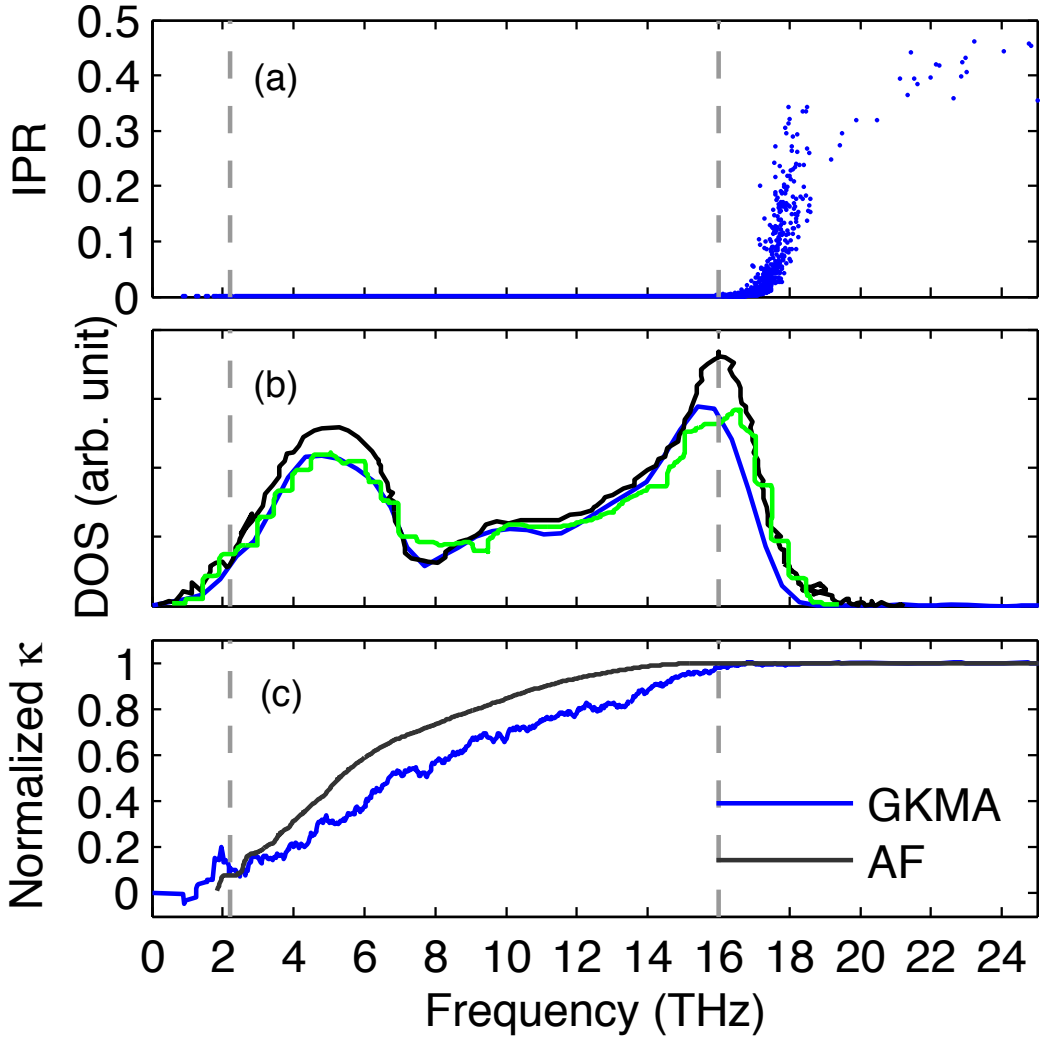

Figure 3.3 (a) Inverse participation ratio of modes in a-Si; (b) Phonon density of states, all three are from lattice dynamics simulation, black curve is from [18] and green curve is from [23]; (c) Normalized thermal conductivity accumulation vs. mode frequency for a-Si at 300K using GKMA and A-F theory at 300K. The dotted gray lines are estimated transition between propagons and diffusons & between diffusons and locons, based on direct inspection of the mode character.

In Fig. 3.3(c), the GKMA result, which includes all degrees of anharmonicity, predicts a similar trend as the A-F result at room temperature, which does not incorporate the effects of anharmonicity on the mode-mode interactions. At first this might seem to suggest that anharmonicity is not important. However, examination of the 2D cross-correlation terms (e.g., Eq. (2.38)) shown in Fig. 3.4, indicates that there is significant correlation between modes with different frequencies. In Fig. 3.4(a) the diagonal terms are the largest, but they only account for ~ 70% of the total thermal conductivity at room temperature. Therefore cross-correlations, which arise due to anharmonicity, are responsible for approximately 30% of the thermal conductivity. What is also remarkable about the result in Fig. 3.4 is the fact that there is a distinct change in the magnitude of the correlations around 16 THz. This transition coincides with the transition to localized modes (e.g., locons – see Fig. 3.4). Here it is important to note that no information regarding the nature of the modes (e.g., propagon, diffuson, or locon) was used to generate Fig. 3. 4. Every mode in Fig. 3.4 was treated the same and no filtering was used to highlight the feature at 16 THz. Instead, a natural feature in the mode-mode correlations arises at the frequency where the mode character switches from spatially delocalized to localized. In Figs. 3.4 (b) and (c) we have filtered out the auto-correlations (cross-correlations only) and cross-correlations (auto-correlations only) respectively to make the features more clear. Figure 3.4 (c) shows that the locons do not have strong auto-correlations and the accumulation in Fig. 3.3 (c) is consistent with previous assertions that locons exhibit a negligibly small contribution to thermal conductivity. One result of the A-F analysis is that the correlations between modes (e.g., interactions) should be most significant when the frequency of two modes is similar. However, using

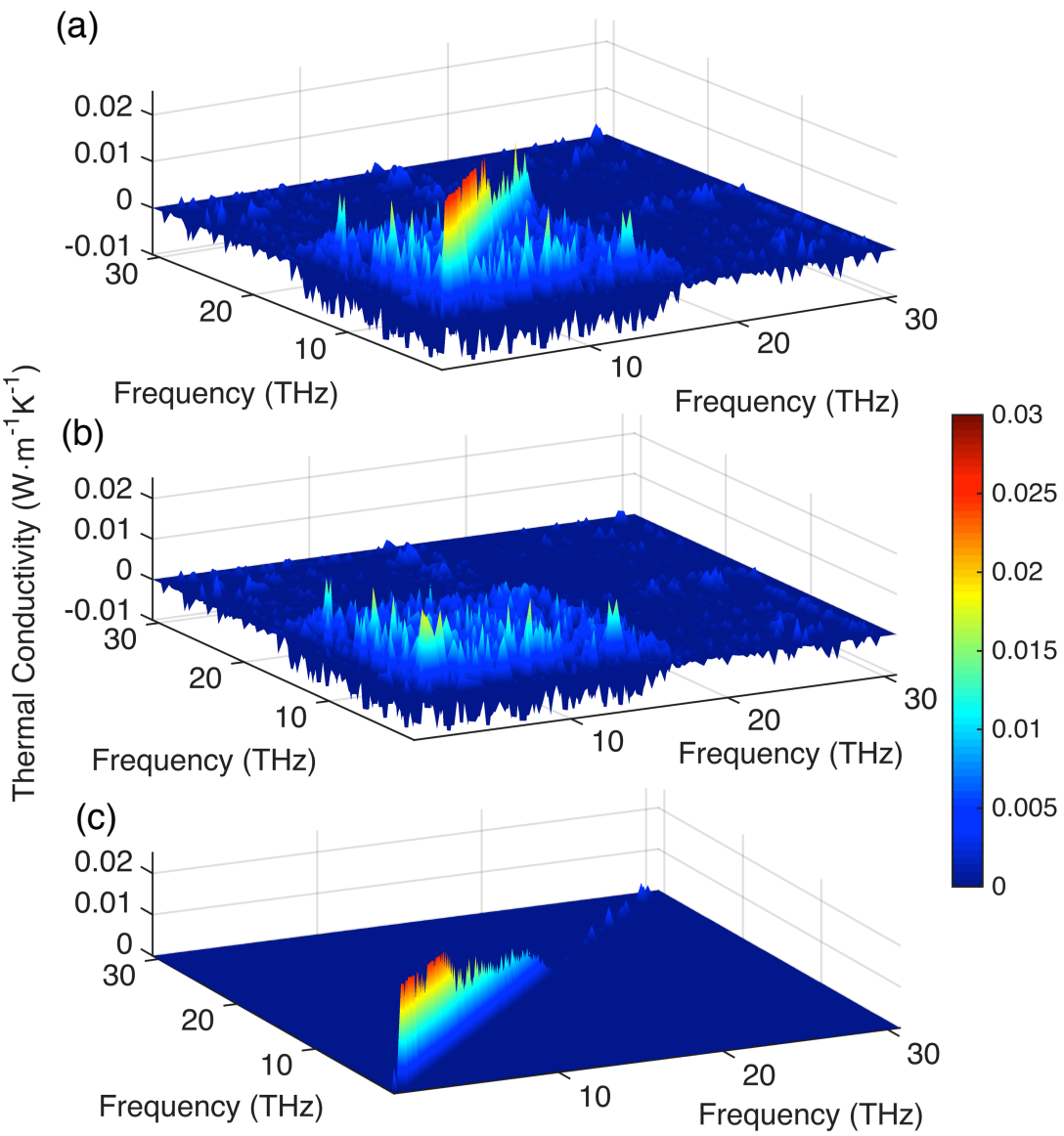

Figure 3.4 (a) Thermal conductivity contributions from mode-mode correlations of amorphous silicon; (b) Thermal conductivity contributions from just mode-mode cross-correlations of amorphous silicon; (c) Thermal conductivity contributions from only mode-mode auto-correlations of amorphous silicon.

the GKMA approach, Fig. 3.4 (b) suggests that interactions between modes of many different frequencies can all interact, as there is no obvious increase as one approaches the diagonal. It is interesting to note, nonetheless, that despite these differences, both GKMA and the A-F model yield a similar normalized accumulation plot (see Fig. 3.3

(c)), even though the total value at 300K predicted by A-F (1.4 W/mK) is ~ 30% lower than GKMA result. The same mapping (2D) of mode-mode correlations for crystalline silicon is presented in Fig. 3.7 for comparison.

In comparing the magnitudes of thermal conductivity values produced by GKMA and the A-F method, the A-F result underestimated the total thermal conductivity of amorphous silicon by 30% at 300K as shown in Fig. 3.5(c) and 3.6. Here the most relevant experimental result is taken to be the measurements of Cahill et al. [70], because it included the minimum hydrogen concentration (1%) and the hydrogen concentration in the simulations is 0%. It is acknowledged that there is a wide spread in the measured thermal conductivities for a-Si [70], but the differences must somehow relate to the underlying structure and composition of the actual samples used. Conceptually, if the atomic level composition and structure were well-known, one can simply construct super-cells that exactly match the experimental structures. If this were possible, the resulting thermal conductivities should match if the theory is correct, and even more importantly the GKMA approach would be able to provide insight on why the thermal conductivity becomes so high in certain cases [61] by elucidating which modes are responsible for the difference.

Since the GKMA method allows us to determine the thermal conductivity accumulation with respect to phonon frequency, we can apply a quantum correction to the classical MD GKMA results at different temperatures and compare to the experimental data [59,70] at all temperatures using Eq. (2.51). As discussed in Chapter 2, since classical MD trajectories do not yield the correct quantum mode amplitudes observed at low temperatures, MD incorrectly predicts shorter relaxation times, due to

artificial interactions with high frequency modes that are actually suppressed. However, in the situations where the phonon-phonon anharmonic interactions are not the primary mechanism governing the low frequency mode thermal conductivity contributions, one would imagine that the error associated with incorrect mode-mode interactions at low temperatures can become negligible. Furthermore, in such a situation, one would expect to achieve good agreement with experimental data, even with interatomic potentials that poorly describe the bulk behavior, such as the Tersoff potential. For example, consider using MD to calculate the temperature dependent thermal conductivity of a silicon nanowire [71–73], where the majority of the phonon contributions are limited by scattering with the boundaries. In such a situation the net relaxation time for most modes is dictated by the nanowire dimensions and not the detailed mode-mode interactions. This is especially the case for the low frequency modes, which are the only modes that remain excited at low temperatures. As a result, in such a situation, one would imagine that application of a quantum heat capacity correction would subsequently lead to good agreement with experimental data.

It is argued here, that the situation for disordered materials is likely the same as the nanowire case, in the sense that another more dominant scattering mechanism, such as impurity scattering [43,74] or structural scattering [12] dominates the contributions of low frequency modes at low temperatures. As a result, one would expect that even a model such as the Tersoff potential, which has been noted to poorly describe the thermal conductivity of crystalline silicon, can be sufficient for describing the behavior in a-Si. Here, we test this assumption by applying a quantum correction to the GKMA results, which only imparts a correction to the specific heat component of each mode's thermal

conductivity contribution via the ratio of the quantum to classical specific heat [1] (See Eq. (2.51)).

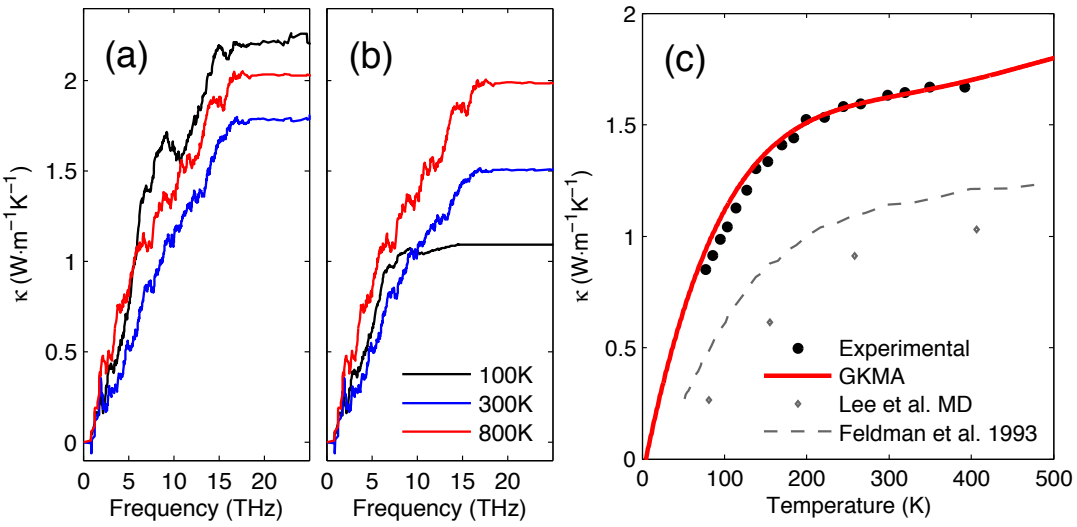

Figure 3.5 Thermal conductivity accumulation of a-Si at 100K, 300K and 800K without (a) and with (a) quantum correction; (c)Thermal conductivity vs. Temperature for a-Si comparing with experiments[70] and simulation results from other methods [21,75].

Figure 3.5(c) shows a comparison of the quantum corrected thermal conductivity using GKMA as compared to experiments, which shows best agreement of all models to date [21,70,75]. The GKMA results in Fig. 3.5(c) were generated by a linear interpolation of the normalized thermal conductivity accumulation functions at 100K, 300K, and 800K. The un-normalized accumulations at each temperature are shown in Fig. 3.5(a) and (b), which indicates that a significant shift in the contributions occurs at lower temperatures. The fact that the non-quantum corrected MD result increases at lower temperatures shows that in order to obtain the correct temperature dependence, the frequency dependence must be obtained from GKMA first, so that the quantum correction can correctly scale each mode's contribution. At lower temperatures, the quantum correction nullifies the higher frequency contributions. However, it is still

important to correctly calculate seemingly over predicted values with MD for the lower frequencies, which when quantum corrected exhibit excellent agreement with the experimental data [70]. This serves as initial evidence that the thermal conductivity contributions from low frequency modes in disordered materials may be more so governed by scattering with the structure itself (or impurities in the case of an alloy), as opposed to pure anharmonic mode-mode interactions.

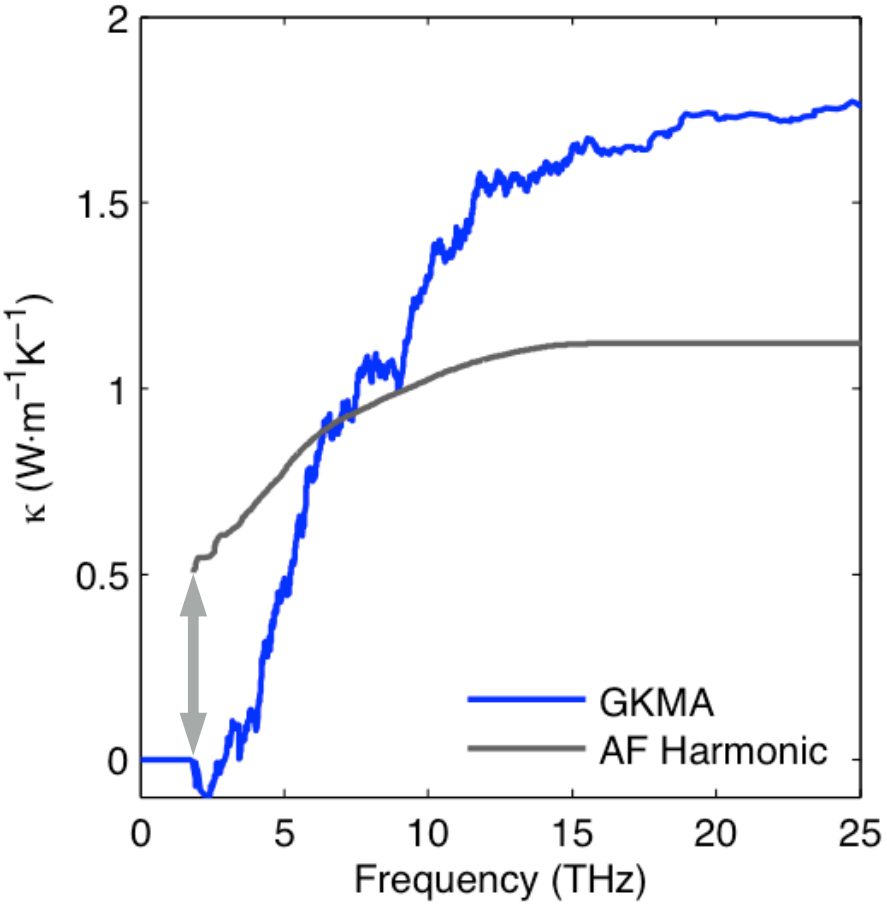

Figure 3.6. Thermal conductivity accumulation with frequency using GKMA and A-F (diffusons) with Tersoff potential for amorphous silicon without normalization. Here, it should be noted that the A-F result is offset by the propagon contribution computed by Larkin and McGaughey [68].

In Fig. 3.6 the magnitude of GKMA and A-F method predicted frequency-dependent thermal conductivity are compared. The A-F result does not start from zero because it includes the contributions from propagons via approximations developed in Larkin and McGaughey's work [68]. Here the propagon contribution is calculated to be 0.5183 W/mK using the implementation in GULP. This implementation requires specification of a cutoff frequency for propagons and then treats the propagons as propagating modes with thermal conductivity contributions described by the PGM. Since they are low frequency modes, similar to acoustic modes, they have a constant velocity and the relaxation times were determined from analytical expression. It is clear that the A-F result is lower from GKMA result and the difference mainly comes from the cross-correlations contribution in GKMA. The A-F result is very close to the auto-correlations from GKMA, which will be discussed this phenomenon in more details in the next chapter, but the cross-terms differ greatly.

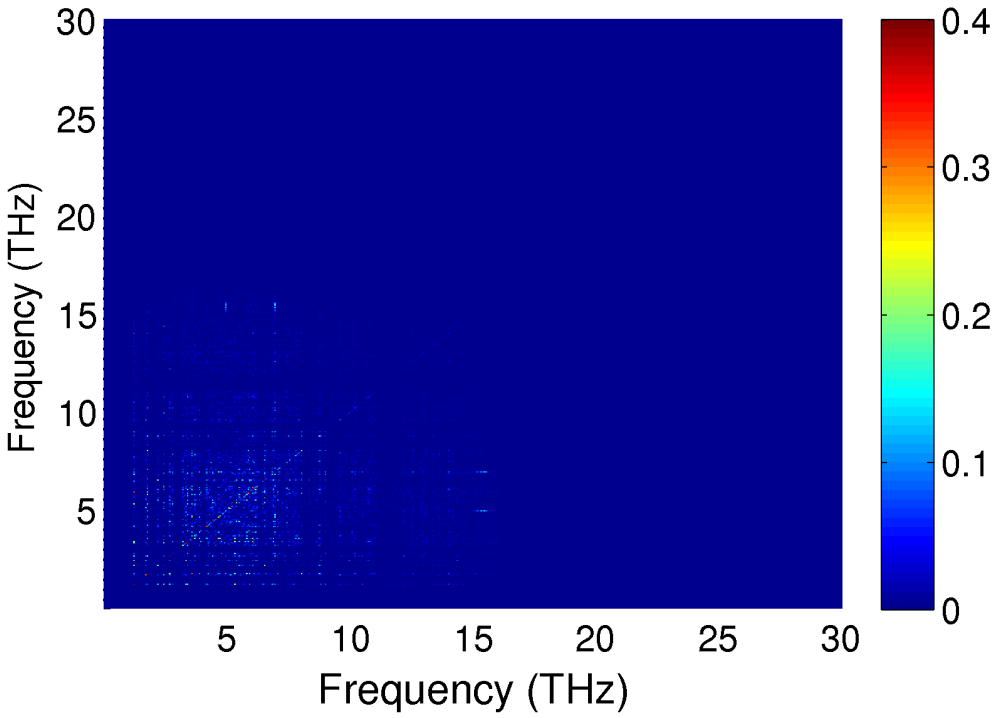

Figure 3.7: Crystalline silicon 2D cross-correlation map

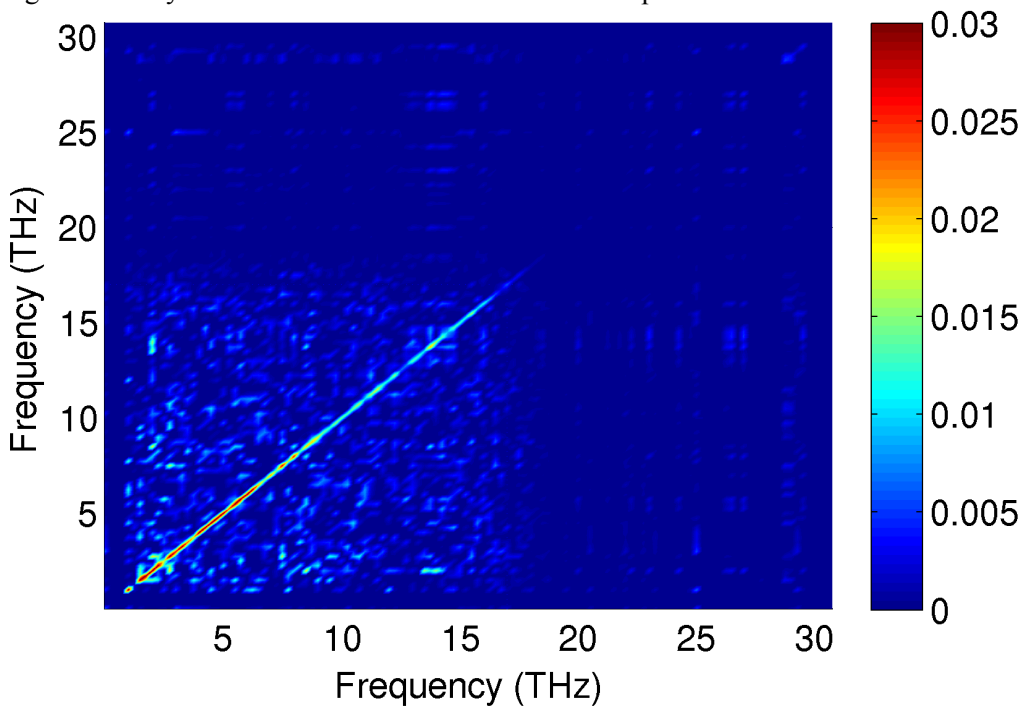

Figure 3.8: Amorphous silicon 2D cross-correlation map

Comparing Fig 3.7 and 3.8, one can observe the major difference of the mode-mode correlations in crystalline vs. amorphous silicon. In Fig. 3.7, as for the crystalline silicon, there are no strong auto-correlations. Instead, there are many mode–mode correlations at different frequencies, especially for the acoustic modes. In Fig. 3.8, there are three differences one can find comparing with crystalline silicon. Firstly, the diagonal terms, which are the auto-correlations, are dominating. Secondly, the off-diagonal terms are not negligible, and there is no clear pattern for the correlations below 16 THz (the cut-off frequency). The third insight is the natural appearance of a band gap between diffusons and locons at around 16 THz as discussed earlier, which implies there is a distinct difference in behavior that accompanies the difference in spatial delocalization.

After the successful application to a-Si using GKMA, one may wonder if it is a coincidence like A-F method on a-Si. We decide to study a few other amorphous solids to further prove the validity of GKMA on disordered materials.

3.3 Amorphous silica

The next amorphous materials we studied using GKMA is silica. Silica is of widespread technological significance and therefore understanding its thermal transport physics is of significant and broad interest. Of particular importance is the fact that the thermal conductivity of amorphous silica (a-SiO_2) increases with temperature beyond room temperature, which is somewhat difficult to explain with MFP based arguments. Furthermore, the model developed by A-F, for example, predicts essentially constant thermal conductivity above 200 K [23] and therefore it is important to examine the role of anharmonicity in the thermal conductivity of a-SiO_2.

Using the GKMA method, we then calculated the modes and their respective contributions to thermal conductivity for a-SiO_2. The atomic interactions between amorphous silica atoms are described by Tersoff potential with parameters published by Munetoh et al. [65]. The a-SiO_2 structure was generated by the melting-quenching method. The detailed procedures for generating a-SiO_2 from crystalline silica have been described by Ong *et al*. [76] using the Tersoff potential. After quenching, the structure was annealed at 1100 K for 10 ns to avoid the meta-stability reported by Larkin *et al*. [68]. After generating the a-SiO_2 structure, we calculated the DOS, and compared with experiments [77]. The agreement is overall reasonable, although there is significant discrepancy at lower frequencies. Nonetheless, Fig. 3.9 shows that even though there is some discrepancy at low frequencies the specific heat as a function of temperature is still well reproduced.

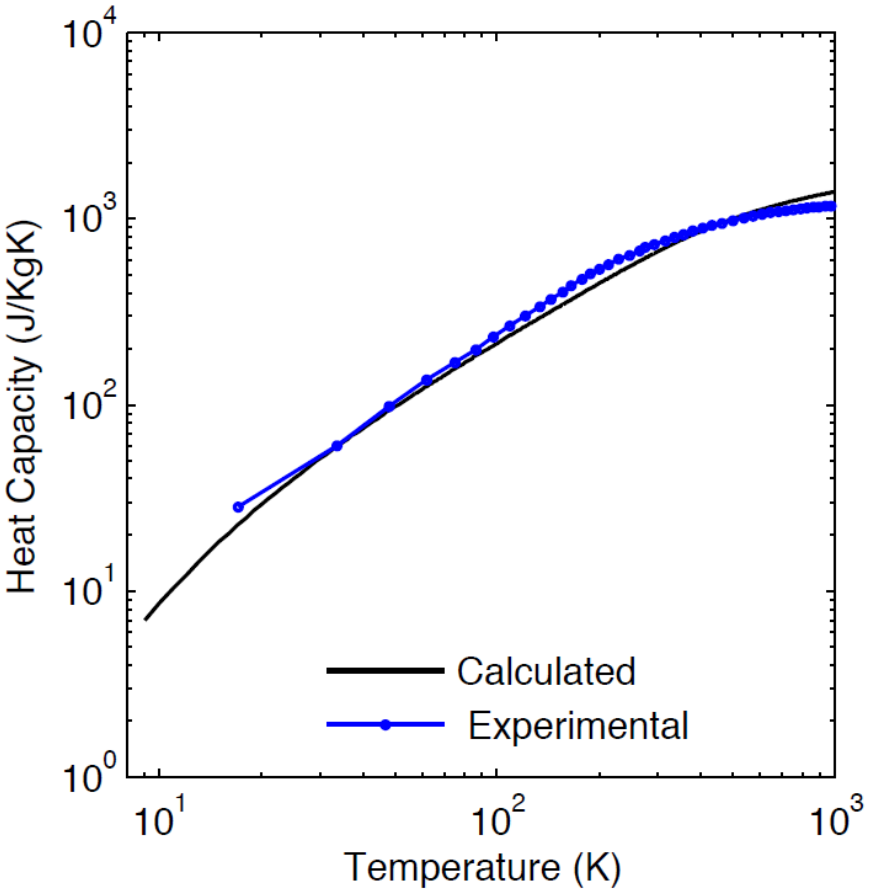

Figure 3.9. Heat capacity of a-SiO_2 from the Tersoff potential, as compared to experimental results [78].

After we obtained the a-SiO_2 structure, we applied SCLD (i.e., at gamma point $k = 0$) for the supercell (4608 atoms) with periodic boundary conditions to obtain the normal mode eigenvalues and eigenvectors which allow one to visualize the normal mode shapes. The SCLD calculations were performed using the GULP [69]. Before SCLD calculation, one needs the relaxed structure, which is computed at 0K with zero pressure. The supercell is approximately cubic has 4608 atoms, with a length of ~ 40.44 $\mathring{A}$. The density for the relaxed structure is 2317 kg/m^3, which is 4% larger than the experimental value 2220 kg/m^3 [79]. The eigenvectors and harmonic frequencies are then obtained using GULP.

Once all the eigenvectors have been calculated, we read them into LAMMPS in order to calculate the mode level thermal conductivity contributions using GKMA. All MD simulations were performed using a time step of 0.1 fs. After equilibration for 100 ps at 300K using NVT, the heat current, and mode heat current were captured for another 2 ns (2 x 10^7 time steps) using NVE. After supplying the eigenvectors once at the beginning of the MD simulation, one is able to obtain the heat current and kinetic energy of each mode. Figure 3.10 shows total heat current auto–correlation function and its integral with time separation. The auto-correlations decay very fast, within 10 ps, as the integral, which is proportional to the thermal conductivity, converges in less than 30 picoseconds. The integral of the heat current autocorrelation function is cut off at 30 ps [80] since the largest relaxation time in the supercell is less than 10 ps. After the modal heat current is computed, the modal thermal conductivity is determined by calculating the correlation between modal heat current and the total heat current.

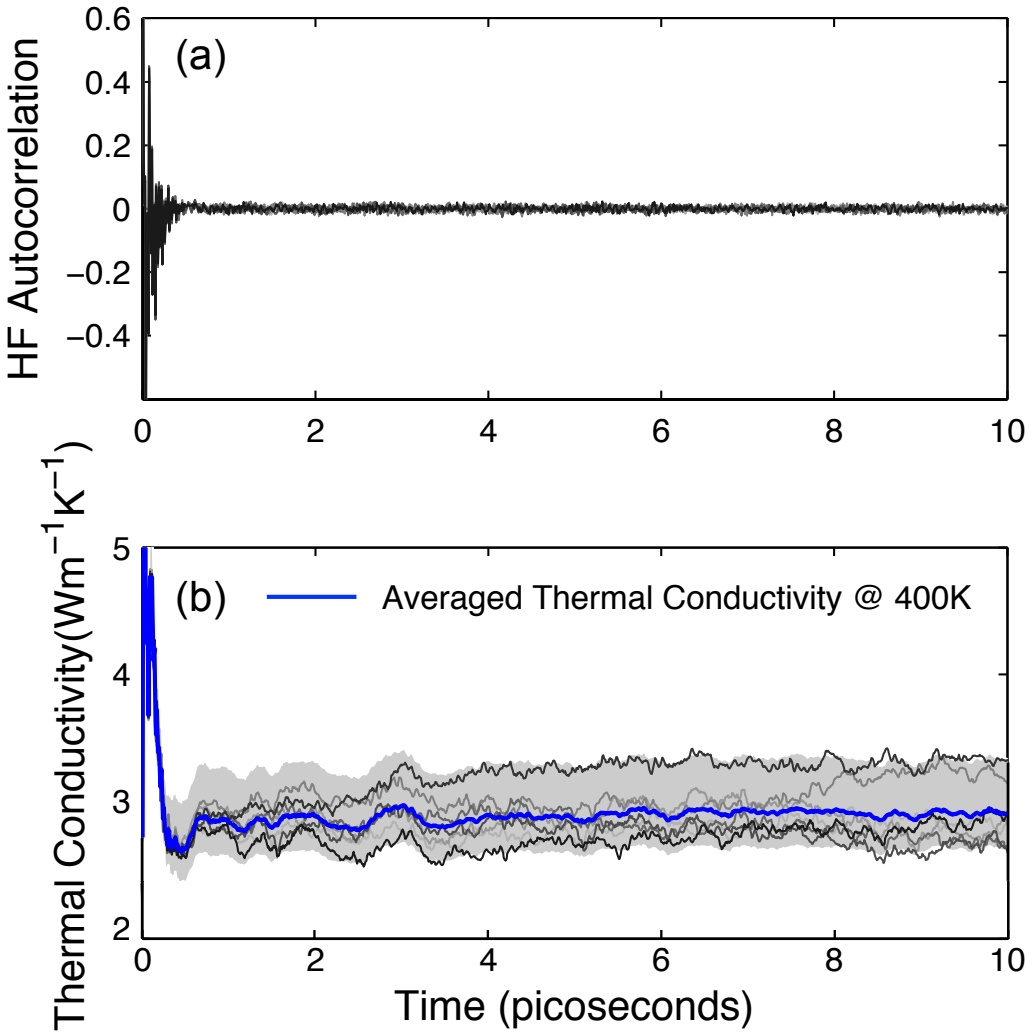

Figure 3.10 (a) Total heat current autocorrelation functions (10 ensembles) and (b) integrations with time (in units of thermal conductivity) at 400K. The blue curve in (b) represents the averaged thermal conductivity from ten ensembles. The individual ensemble results are plotted as the grey curves, the shaded region represents the confidence intervals for the ensemble averaging. The width of the interval indicates the degree of certainty (12%).

There are a few schemes to reduce the computational cost of GKMA as discussed in Chapter 2. The first way is to combine a group of modes together. Without calculating individual mode heat currents separately, one can combine a group of mode's contributions to the velocity of a given atom together and then substitute it into the heat current operator. Next, one can sum of a group of n modes' heat current once instead of as n separate individual contributions. Mathematically, the correlation between

combined mode heat currents and the total heat current is exactly equal to the sum of all of the correlations between individual heat currents and the total heat current. The only difference this combination scheme will make is on the specific heat correction. We have to take the averaged frequency of the combined modes in one interval to calculate the specific heat suppression. Here, the frequency interval we used is ~ 0.15 THz, which is small enough to have negligible effect to the final system thermal conductivity. We have tested that when using smaller frequency interval, the GKMA results do not change.

Another scheme is to reduce the frequency of the mode heat current calculations. Although the simulation time step is 0.1 fs for a-SiO_2, we do not need to calculate mode heat current at every time step. When the heat current is calculated every 5 fs, we observed no difference in thermal conductivity as compared to when a smaller time step was used. This then reduces the cost associated with the GKMA portion of the simulation itself, 50X lower. In order to efficiently conduct the calculation, we parallelized the algorithm of calculating the heat current, mode heat current and mode kinetic energy by implementing the algorithm in the force-routine of the Tersoff potential in LAMMPS [63].

The IPR and phonon density of states are shown in Fig. 3.11 (a) and (b). The IPR quantifies the extent of localization for a given mode [18]. The color-shaded regions in Fig. 3.11(b) represent the quantum specific heat suppression function multiplied by the DOS, $\mathrm{DOS}(\omega)\cdot\frac{\mathrm{C}(\omega)_{\mathrm{q}}}{\mathrm{C}(\omega)_{\mathrm{m}}}$ at three temperatures (100K, 400K, and 800K). Since the classical limit for the volumetric specific heat is constant, the area under the black DOS curve is proportional to the specific heat in the Dulong-Petit limit [81] which is

equivalent to the statement that the volumetric specific heat per mode is k_B / V. The areas of color-shaded zones denote the quantum specific heat at the three temperatures. As the temperature increases, there are continuously more modes excited above their ground states, such that they can contribute to the specific heat. Once this happens, these modes start to contribute to thermal conductivity and as a result, the thermal conductivity of a-SiO_2 continuously increases from 10K to 1200K. Figure 3.11 (c) shows the thermal conductivity accumulation with frequency at different temperatures. The accumulations above 400K are very similar, which indicates that the anharmonic effects do not drastically change the mode-mode interactions above 400K. The increase in thermal conductivity above 400K is mainly due to more diffusons and locons starting to become excited above their ground state after which they are able to contribute to the thermal conductivity.

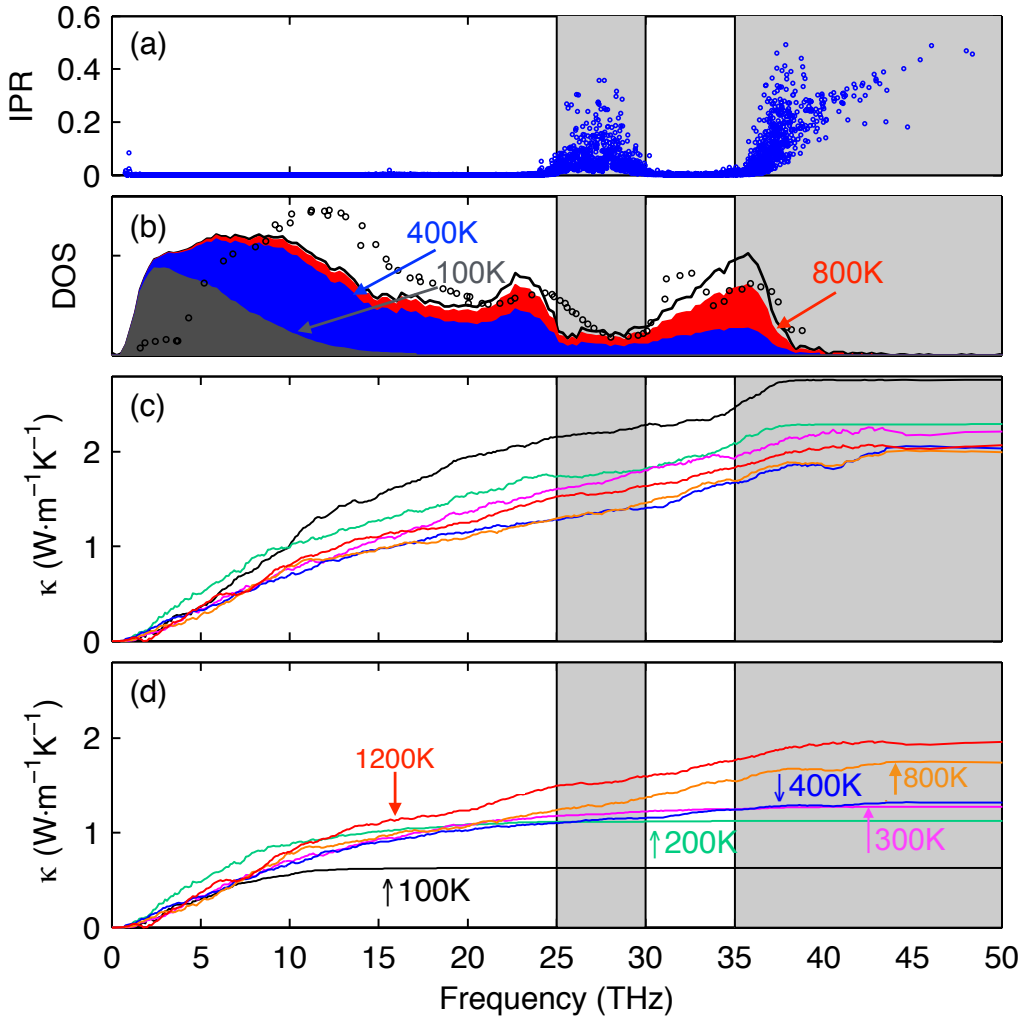

Figure 3.11. (a) IPR of modes in a-SiO_2; (b) Phonon density of states (solid line) and experimental results (black circles) [82]. The three color-shaded areas demonstrate how Bose-Einstein statistics suppress the heat capacity associated with certain modes, which was calculated by multiplying the quantum correction ($\frac{C_q}{C_m}$) times density of states. The red, blue and gray regions represent 800K, 400K, and 100K respectively and the suppression is significant for 100K; (c) thermal conductivity accumulation vs. mode frequency for a-SiO_2 using GKMA at different temperatures (100K, 200K, 400K, 800K, 1200K) without the quantum specific heat correction; (d) with quantum specific heat correction. The gray shaded areas represent locons.

Figure 3.11 (c) and (d) shows the thermal conductivity accumulation vs. frequency before and after quantum specific heat corrections at five different temperatures for a-SiO_2. Figure 3.12 shows how the predictions improve, as more accurate temperature dependent information is included. Initially the thermal conductivity

is calculated directly from classical MD, and as expected, the temperature dependence qualitatively differs from the experimental data [59] as shown in Fig. 3.12 (a). The data in Fig. 3.12 (a) corresponds to evaluating Eq. (2.35) and setting $f_Q = 1$ for all modes, and it should be noted that we averaged over 10 ensembles for each data point in Fig. 3.12 (a) for the GK calculation. However, after the quantum specific heat correction is applied to GKMA results, the overall experimental trend is obtained, but the results still differ significantly if only the GKMA accumulation is used for a single temperature (i.e., 400K). Figure 3.11 (b) corresponds to evaluating Eq. (2.35) with f_Q equal to the quantum to classical specific heat ratio, but the temperature dependence of both f_κ and ω is neglected, as we have only used the values of f_κ at 400K from GKMA and harmonic frequencies ω_0 at 0K from LD. In reality, the accumulation, which is obtained from the thermal conductivity contributions f_κ, itself is a function of temperature, as indicated by Fig 3.11 (c). The accumulation, however, only exhibits moderate temperature dependence, which can be roughly approximated by linear interpolation at a few key temperatures. Thus, once the quantum correction (Q) and the accumulation (κ) temperature dependence are applied, the agreement with experiments improves significantly. We then correct for the temperature dependence of the phonon frequencies (ω) themselves (e.g., softening),

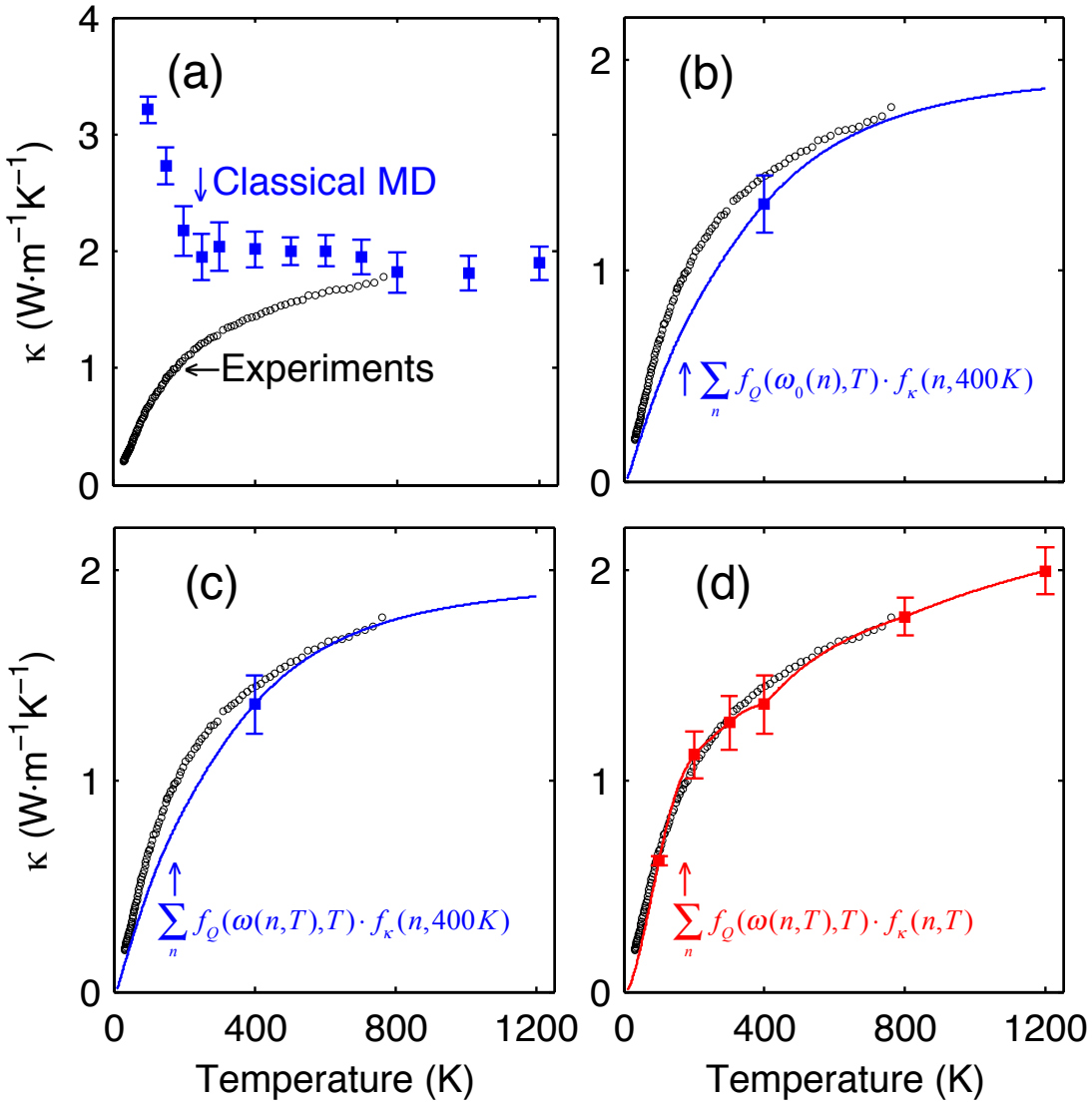

Figure 3.12 (a) shows the GK results with error bars comparing with experiments (black circles). The error bars correspond to the standard deviations observed for independent ensembles; (b) is the result of using 400K GKMA data with quantum specific heat correction; (c) is based on the results in (b) with the addition of temperature dependent frequencies at 400K; (d) shows the thermal conductivity using GKMA results at 100K, 200K, 300K, 400K, 800K and 1200K (interpolated in between) with the quantum specific heat correction and temperature dependent frequencies.

which can be determined from a Fourier transform of each mode's kinetic energy [45]. This softening tends to shift the frequencies lower by ~ 10% at 800K and 6% at 400K, which is important, because the quantum correction is sensitive to the mode frequencies. In Fig 3.12 (c), the thermal conductivity predictions shift slightly to the left, once the

frequency softening $\omega(n,T)$ is incorporated into the calculations. In Fig. 3.12, we have used the subscripts Q, κ, and ω to denote the quantum specific heat temperature dependence, thermal conductivity accumulation temperature dependence and mode frequency dependence respectively. GKMA [16] fully includes anharmonicity resulting in different quantitative predictions than the A-F method, which computes the mode diffusivity based on harmonic approximation [25] and assumes the mode diffusivity is not temperature dependent. Instead of using temperature independent thermal diffusivity, we have interpolated the values at several temperatures to incorporate the temperature dependence of f_κ.

After all the temperature dependence and interpolations have been accounted for, the magnitude and trend of the temperature dependent thermal conductivity exhibits excellent agreement with experiments as shown in Fig. 3.12 (d). We thus recommend that all three-temperature dependencies should be included to obtain the most accurate predictions using Eq. (2.49). In Fig. 3.11, we have included the uncertainty associated with sampling a limited number of ensembles, which is given as the standard deviation of the GK results at that temperature.

As discussed in the Chapter 2, researchers [41] have shown that applying quantum specific corrections to crystalline materials is not in general rigorously correct, because the coupling between modes is dependent on their respective amplitudes. However, we argue that for amorphous materials, this effect is negligible only the quantum correction on specific heat is needed to reproduce experiments properly.

Because the quantum effect on "scattering rates" is negligible for amorphous materials. Furthermore, by applying the quantum correction to the 2D mapping of mode-mode

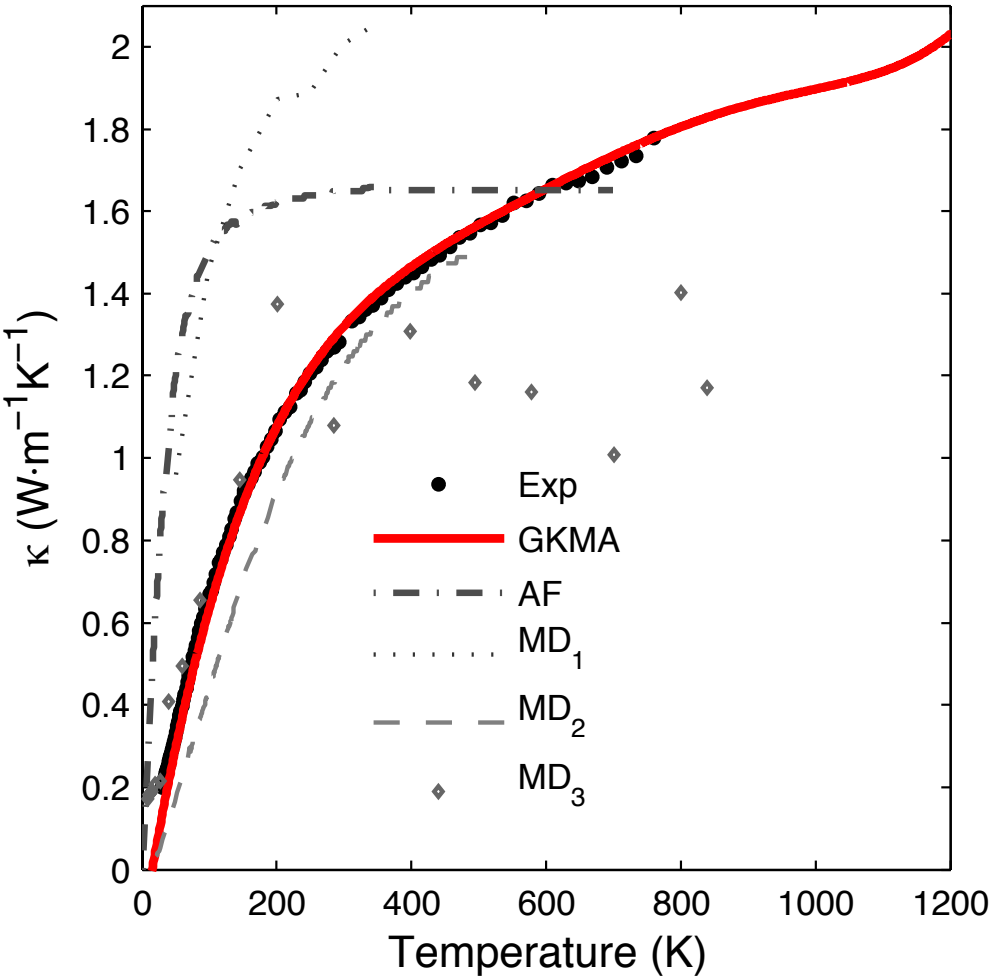

Figure 3.13 Thermal conductivity of a-SiO_2 vs. temperature as compared to other models and experiments: The red curve is the temperature dependent thermal conductivity of a-SiO_2 from GKMA calculations with error bars showing the standard deviation between independent simulations, the experimental results (black circles) are from reference [27], A-F is Allen-Feldman theory prediction from reference [23] using Beest-Kramer–van Santen (BKS) potential [83,84], MD_1 is a non-equilibrium molecular dynamics simulation result from Shenogin *et al.* [23], MD_2 is the MD result with quantum corrections from Jund and Jullien [85].

correlations (see Eq. (2.38)), we eliminate the effects of high frequency and low frequency mode interactions, as they would manifest in the heat current correlation contributions. This in essence eliminates the effect that high frequency modes have on

low frequency modes, which is incorrectly included in a classical MD simulation. Comparing with other methods, GKMA demonstrates much better agreement with experiments for a-SiO_2, as shown in Fig 3.13, which derives from the more complete inclusion of the mode dependence, anharmonicity and its temperature dependence.

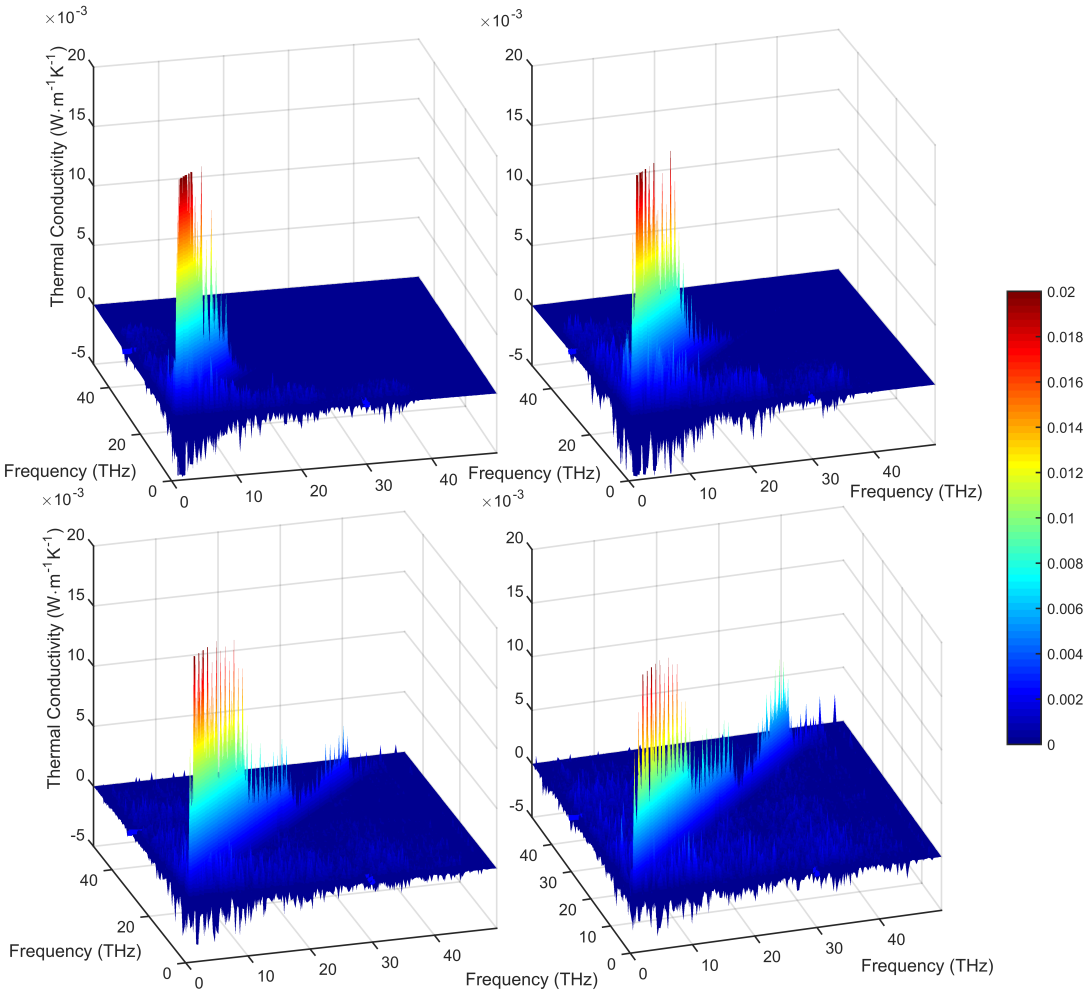

Figure 3.14. (a) Cross-correlation map of thermal conductivity contributions including the quantum specific heat correction. The values are determined from the mode-mode cross-correlations for a-SiO_2 at 100K, (b) at 200K, (c) at 400K and (d) at 800K.

Using Eq. (2.38), one can calculate the mode-mode correlations as shown in Fig. 3.14. Using the summation of all correlation functions between pairs of modes $\sum_{n}^{3N}\sum_{n'}^{3N}\kappa(n,n')$, the resulting sum yields the Green-Kubo thermal conductivity at the simulated temperature, which represents the total integrated volume of the 3D map in Fig. 3.14.

In this section, we applied the GKMA method to a-SiO_2 and have incorporated three sources of temperature dependence. Our results indicate that in order to obtain the accurate predictions, one should incorporate a quantum correction on the heat capacity, the temperature dependence of the GKMA thermal conductivity contributions as well as the softening of the mode frequencies themselves. With these effects included, we have demonstrated the best agreement with experiments to date, as compared to all previous models.

3.4 Amorphous carbon

For the above two amorphous solids, we found good agreement with experiments. In order to further validate GKMA, we choose third amorphous solids to study, which is the amorphous carbon. Amorphous carbon (a-C), also known as diamond-like carbon (DLC), have been widely applied as solid lubricants, protective coatings, and wear-resistant coatings [86–88]. Prior work has measured the thermal conductivity of a-C layers [60,89], but the phonons that are responsible for its thermal conductivity have not been studied, which would highlight any potential pathways towards increasing it.

What makes a-C more interesting is that the MD simulations predict the thermal conductivity of a-C to be very high (> 10 W $m^{-1} K^{-1}$) at room temperature, which is inconsistent with the experiments (~ 3 W $m^{-1} K^{-1}$). This is because at room temperature only 36% of the phonons in a-C are actually excited above the ground state, and classical MD is unable to incorporate the quantum effect on the heat capacity of phonons, it is possible that this issue is the primary source of the discrepancy between MD-GK and experiments. This discrepancy can be resolved if one uses GKMA to calculate the contributions of different phonons made to the thermal conductivity as a function of phonon frequency, and apply a quantum correction to the phonon/normal mode heat capacities to obtain reduced contributions for the many modes that are not fully excited, thereby resulting in a reduced thermal conductivity that will agree properly with experiments.

Furthermore, using GKMA, one can also find out the dominant phonons in a-C. As discussed in Chapter 1, in amorphous materials, the normal modes of vibrations, (e.g., phonons), are differentiated into three categories, namely propagons, diffusons and locons [40,90]. Propagons and diffusons are both delocalized modes, [21,90] but only propagons exhibit spatially periodic repeating vibrations that correspond to that of a propagating mode. Diffusons, however, do not propagate, since there is almost no spatial periodicity in their vibrations. Whether propagons or diffusons contribute more to the thermal conductivity can now be answered using GKMA results.

EMD simulations were performed using LAMMPS [63]. The a-C structure is generated using a melt-quenching method as described by Li et al. [91] and we used the modified Tersoff potential [62] proposed by Sha et al. [92] that has been tested to

accurately reproduce the mechanical properties of DLC and DLCH (hydrogenated diamond-like carbon). In order to offer the most fair comparison with the experimental results, we used a DLC structure with a density of 3.0 g/cm^3, which is identical the DLC measured in the experiments [60]. This is important, because the thermal conductivity of a-C is known to depend strongly on the density, which ultimately determines the sp2/sp3 bonding ratio (e.g., graphite/diamond like bonding). After quenching the structure to the desired density (3.0 g/cm^3), we relaxed the structure first using a NVT for 500 picoseconds. After equilibration, all simulations are run with 0.25 fs time-step under NVE ensemble for 5 ns to collect sufficient statistics for the thermal conductivity computation. The total heat current and mode heat current are calculated every 5 fs to save computational time, and it was verified that the total thermal conductivity does not change with the frequency of the heat current calculations (i.e., outputting the heat current every 5 fs yields the same answer as every 0.25 fs). The LD calculations were conducted in GULP [69], which resulted in the eigenvectors and frequencies.

Figure 3.15 (a) shows the IPR of modes in a-C at different frequencies [16,40], which highlights the third category of modes, which are locons. Locons are localized modes that typically occur at high frequencies, as one can see that the transition between diffusons and locons occurs around 70 THz. Since the locons are not excited at room temperature, they are unable to contribute to the thermal conductivity. Figure 3.15(b) shows the calculated density of states for a-C and Fig. 3.15(c) shows the thermal conductivity accumulation with and without the heat capacity quantum correction at room temperature (300K). Due to the stiff bonds and light mass of carbon atoms, the frequencies in a-C are high. Consequently, Figs. 3.15(b) and (c), show that only a small

fraction of the modes (< 36%) can contribute to the thermal conductivity at room temperature.

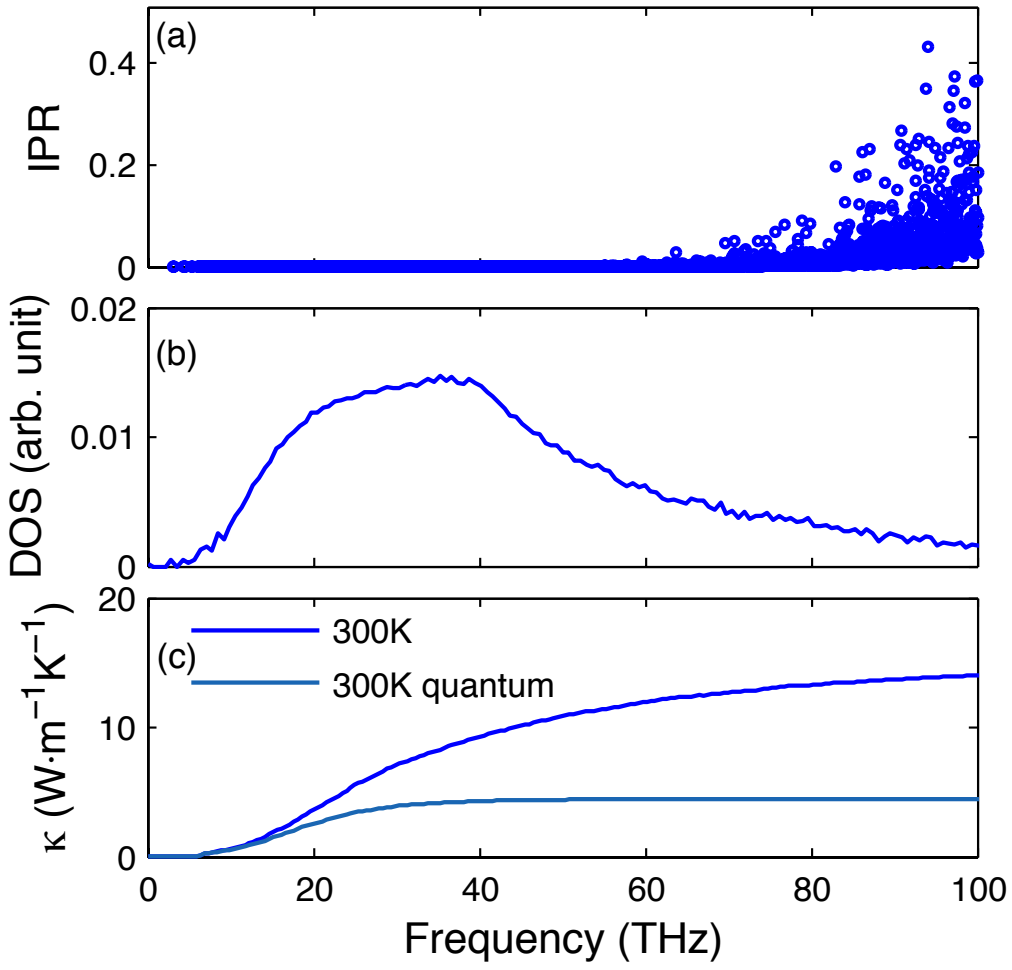

Figure. 3.15 (a) IPR of modes in a-C; (b) Phonon density of states of a-C; (c) thermal conductivity accumulation vs. mode frequency for a-C using GKMA at different temperatures with and without the quantum specific heat correction;

Figure 3.16 shows the relaxation times for low frequency modes (< 40 THz) at multiple temperatures (100K, 200K, 300K), calculated using normal mode analysis [93,94]. The mode relaxation times decay rapidly following a ω^2 trend for the modes below 8 THz. Another interesting observation is that the relaxation times are not strongly temperature dependent, which is different from a-Si and a-SiO_2 [16,93]. In order to

quantify the change in relaxation times with temperature, we compared the ratio of the relaxation times at 300K to 100K for a-C and a-Si. As shown in Figure 3.17 (b), the

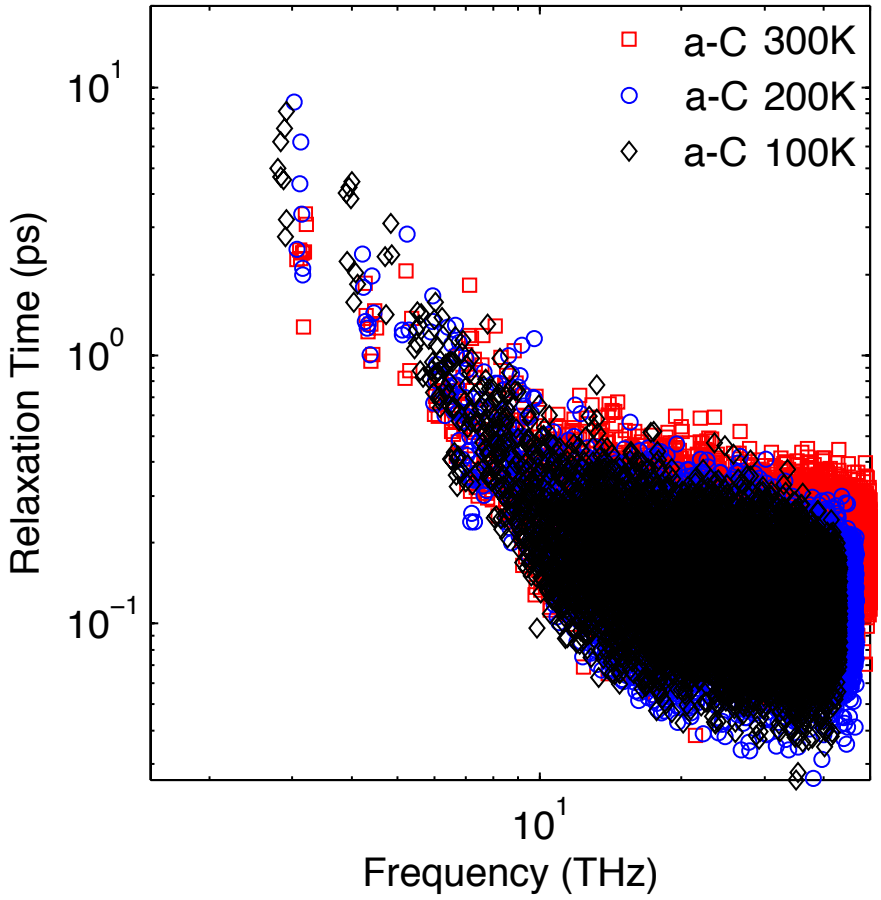

Figure. 3.16 Relaxation time calculated from time-domain normal mode analysis at different temperatures (100K, 200K, 300K) for a-C.

relaxation times reduce from 100K to 300K in a-Si, where on average the values at 300K are ~ 58.8% of their values at 100K. This is due to the increased anharmonicity and interactions with other modes, which reduces the time a mode can remain correlated with itself. However, in Fig. 3.17 (a), the same ratio between relaxation times at 100K and 300K for a-C is on average slightly larger than unity ~ 125%. Given the large spread in the relaxation time ratio, the average serves as only a rough indication of the behavior,

yet it is quite remarkable that on average the relaxation times are roughly equivalent at the two temperatures. Furthermore, even though there is a wide spread in the relaxation time ratios, the average still provides some meaningful perspective since the non-quantum corrected GK thermal conductivity ratios ($\kappa_{100K}/\kappa_{300K}$) for a-Si and a-C are 1.25 and 2.25 respectively. This result is interesting, because it supports the arguments put forth [95] that the relaxation time is not even an appropriate descriptor for describing transport via non-propagating modes. We will discuss this topic in details in the next chapter.

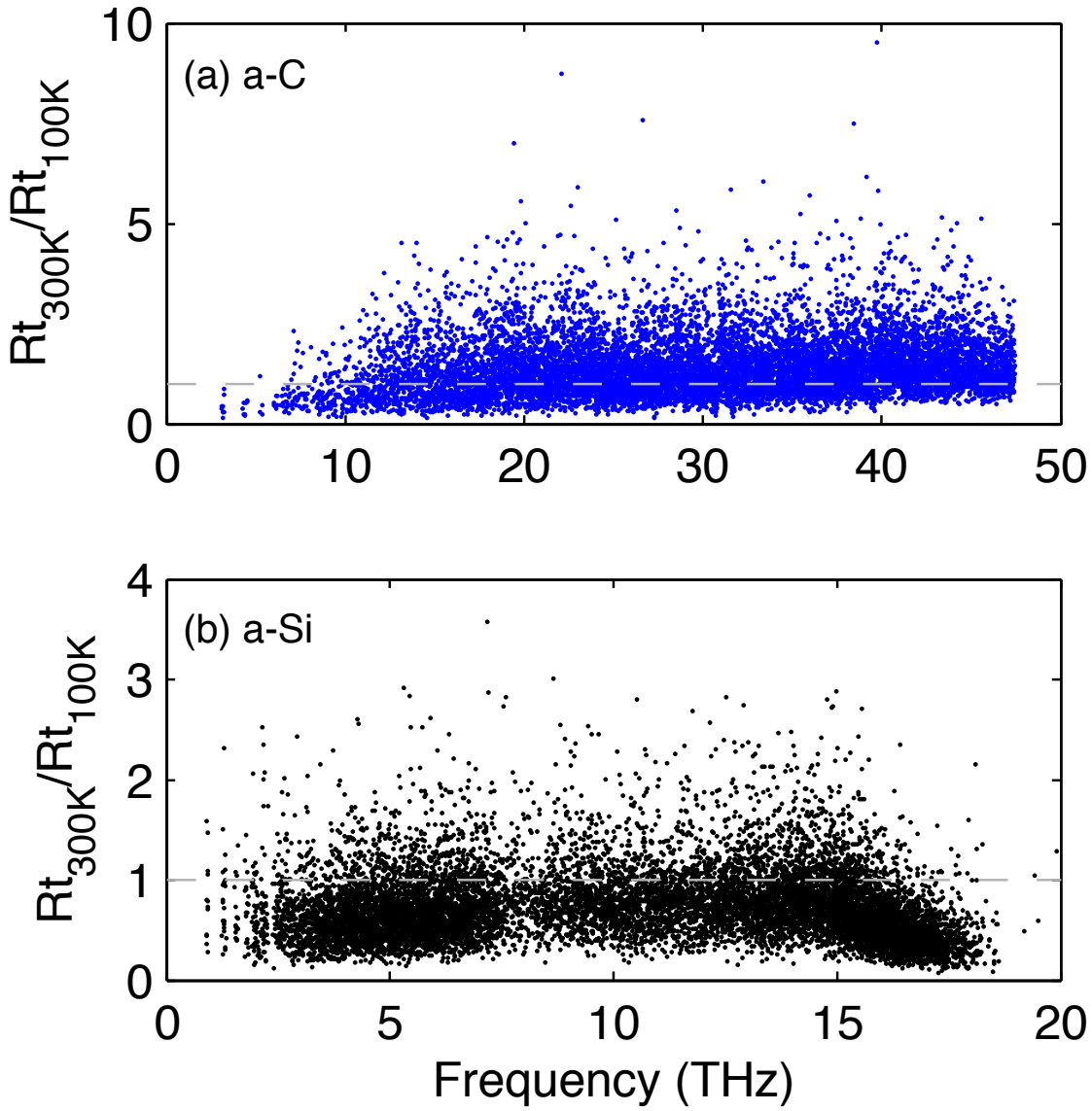

Figure 3.17 The ratio of the relaxation time at 300K over relaxation time at 100K for (a) a-C and (b) a-Si.

Figure 3.18 shows a 3D view of the mode-mode correlations, where the two axes in horizontal plane represent the frequencies of the two modes interacting, while the vertical axis is the magnitude of the correlation between the two modes and represents the thermal conductivity contributions in Fig 3.18. The diagonal elements represent the auto-correlations, which is the dominant contribution for a-C. Interestingly, it is also clear from Fig. 3.15 that it the diffusons between 10-40 THz comprise 70% of the room

temperature thermal conductivity. By inspection of the normal mode shapes, the frequency range where the mode character switches from that of propagons to diffusons occurs around 6 THz. This then suggests that propagons only comprise 13% of the thermal conductivity at room temperature. The result is somewhat counter-intuitive given the fact that room temperature is only 6% of the Debye temperature for a-C, which is close to the regime where many crystals such as silicon experience their peak thermal conductivity where anharmonicity begins to dominate over other scattering mechanisms. The intuition inferred from studying crystalline materials would then suggest that at such a low temperature, the dominant phonons should have low frequencies and long MFPs given the suppression of most other modes. However, the results indicate that unlike a crystalline material, in a-C the lowest frequency modes do not have the highest thermal conductivity contributions on a per mode basis and they do not dominate the thermal conductivity far below the Debye temperature.

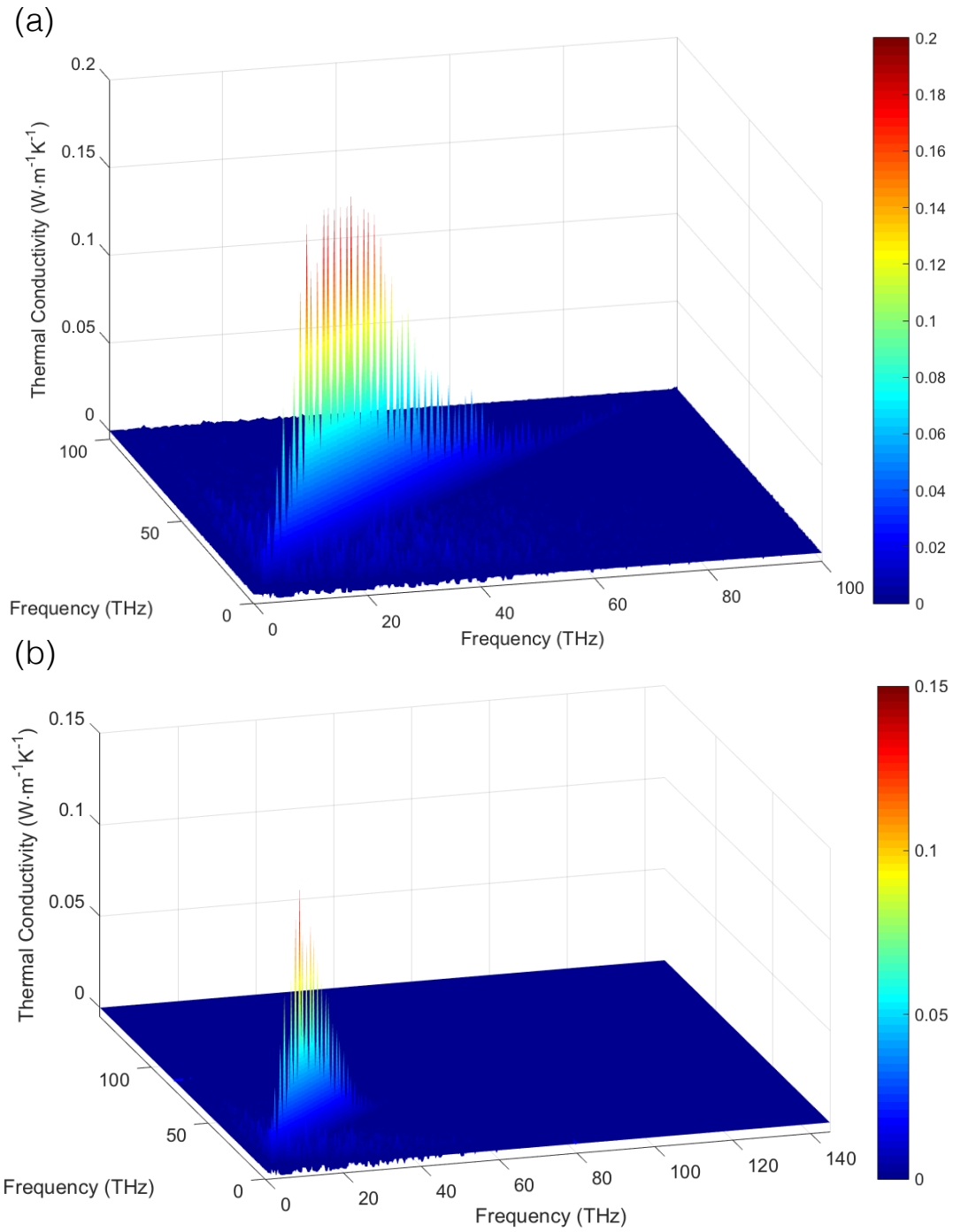

Figure. 3.18 Thermal conductivity contributions from mode-mode correlations with (a) and without (b) quantum correction (300K) of a-C.

Figure 3.19 shows the comparison of GKMA and GK predictions at three different temperatures (100K, 200K, 300K) along with experimental data from Shamsa et al. [60].

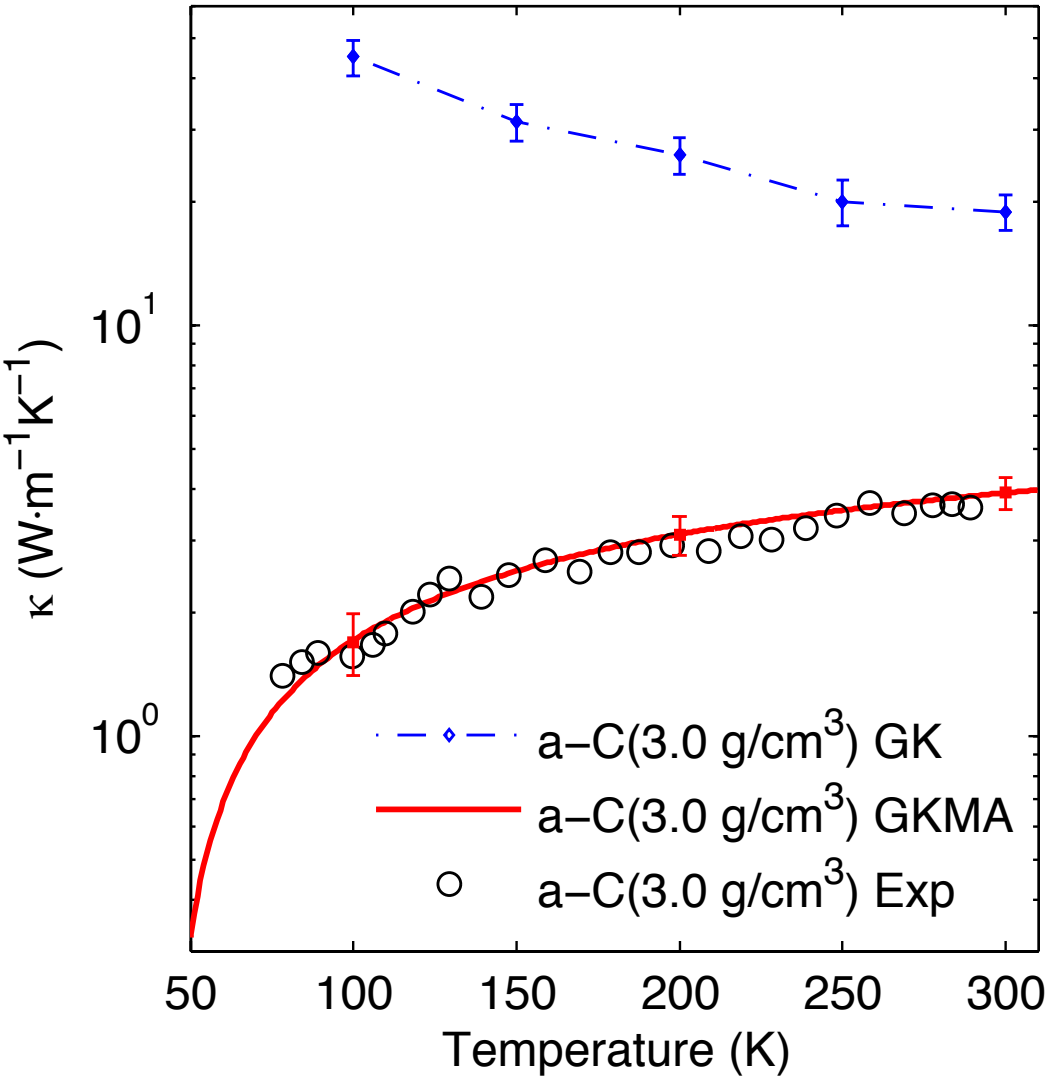

Figure. 3.19 Thermal conductivity vs. Temperature for a-C comparing with experiments [60].

The GK predicted thermal conductivity is much higher than the experimental values and the trend is incorrect. GKMA produces accurate results comparing with experiments. It proves that the mode-mode interactions contained in the classical MD simulations are

meaningful, because the quantum correction on the heat capacity, enabled by GKMA, brings the predictions into excellent agreement with experiments. The data in Fig. 3.18 shows minimal interactions between low and high frequency modes, and thus, the hypothesis that the quantum effect on phonon-phonon interactions is negligible, confirmed by the good agreement obtained by only including the quantum effect on the heat capacity for amorphous materials. At room temperature, more than 60% of the modes in a-C are not excited and therefore cannot contribute to the thermal conductivity and it is quite remarkable that when these contributions are suppressed by the quantum heat capacity correction, the remaining contributions reproduce the experimental values and trend correctly. In sum, the GKMA results on a-C support our earlier claim that the quantum specific heat correction is adequate for thermal conductivity prediction of the amorphous materials.

We have calculated the mode thermal diffusivity contributions at 5 temperatures for amorphous carbon. For the intermediate temperatures, we have also linearly interpolated the mode thermal diffusivity using the data for 100K, 150K, 200K, 250K and 300K. The GKMA results for individual mode diffusivities are then multiplied by the specific heat at the temperature of interest. And we applied the quantum specific heat correction [16] and anharmonic frequency correction [93]. The quantum heat capacity correction factor is the ratio of the specific heat calculated by Bose-Einstein statistics and the classical volumetric specific heat in Eq. (2.50). The predicted thermal conductivity vs. temperature from 0K and 500K is shown below in Figure 3.20.

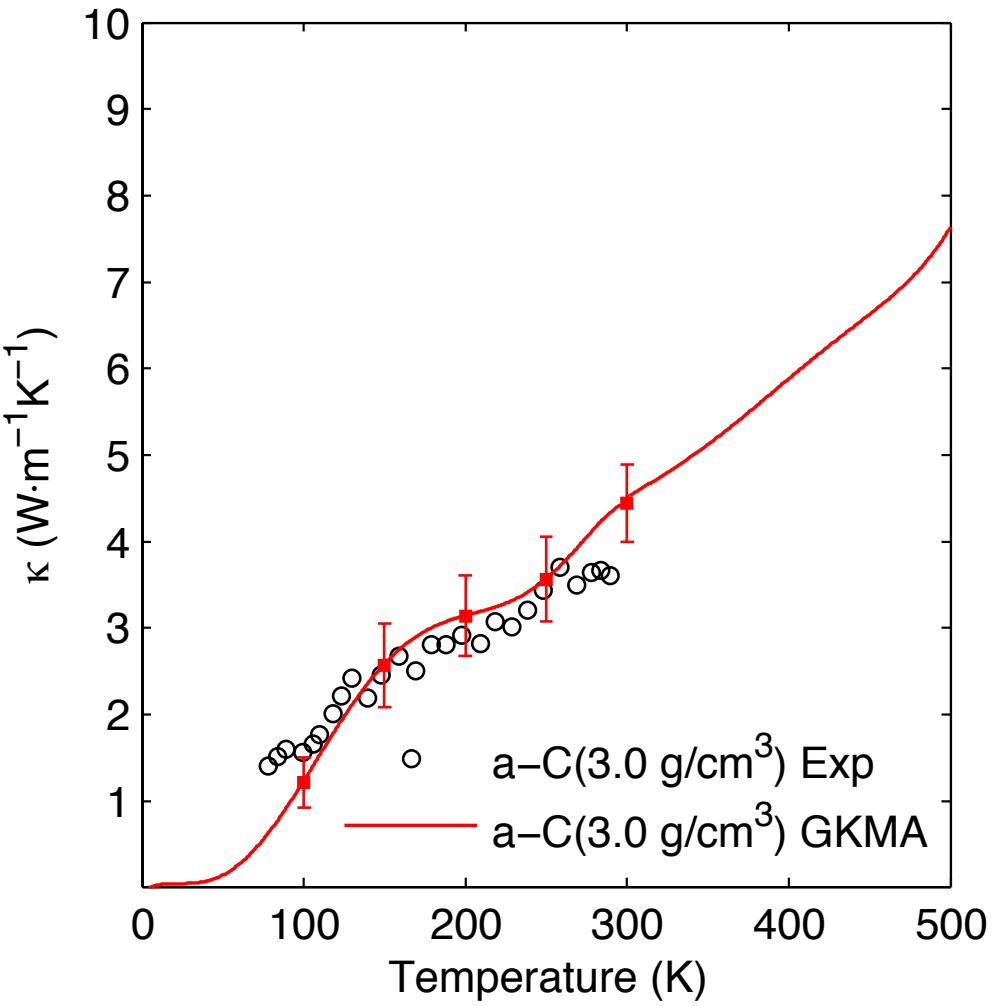

Figure 3.20 The GKMA predicted thermal conductivity for temperature range from 0K to 500K from interpolation between 5 temperature results and extrapolation to 500K, using the accumulation at 300K.

Due to the computational cost associated with GKMA, we have not done ensemble averaging for each simulation as is usually done for normal GK calculations [26,72,96]. However for the amorphous carbon we tested here, the statistical variance of the GK results is small, and from our prior experience studying other amorphous materials, the shape of the thermal conductivity accumulation shows minimal changes with additional ensembles.

In this section, we used GKMA method to study the mode level contributions to the thermal conductivity of a-C, using the Tersoff potential. The phonons in a-C range from 0 to 100 THz and at room temperature (300K) or lower, less than 36% of the modes are excited. As a result, the native GK method over predicts the thermal conductivity by a factor of ~ 3X, but by obtaining the individual mode contributions through GKMA, application of a quantum heat capacity correction suppresses the contributions of high frequency modes, bringing the corrected results into excellent agreement with experiments. The modal analysis also revealed that even though the thermal conductivity of a-C is strongly temperature-dependent the relaxation times are not, and thus it brings into question whether or not relaxation times are useful descriptors for non-propagating mode contributions. Lastly, it was found that, at room temperature, propagons only comprise 13% of the thermal conductivity and thus the majority of the thermal conductivity of a-C comes from diffusons, even though 300K is only 6% of its Debye temperature.

Until now, we studied three amorphous solids (a-Si, a-SiO_2, a-C) using GKMA. The good agreement with experiments for all three indicates the GKMA is the most accurate thermal conductivity calculation methods for amorphous solids so far. The thermal conductivity of another type of materials that has not been fully understood is polymers. As discussed in Chapter 1, single polymer chain has shown divergent thermal conductivity in previous studies, which has not been fully understood. In the next section, we use GK and GKMA to study single polymer chains. The initial GK and GKMA results of single Pth chain are shown. More detailed analyses are discussed in Chapter 4.

3.5 Single polymer chains

1D polymer chains have been studied previously [31–34,97], specifically individual polymer molecules that exhibit divergent thermal conductivity. For polymer chains, Henry and Chen [28] discovered that in a realistic model for the interactions between atoms in a PE chain, it is possible to observe divergent thermal conductivity. The observation entails a direct calculation of the thermal conductivity via EMD simulations with the adaptive intermolecular reactive bond order (AIREBO) potential, which includes anharmonicity to full order.

The divergence is found from the heat flux/current auto-correlation (HFAC) function. The quantity $\left\langle Q_z(t)Q_z(t+t')\right\rangle$ in Eq. 2.2, which is often termed the HFAC, measures the strength of correlation in the atomic motion. For all materials that have been studied using EMD, the HFAC decays with increased time delay t' and the integral of it converges to a finite value. Convergence of Eq. 2.2 with increasing integration time is usually achieved within 500 ps for all previously studied materials at room temperature, including carbon nanotubes [8,24,96,97]. However, even when extended to 5 ns, the thermal conductivity of individual PE chains did not converge and continued increasing [28]. This divergence is associated with non-ergodic behavior, as some aspect of the trajectory repeats in order to remain correlated over such a long period of time.

The previous study by Henry and Chen [31] suggests that the divergence in PE was caused by cross-correlations between mid-frequency longitudinal acoustic modes. In essence they argued that the normal modes do in fact attenuate, however, the mode-mode interactions remain correlated in time, which violates the stosszahlansatz assumption [30]

that underlies the BTE. The BTE treatment for phonons is essentially the PGM. The stosszahlansatz assumption, which was made by Boltzmann during the derivation of the BTE, simplifies the particle collision integral, by assuming each collision is independent of all previous collisions and that successive collisions are not correlated. In the context of phonons, this translates to an assumption that successive phonon scattering events are unrelated, and therefore when one collision occurs there is no effect on subsequent collisions. Henry and Chen [31] introduced a correlation-based paradigm stemming from the GK formula and argued that one cannot use a PGM/BTE (i.e. relaxation time) based formalism to explain the phenomenon, because the stosszahlansatz assumption is violated. This argument was substantiated by estimating the relative contributions of different correlations within the GK formalism, by substituting Q_z with the expression used in the PGM $Q_z = \frac{1}{V}\sum_k \sum_p h\upsilon v_z \delta n(t)$, where v_z is the group velocity along the chain backbone direction and δn is the deviation from the average occupation.

A key shortcoming of the method they employed was that it can only serve as an estimate [31]; summing all correlations does not necessarily reproduce the full GK result exactly and thus it is difficult to quantify precisely which interactions (i.e. correlated scattering events) are most responsible for the divergence. One unresolved question from the study is pinpointing which phonon mode is most responsible for the divergent thermal conductivity. GKMA however is a suitable tool to identify the divergent mode in single polymer chains. Because GKMA can follow the same trajectory in the divergent GK simulation, and the sum of the mode heat current correlation always gives back the GK result.

We use a different potential from AIREBO, namely the reactive force field (ReaxFF) [98]. ReaxFF is similar to AIREBO in that it is a bond order potential. However, the mathematical descriptions differ significantly. ReaxFF is constructed to be as general as possible, capturing all conceivable interactions from covalent terms, columbic interactions, and van der Waals forces. In addition to using a different potential, we choose a different polymer chain to study, single Pth chains.

We use the ReaxFF potential and confirm its utility describing phonon transport in Pth by first computing the thermal conductivity of amorphous Pth as 0.3 ± 0.1 W m^{-1} K^{-1}, which is in reasonable agreement with experiments 0.19 ± 0.02 W m^{-1} K^{-1} [99]. We then proceed to conduct MD simulations of chains with periodic boundary conditions (PBC) to determine whether or not the divergence manifests. The relaxed structure with a 0.796 nm long unit-cell is used as the initial structure. The simulations used here employ PBC along the axial direction of the chain and a 0.15 fs time step, and are run at equilibrium in the NVE ensemble for 20 nanoseconds, with 100 picoseconds of equilibration time. EMD simulations of different numbers of unit cells exhibit interesting results for single Pth chains. More than 80 independent simulations in total are conducted to ensure the divergent cases are not anomalies, but instead occur often enough to be non-negligible in the ensemble average. Although only 20% of cases diverge, if one considers calculation of the ensemble average, the averaged thermal conductivity diverges as a result. We calculate the thermal conductivity for 10, 20, 30, 40, 80, 90, 120, and 150 unit cell chains, with the 30, 90 and 150 unit cell length chains exhibiting divergent thermal conductivity. Similar to Henry and Chen's [28] results for PE, there are some simulations that exhibited clear convergence and others that exhibit clear divergence, with many

cases falling in between these extremes. The only difference between each case is the random initial velocities used. A comparison of example convergent and divergent cases is shown in Fig. 3.21.

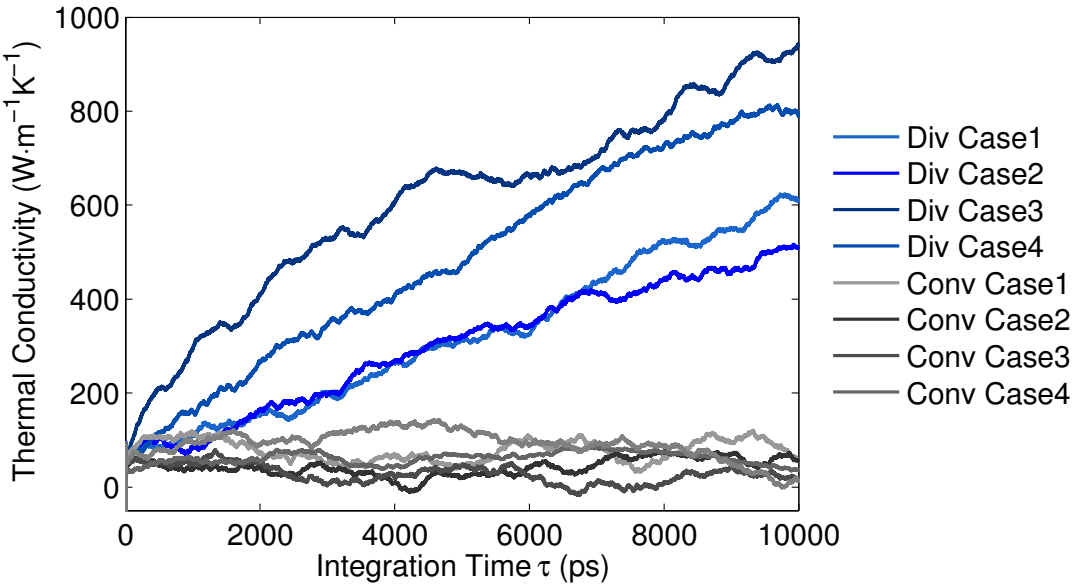

Figure 3.21 Green-Kubo thermal conductivity integrals for individual 30 unit cell long polythiophene chains with periodic boundary conditions

We have carefully examined the energy and momentum conservation as well as the movement of the center of mass during the simulations and have ruled out the possibility that the divergence is due to an aggregated effect of small numerical errors or non-zero bias in the average heat current. Furthermore, no obvious significant difference in the total heat current was observed for convergent vs. divergent results.

In order to pinpoint the mode that is responsible for the divergent thermal conductivity, we used GKMA to conduct modal analysis on a single Pth chain. GKMA is guaranteed to recover the exact value of the total thermal conductivity in GK calculations, and the simulations are based on deterministic dynamics. One can repeat simulations of interest using the same initial conditions and examine the contributions in

increasing levels of detail to maximize computational efficiency. With GKMA we can also calculate the eigenmode contributions to thermal conductivity directly rather than relying on the PGM, whose accuracy is questionable in such systems given the potential violation of the stosszahlansatz assumption. However, calculating mode by mode using GKMA with ReaxFF potential is very expensive; hence we decided to use the partial summation method to reduce the calculation load. After obtaining the eigenvectors from LD calculation, we sum up the entire mode heat currents on the same branch in GKMA. By doing so, the computational expense is reduced significantly. Based on previous studies [31], the modes on the acoustic branches are responsible for most of the lattice thermal conductivity. Hence we study all four acoustic branches individually and sum all the optical branches together. Figure 3.22 shows the thermal conductivity contributions from different phonon branches. Summing the thermal conductivity from the four acoustic branches and the optical branches gives back the exact GK thermal conductivity. In Figure 3.22, we find that the transverse acoustic modes that correspond to vibrations in the plane of the aromatic rings (TA-y) and out of the plane (TA-x) contribute most to the total thermal conductivity in 30 unit cell chains. All other branches contribute negligibly to the total thermal conductivity. Since the correlation function between mode heat current and total heat current is allowed to have a negative value, one would expect both positive *and* negative contributions if the contribution from the branch is oscillating around zero, despite the fact that the total thermal conductivity is always positive. Based on the results from Figure 3.22, we discover that the modes responsible for the divergence of Pth are different than those in PE. The most important branches are two transverse acoustic branches, rather than one longitudinal acoustic branch in the single

PE chain. See Chapter 4 for a discussion about which mode on the transverse acoustic branch is responsible for the divergence, and what causes the divergence to happen in a single polymer chain.

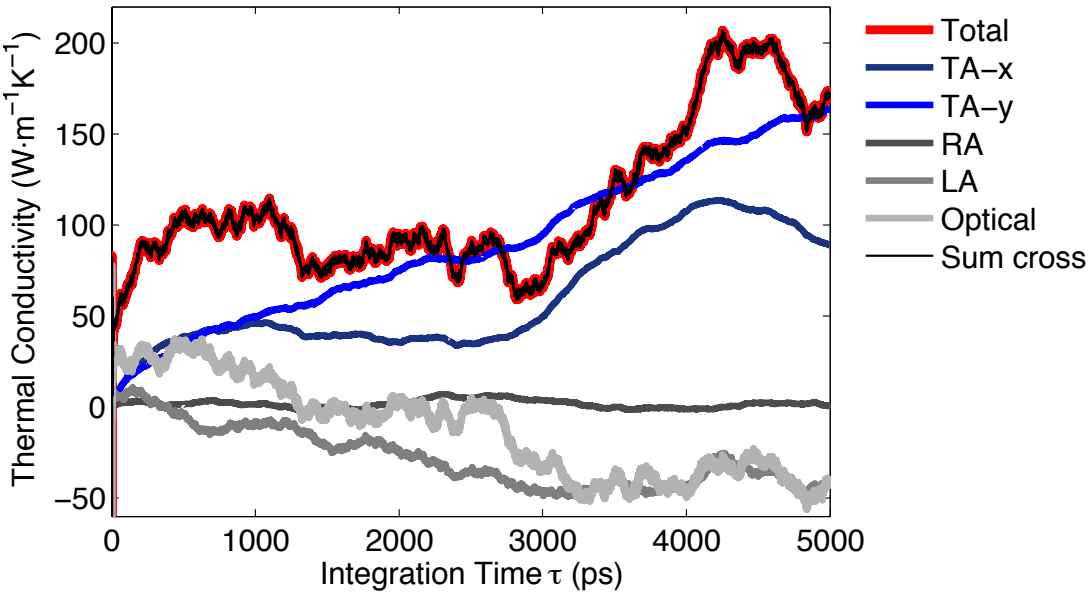

Figure 3.22 Pth thermal conductivity contribution from different branches.

Thus far, we have applied GKMA on three amorphous solids and one single polymer chain. For the amorphous solids, GKMA results demonstrate the best agreement with experiments. Additionally, we identified the phonon branches that are responsible for the divergent thermal conductivity found in single Pth chain. In the next chapter, we will describe a few interesting cases that we observed when analyzing GKMA results. These phenomena cannot be rationalized by the PGM, hence a new physical picture is needed to explain them.

CHAPTER 4

NEW INSIGHTS OF THERMAL TRANSPORT IN NON-CRYSTALLINE MATERIALS

In Chapter 1, we discussed that one cannot use PGM to study disordered materials due to lack of the definition of wavelength, hence phonon velocity for all types of modes. In Chapter 2, we introduced a new correlation paradigm and GKMA formulation to solve this issue. In Chapter 3, we showed the GKMA applications on a few materials including a-Si, a-SiO_2, a-C and single Pth chain. GKMA shows excellent agreement with experiments for all the amorphous solids that we have tested, which validates the GKMA formulation for disordered materials. In the proceeding chapter, we will use GKMA to explain a few phenomena that cannot be justified by the PGM.

Although one cannot apply PGM rigorously on amorphous materials, researchers try to use PGM based methods [14,61] with approximations to understand the thermal transport properties of amorphous solids. Let us assume PGM is still applicable on disordered materials. Then PGM entails a few inferences directly or indirectly. One would argue that the proportional relationship between thermal conductivity and relaxation time still exists for amorphous solids. Hence one can still use some effective MFP to study amorphous solids' phonon properties. Following the same logic by assuming that PGM is applicable to amorphous solids, one would claim the locons do not contribute to the thermal conductivity, because locons have zero velocity due to the localization. Based on Eq. (1.3), they should have zero thermal conductivity contribution. Based on PGM results on crystalline materials, the anharmonicity reduces the relaxation

time, hence decreases the thermal conductivity. If PGM is still applicable, one should find anharmonicity decreases the thermal conductivity in amorphous materials. Diffusons which are non-propagating modes, do not have a well-defined phonon velocity, hence one would think the boundary scattering has little effect on their contributions to the thermal conductivity. Based on PGM, the only explanation for the divergent thermal conductivity of the single Pth chain is the infinite relaxation time. With GKMA and the correlation paradigm, we are now able to explicitly check the validity of the above inferences. By doing so, we can conclude whether PGM is applicable on disordered materials and single polymer chains or not and gain more insights on the thermal transport in non-crystalline materials.

4.1 The need for a new physical picture

As discussed in Chapter 2, essentially all understanding of phonon transport is based on the PGM**.** The PGM ascribes every phonon with the following contribution to the heat current, $Q = \hbar\omega \cdot \mathrm{v}_g / V$ as shown in Eq. (1.1). This, however, becomes problematic for materials that do not have well-defined phonon dispersion and therefore do not have well-defined velocities. In reality all phonons share two properties, which is that of a well-defined frequency and time scale over which the amplitude remains correlated (e.g., a relaxation time), since they are most generally/mathematically just quantum oscillators. Wavelengths, wave vectors, velocities and MFPs, on the other hand, are not general properties of normal modes of vibration, because they become ill-defined when there is disorder [18]. Despite this lack of generality, the PGM has been used almost ubiquitously across all material classes [2,4,7,39,100–103]. Due to the limitation

of PGM, the validity of PGM to describe the transfer of heat in non-crystalline materials is questionable.

In the previous chapter, GKMA has been used to accurately predict the thermal conductivity of several amorphous solids. Using GKMA, one can obtain not only the temperature dependent thermal conductivity but also the modal contributions to thermal conductivity contributions. Using the mode thermal conductivity at different temperatures, we can now examine the validity of the PGM on mode level. In the proceeding chapter, five case studies are conducted to exam the validity of the PGM on amorphous solids and single polymer chains. The first test is to check the relationship between phonon relaxation time and mode thermal conductivity. If PGM is applicable on the amorphous materials, based on Eq. (1.3) $\kappa = \frac{1}{3}\sum_{\mathbf{k}p} C_{\mathbf{k}} \mathbf{v}_{\mathbf{k}p} \cdot \mathbf{v}_{\mathbf{k}p} \tau_{\mathbf{k}p}$, the relaxation time should be proportional to the mode thermal conductivity. Using GKMA and NMA, we now can compute both the mode relaxation time and mode thermal conductivity as shown in Fig. 4.2. We find there is no simple proportional relationship between them. This serves as the first evidence that the PGM is not suitable to describe the thermal conductivity in disordered materials and we need a new physical picture to understand the disordered material's thermal conductivity. The second case is on the locons' contribution to the total thermal conductivity. Locons are localized modes, which are constrained in the localized region. These modes are not travelling. Hence their group velocity should be zero. According to Eq. (1.3), they cannot contribute to the thermal conductivity. However, it is not true for all the amorphous materials that we tested. As shown in Fig. 4.5, locons' contribution is not negligible for a-SiO_2. This becomes second

evidence that PGM is not suitable for amorphous solids and a new physical picture is needed. The third case study is on the anharmonicity effect on the thermal conductivity. In crystalline materials, the anharmonicity increases the scattering rates between phonons such that it reduces the relaxation time and the thermal conductivity. However, in amorphous materials, we observe a reverse trend that mode thermal conductivity increases when the anharmonicity increases which again cannot be explained by the PGM, as shown in Fig. 4.13. The fourth test is on the size effect of the diffusons. Diffusons are non-propagating modes, hence they should not have any size effect since they cannot travel beyond the system boundary based on PGM. However we discover that the diffusons have size effect in 14 nanometers thick amorphous silicon thin film, as shown in Fig. 4.16. To understand the size effect of diffusons, one needs a new physical picture other than the PGM. The fifth test is on the single polymer chain which is a crystalline material. According to PGM, the divergent thermal conductivity must come from infinite relaxation time since the group velocity is finite and specific heat is a constant for a mode. However, the relaxation time in all cases (divergent or convergent cases) is finite and has similar magnitude, as shown in Fig. 4.23. Using GKMA, we are able to explain the divergent thermal conductivity with the four lowest frequency (divergent) modes on the transverse acoustic branch, as shown in Fig 4.22. In sum, we will demonstrate five cases that PGM fails to explain, which proves that PGM cannot be applied on single polymer chains. GKMA and correlation based paradigm however are able to explain all these cases. Hence these cases substantiate the validity and correctness of the correlation paradigm for disordered materials. Now, let us start the analysis on the relaxation times.

4.2 Relaxation time can become an invalid descriptor

From the PGM perspective, thermal conductivity depends on the individual mode heat capacities (c), phonon group velocities (v_g), and relaxation times (τ) as, $\kappa \propto \frac{1}{3} c \mathrm{v}_g^2 \tau$. Considering the fact that the thermal conductivity of solids spans about 5 orders of magnitude (0.1-10,000 W $m^{-1}K^{-1}$), it is instructive to examine which variables in Eq. (1.3) must be responsible for the range of κ observed in nature. For example, the heat capacities are essentially determined by the phonon density of states and the velocities scale with the speed of sound. The heat capacity from phonons in virtually all materials reaches the same maximum value at high temperatures, which is $3k_B$ per atom. Similarly, the speed of sound in solids is generally in the range of 1,000-10,000 m/s. Thus, the PGM asserts that it is the relaxation times that are the primary descriptor for explaining why transport is inhibited or more facile in different materials. Furthermore, the temperature dependence of thermal conductivity in a given class of materials is largely determined by the temperature dependence of the relaxation times [104,105]. Given this rather general theoretical framework imparted as a natural consequence [1,2] of taking Eq. (1.3) to be true, and the fact that the relaxation times are predominantly responsible for the temperature dependence of thermal conductivity above cryogenic temperatures, one can devise a scheme by which to assess the validity of the PGM.

The validity of the PGM becomes questionable for amorphous materials, due to the inability to define the phonon velocities. Here it is important to emphasize that periodicity is an inherent requirement for rigorously defining the phonon velocities, since

it requires that one define the phonon wave vectors, which in turn require periodicity. Therefore in an amorphous material, where there is no long-range periodicity, it is useful to assess whether or not one can still utilize the PGM framework in order to make sense of the thermal conductivity. If for example, one can still rationalize the behavior of amorphous materials with the PGM, then one can think of somehow defining an effective MFP for different modes and continue with the general viewpoint that has been used for almost all other materials. However, if after such an assessment one determines that the PGM is inapplicable, then one must then proceed to consider alternative descriptions of the heat flow and a revised physical picture for the transport.

To assess if one can rationalize the PGM for a given class of materials one can use a combination of experimental data for thermal conductivity (κ) and atomistic level calculations of the mode heat capacities (c) and relaxation times (τ) to then back-calculate the corresponding velocities (v_g) that would have to be ascribed to each mode in order to reproduce the experimental thermal conductivity. Here, the idea that one can back-calculate the velocities, is based on the basic assertion that κ, c, and τ together contain all of the temperature dependence, and any temperature dependence associated with v_g is negligible.

No matter how one tries to rationalize the velocities of phonons, it is difficult to imagine that somehow the velocities would not scale with the elastic modulus (e.g., the bulk and shear modulus) or at least be limited to values on the same order of magnitude as the speed of sound (e.g., assuming they are not polaritons [106,107]). Furthermore, one would also expect that any temperature dependence associated with the velocities of

modes in a given material must still exhibit similar temperature dependence to the speed of sound or modulus, which generally do not show strong temperature dependence for amorphous materials [15]. For example, in the case of a-Si [109] and a-SiO_2 [110,111], the change in modulus with temperature is less than 10% for both a-Si between 200-800K and a-SiO_2 between 100-1200K. Consequently, the sound velocity, which is proportional to the square root of the modulus, then only changes by less than 4% over these respective temperature ranges. Hence an important, yet physically well-reasoned assumption herein is that phonon velocities ($v_g(n)$), whether defined or ill defined, must still exhibit negligible temperature dependence (e.g., $\frac{dv_g(n)}{dT} \approx 0$) as compared to the heat capacity and relaxation times. This logic then yields a framework whereby one can use a combination of experimental data and relaxation times derived from LD and MD to assess if the resulting calculation for the phonon velocities is sensible. Towards this end, we calculated the mode relaxation times from NMA [8,39,45] using the Tersoff potential [62,65] for a-Si and a-SiO_2 [16,93]. We calculated individual mode relaxation times at six different temperatures (30K, 100K, 200K, 400K, 800K, 1200K) for a-SiO_2. Then we simply interpolated between the data obtained at each temperature to yield a continuous function for each mode's relaxation time as a function of temperature from 30K to 1200K. It is well appreciated that relaxation time results derived from classical MD are incorrect at low temperatures. However, based on Turney, McGaughey and Amon's work[41], it appears reasonable to expect that the classical MD relaxation times are within an order of magnitude and should generally exhibit the appropriate scaling with temperature, which, as will be shown later, is most critical to the subsequent conclusions. Therefore, assuming the PGM is valid, we then calculated the velocity squared via,

$v_g(n)^2 = 3\kappa(T)/\left[c(T,n)\tau(T,n)\right]$ for each mode. At 30K, there are only a few modes are excited, in other words, most of modes $c(n,30)$ is negligible. We choose $c(n,T) < 0.001$ as a criteria to set mode n is excited or not at temperature T. After we calculated the phonon velocities of a few modes that are excited at 30K, we increased temperature to be slightly higher (30.072K). Since there are total 13824 modes in the system, we divided temperature into 10000 bins so that each temperature increase only excites a small number of modes. When the temperature changes, the relaxation time and specific heat are changing for all modes. The contribution of thermal conductivity $\sum_{n}^{n'} k(n,T)$ from the modes that phonon velocity has been calculated is changing with the relaxation time and specific heat. The difference between experimental value $k(T)$ and $\sum_{n}^{n'} k(n,T)$ is used to determine the phonon velocity of newly excited modes at this temperature using $v_g(n)^2 = \left[\kappa(T) - \sum_{n}^{n'} k(n,T)\right]/\left[c(T,n)\tau(T,n)\right]$. Iteratively, we calculated the square of phonon velocities for all modes.

Conceptually, one can argue that there does not exist a unique solution for v_g^2, but in practice there is. Since one cannot rationalize the velocities having strong temperature dependence, they are constant and therefore unique for every frequency. As a result, one can simply begin by solving for the velocities at low temperatures where the majority of the modes' heat capacities are effectively zero. In this temperature range one can easily find a unique solution to v_g^2, because only a small portion of the low

frequency modes can contribute to the thermal conductivity. Once v_g^2 for low frequency modes are determined, one can then gradually progress to successively higher temperatures, solving for a unique function $v_g(n)^2$ at successively higher and higher frequencies with mode relaxation time $\tau(T,n)$ and specific heat $c(T,n)$ at this temperature.

The calculated mode-wise squared velocity $v_g(n)^2$ and the magnitude of the real and imaginary part of the velocity (e.g. since now the phonon velocity can become imaginary if v_g^2 is negative) is shown in Fig 4.1 Note that in Fig. 4.1, $v_g(n)^2$ is normalized by the longitudinal velocity (6500 m/s) calculated from bulk modulus [68]. From Fig. 4.1 (a) it is apparent that $v_g(n)^2$ is negative for many mid-frequency modes. Hence as shown in Fig. 4.1 (b), there are a great number of modes that would have to have imaginary group velocities in order to reproduce the experimental data. The most significant contributor to this requirement is the rise and then sharp drop in relaxation times between 20-30 THz (see Fig. 4.2 (d)). This feature in the relaxation times requires imaginary velocities, if these phonons' contributions to the thermal conductivity are proportional to their relaxation times. Furthermore, Fig. 4.1 (b) shows that the magnitude of $v_g(n)$ is unreasonably large (> 100X the speed of sound) for some middle and high frequency modes. Neither of these two results are sensible or can be rationalized. Imaginary velocities have no sensible interpretation in the PGM and velocities that are orders of magnitude greater than the speed of sound are nonsensical, even if one assumes the real quantum relaxation times are an order of magnitude larger. These two

observations then lead us to conclude that one cannot self-consistently rationalize the usage of the PGM in a-SiO_2 and it is likely that the lack of applicability may extend to many, if not all, amorphous materials.

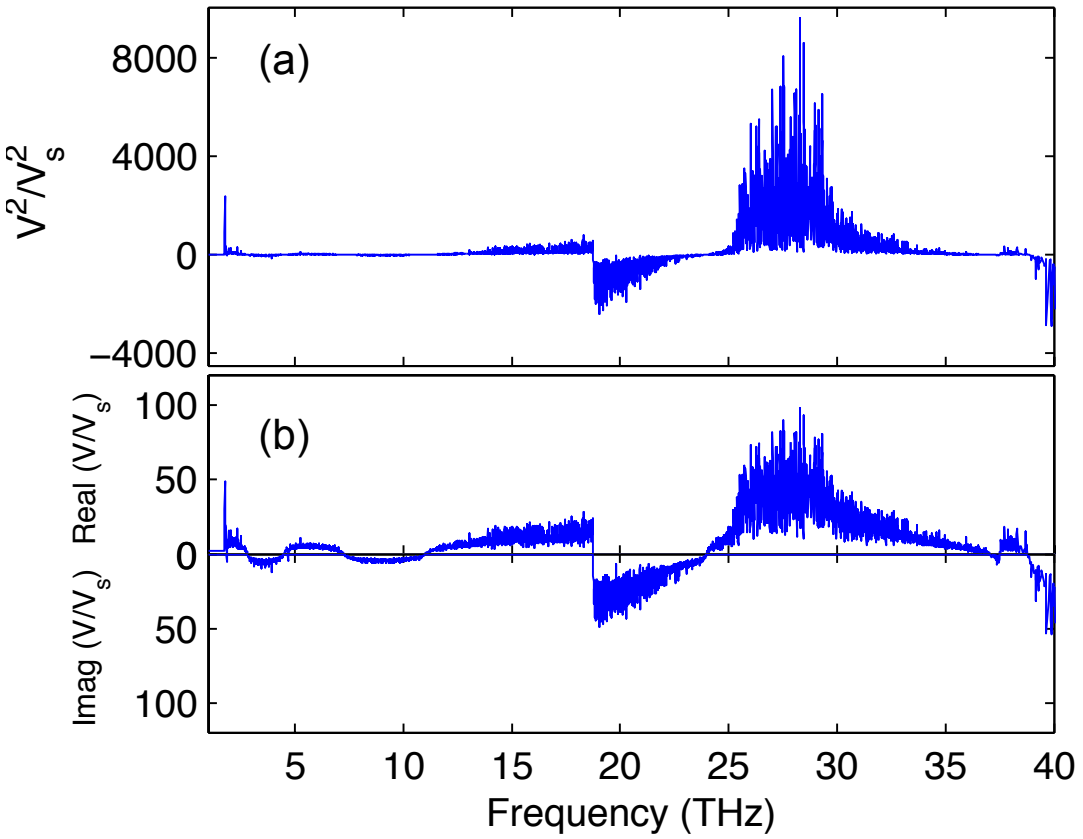

Figure 4.1 (a) Normalized mode phonon velocities squared, (b) normalized mode phonon velocities that are real and imaginary for aSiO2 calculated from PGM model.

To understand the thermal conductivity of amorphous materials more properly, we use the GKMA method [16]. The previous chapter has shown that GKMA yields excellent agreement with experiments on the thermal conductivity of amorphous materials, especially a-Si and a-SiO_2 [16,93]. Thus its results can be regarded as not only accurate, but also meaningful towards deriving improved insight and assessing the validity of the PGM. However, one can still argue that even though GKMA provides a

fundamentally different physical picture for the transport (e.g., based on correlation and not scattering [31,93]), that somehow one can possibly still view the problem from a PGM point of view, via some effective MFP treatment. Here, we examine this question more deeply and show that the behavior in amorphous materials is distinctly different from what can be rationalized by the PGM and thus the PGM is a fundamentally problematic way of viewing phonon transport in amorphous materials, since one cannot rationalize the usage of a MFP based explanation.

Here we used the same atomic structure of a-Si and a-SiO_2 [16,93] and all of the same simulation procedures have been employed here. All the MD simulations are conducted in LAMMPS [63] and LD calculations were performed using GULP [69]. In Fig. 4.2 (a) and (b), the thermal conductivity accumulations with respect to frequency $\kappa(\omega)$ are shown at different temperatures. The accumulation here is directly calculated from GKMA without a quantum specific heat correction. All modes are excited in MD and therefore they all have identical heat capacity $\frac{k_B}{V}$. As a result, classical GKMA results do not incorporate the temperature dependence of the heat capacity. After dividing by the constant heat capacity $\frac{k_B}{V}$ for every mode, one can then think of the accumulation as a thermal diffusivity accumulation, where $D = v^2\tau$. If one were to then try and rationalize the results in terms of the PGM, one would expect that the corresponding thermal diffusivity contributions must follow the same temperature dependence as the relaxation times determined from MD.

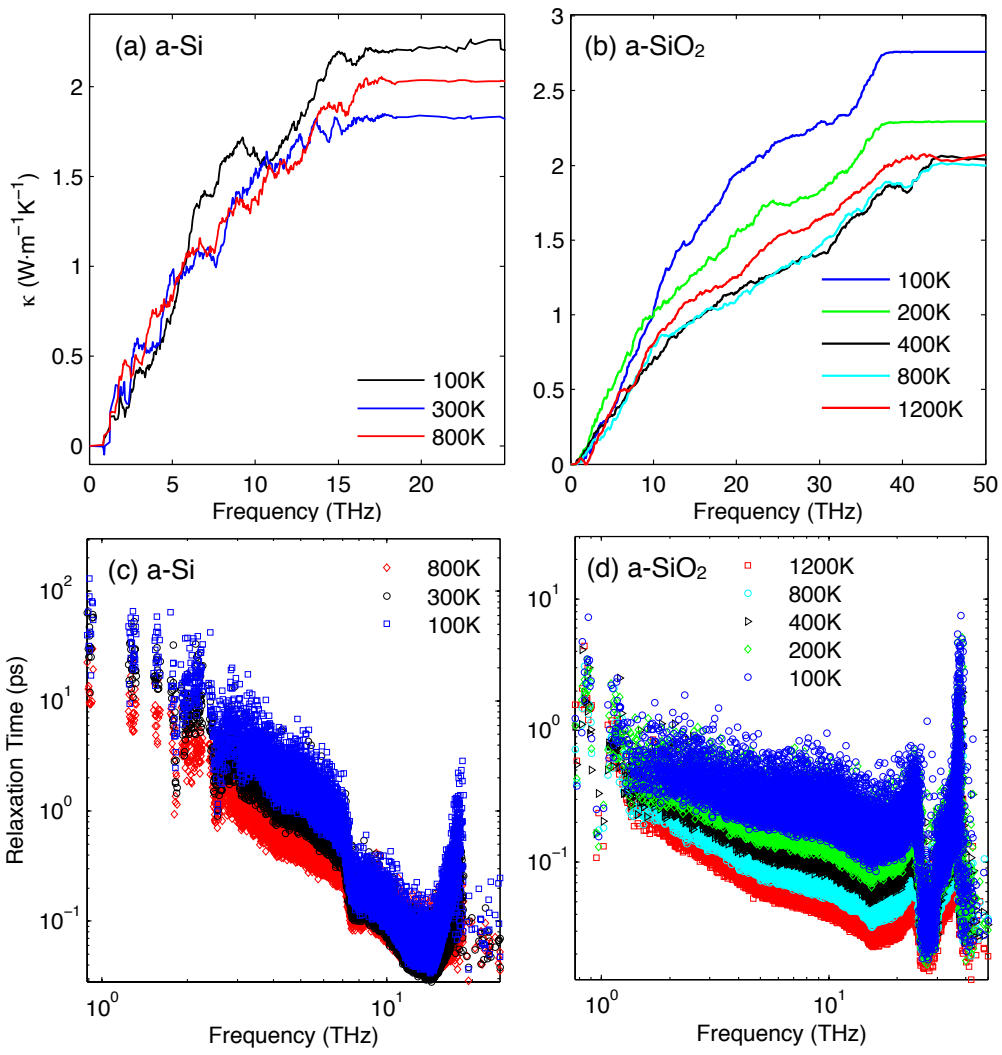

Figure 4.2 Thermal conductivity accumulation and relaxation times calculated from GKMA. Thermal conductivity accumulation for (a) a-Si and (b) a-SiO_2, and relaxation times for (c) a-Si and (d) a-SiO_2.

In both a-Si and a-SiO_2, the relaxation times drop significantly as temperature increases. However the thermal conductivity contributions shown in Fig. 4.2 (c) and (d) do not decrease in the same way. From the relaxation time $\tau(\omega)$ and thermal conductivity accumulation $\kappa(\omega)$ in a-Si and a-SiO_2, the trend required for consistency with the PGM is not observed. In a-SiO_2, for example, above 400K, the thermal conductivity accumulations are approximately identical, even though the relaxation times

decreased by about a factor of two. Furthermore, at 400K, 800K and 1200K, there is no clear reduction of thermal conductivity, and it should be emphasized that the temperature dependent thermal conductivity obtained in these simulations is in excellent agreement with experiments, once quantum corrected as shown in Chapter 3. This further suggests that the thermal conductivity accumulations are both accurate and meaningful.

From Fig. 4.2 (d), it is also clear that the effects of anharmonicity do not seem to alter the thermal conductivity contributions between 400-800K for a-SiO_2. However, at 100K the accumulations are very different from others, which shows that, how anharmonicity affects the thermal conductivity contributions at low temperatures is different than at high temperatures. As for a-Si, comparing 300K and 800K, the relaxation times clearly decrease (Fig. 4.2 (a)), yet somehow the thermal diffusivities increase (Fig. 4.2(c)), which again contradicts the expected behavior based on the PGM.

From the results in Fig. 4.2, one can conclude that thermal diffusivity in amorphous materials does not generally exhibit direct correspondence with the relaxation times. Therefore the idea that all phonon contributions to thermal conductivity can be thought of in terms of relaxation times seems problematic. For modes that do not behave like propagating modes, their contributions to thermal conductivity appear to exhibit almost no connection to their relaxation times and it is desirable to somehow assess this quantitatively. Directly examining the $(\frac{dD(n)}{dT})\Big/(\frac{d\tau(n)}{dT})$, where $D(n)$ is the mode diffusivity leads to values that oscillate about zero, because in GKMA the thermal conductivity is a summation of many positive and negative thermal conductivity contributions from individual modes. Since the mode heat capacity is always positive, the

individual mode diffusivities tend to fluctuate around zero in the GKMA approach, since the correlation functions yield both negative and positive values that ultimately sum to a net positive transport coefficient [16]. Therefore to better quantitatively assess the level of disconnect between the rather consistently decreasing relaxation times, and the often constant and sometimes increasing mode diffusivities, instead of examining the ratio, $(\frac{dD(n)}{dT})\Big/(\frac{d\tau(n)}{dT})$, we examine its accumulation,

$$\sigma(n')=\sum_{n}^{n'}(\frac{dD(n)}{dT}\Big/\frac{d\tau(n)}{dT})/\mathrm{v}_s^2 \qquad (4.1)$$

whereby we are primarily interested in the sign of this accumulation as opposed to its actual value. In essence, σ helps us to assess whether or not the diffusivities and relaxation times are increasing or decreasing together or whether or not they have opposing temperature trends more often than not. By analyzing the accumulation, instead of the argument in the sum, one can discern the net effect of adding many modes together from the individual mode ratios, which oscillate about zero.

In Eq. (4.1), v_s is the (maximum) sound velocity calculated from the bulk modulus calculated from GULP [69], which is used to non-dimensionalize σ. For c-Si we take v_s = 9,000 m/s, and for a-Si the speed of sound is taken as 7,909 m/s. Since we do not have a continuous function for $\frac{dD(n)}{dT}$ and $\frac{d\tau(n)}{dT}$ with respect to temperature, we used $\Delta D/\Delta T$ and $\Delta\tau/\Delta T$ between the temperatures at which GKMA results were computed. This ratio represents the slope in diffusivity, which is proportional to the thermal conductivity contribution, versus the slope in relaxation time, normalized by v_s^2.

Thus, if both diffusivity and relaxation time are increasing or decreasing together for a group of modes in a certain frequency range, the ratio is positive, despite whether the changes occur at the same rate. However, if the ratio is negative, it implies that some modes have increasing diffusivity, yet decreasing relaxation time, which is fundamentally disjoint with the PGM. Similarly, if the slope in σ approaches zero for a group of modes it is because the diffusivity is nearly constant, since Figs. 4.2 (c) and (d) show that the relaxation times in both systems are predominantly decreasing with increased temperature. As a result, if the PGM is valid in amorphous materials, then $\sum_n (\frac{dD(n)}{dT}) \Big/ (\frac{d\tau(n)}{dT}) = \sum_n \mathrm{v}(n)^2 > 0$ and $\sigma(n)$ should always be positive. However, if this ratio is negative, the PGM is inapplicable to amorphous materials in general or at the very least inapplicable to the two materials considered herein.

To validate this, we first calculated σ for crystalline silicon at three temperatures (100K, 300K, 1000K) using GKMA as shown in Fig. 4.3 (a) and (b). As expected, in both temperature ranges, σ is always positive and is roughly constant when comparing the data from different temperature ranges, which suggests that the relaxation time is an appropriate descriptor of the thermal conductivity contributions as determined by the GKMA method, and the PGM is valid. The results in Fig. 4.3 (a) and (b) therefore demonstrate that the proposed approach is useful, since it is consistent with the well-known understanding that the PGM is valid for crystals. For a-Si, on the other hand (see Fig. 4.3 (c)), the modes exhibit positive σ when comparing 100-300K, which implies the relaxation time can be a suitable descriptor in that temperature regime, but Fig. 4.3 (d) shows that between 300-800K there is a marked change in the behavior and σ becomes

negative for most modes. This is also apparent from the fact that in Fig. 4.2 (a), the 800K-accumulation curve is higher than at 300K, yet the relaxation times generally decrease (see Fig. 4.2 (c)).

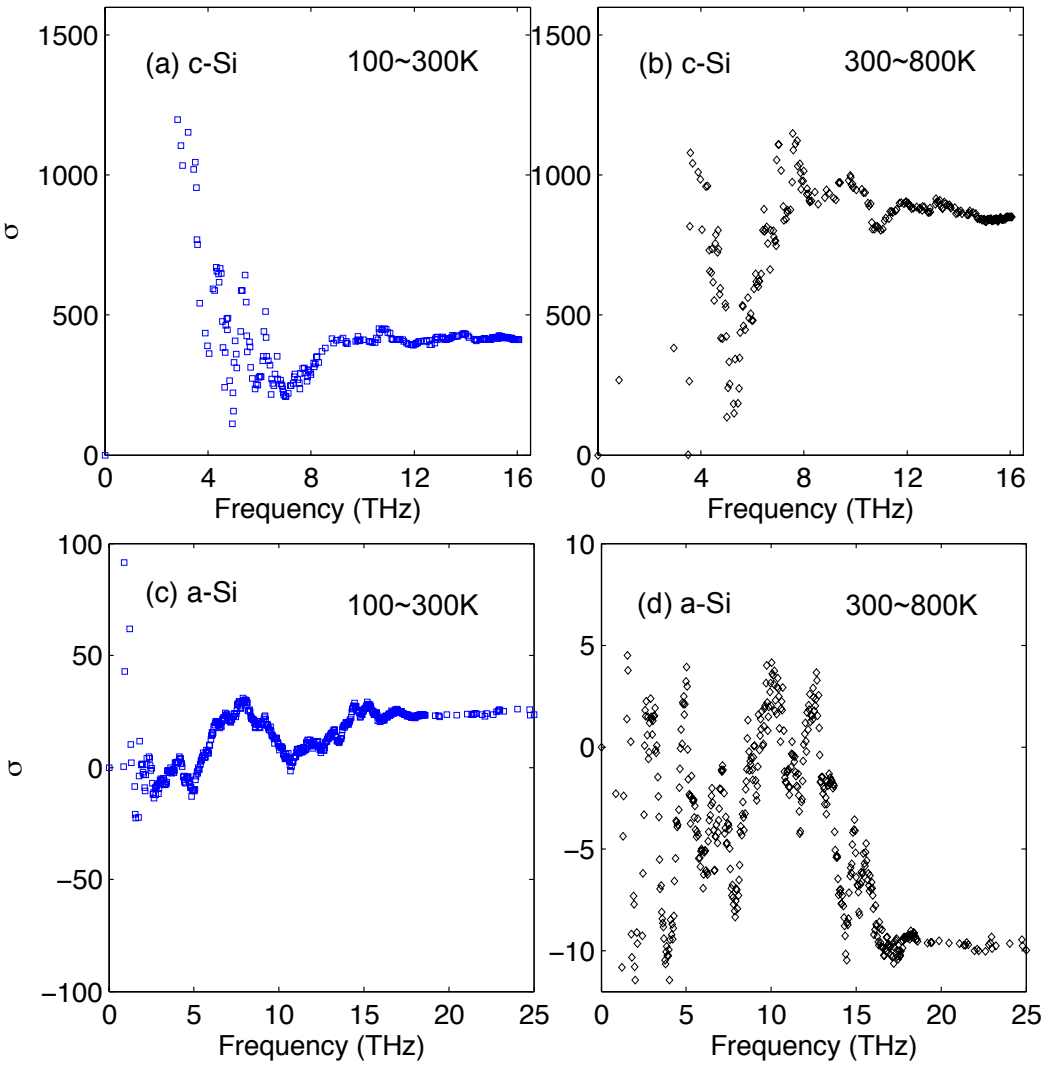

Figure 4.3 The $\sigma(n)$ ratio. (a) 100~300K and (b) 300~800K for c-Si and (c) 100~300K and (d) 300~800K for a-Si.

For a-SiO_2, as temperature increases, the anharmonicity increases and relaxation times decrease, but thermal conductivity contributions for non-propagating modes (diffusons and locons) do not necessarily decrease with relaxation time. Figure 4.4 shows

σ for a-SiO_2, and interestingly, similar to Fig. 4.3 (c) and (d), σ is positive at low temperatures (below 400K) and starts to decrease with temperature and eventually becomes negative in Fig. 4.4 (d). Thus, one can possibly make the argument that the PGM is still somewhat valid below room temperature, but it becomes questionable when temperature of the system is higher.

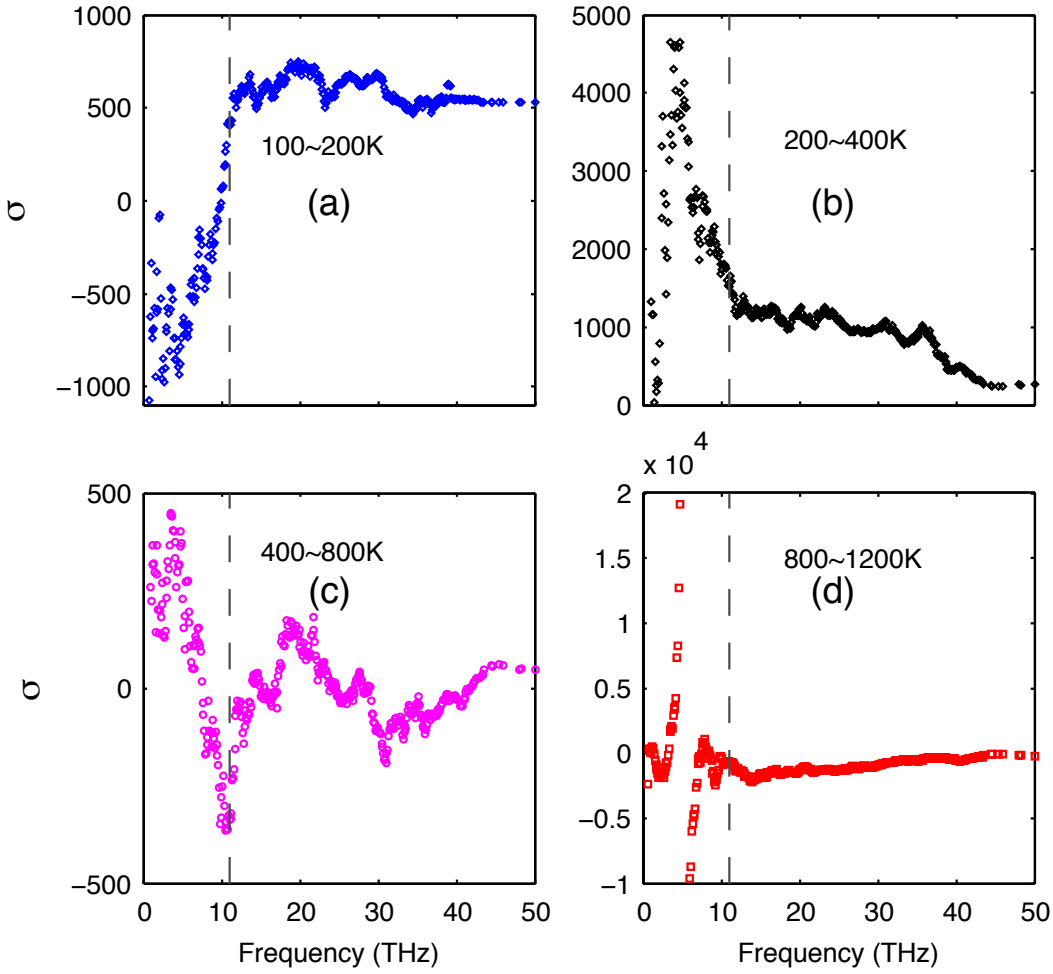

Figure 4.4. The $\sigma(n)$ ratio. (a) 100-200K, (b) 200-400K, (c) 400-800K, and (d) 800-1200K for a-SiO_2. The dashed curve is the estimated cut-off where the ratio of $(\frac{d\tilde{D}(n)}{dT})\Big/(\frac{d\tilde{\tau}(n)}{dT}) \approx 0$, which is primarily caused by the numerator being close to zero (e.g., constant mode diffusivity).

In this section, we have conducted a detailed analysis to assess the validity of the PGM from the relationship between relaxation time and mode thermal conductivity. We use LD derived phonon frequencies and MD derived temperature dependent relaxation times along with experimentally measured thermal conductivities to back-calculate the phonon velocities for individual modes using the PGM. For many of mid and high frequency modes, the phonon velocity must be either imaginary or unrealistically high (> 100X the speed of sound), which is not physical. We therefore conclude that the PGM is not applicable to amorphous solids or at least not to a-Si and a-SiO_2 above room temperature. Using the GKMA method, we calculate the mode diffusivities with inclusion of anharmonicity. Comparing the temperature dependence of mode the diffusivities and relaxation times shows that there is little if any connection between phonon relaxation times and thermal conductivity for the amorphous materials considered herein. Thus, the results provide quantitative evidence that relaxation time is an improper descriptor for the behavior at elevated temperatures in a-Si and a-SiO_2 and is therefore questionable altogether for amorphous materials. It serves as the first evidence that PGM fails on amorphous solids and a new physics picture is needed.

Based on PGM, relaxation time is the most important descriptor for the lattice thermal conductivity. Failure of the relaxation time point of view on disordered materials makes us question other inferences from PGM. Based on PGM, localized modes do not contribute to the thermal conductivity since they do not travel in space. In the next section, we will exam this claim using GKMA results on locon thermal conductivity. Based on the correlation paradigm, the localized modes can still contribute to thermal conductivity by becoming correlated with other modes. In a-SiO_2, we discover the locons

significantly contribute to the thermal conductivity above room temperature, as shown in Fig. 4.5.

4.3 Locons can contribute to the thermal conductivity

Based on PGM, localized modes (locons) have a negligible contribution to thermal conductivity, due to their highly localized nature. However, in a-SiO_2 GKMA results indicate that locons contribute more than 10% to the total thermal conductivity from 400K to 800K and they are largely responsible for the increase in thermal conductivity of a-SiO_2 above room temperature. This is an effect that cannot be explained by PGM and therefore GKMA offers new insight into the nature of phonon transport in amorphous/glassy materials.

The locons are distinguished by the IPR. The IPR quantifies the extent of localization for a given mode. From Fig. 3.10 (b), there are two regions that have localized modes, from 25 to 30 THz and above 35 THz. Given their higher IPR, we classified both of these groups of modes as locons [18], which are spatially localized and typically only involve a small group of atoms in the vibration. Interestingly, the modes between 30-35 THz are diffusons, which are delocalized over the entire system. Thus, a-SiO_2 appears to exhibit two regions of locons [23], which is distinctly different from a-Si [18].

One of the most striking results is the non-negligible contribution associated with locons. Previously, locons have been thought to exhibit negligible contributions to thermal conductivity [40,112], due to their restricted spatial extent, which renders it difficult to imagine how they can transfer a significant amount of heat to another

location. Despite the long held belief that locons are negligible, Fig. 4.5 shows that they contribute significantly to the thermal conductivity of a-SiO_2. It is important to acknowledge, however, that Alexander and coworkers [13,113] proposed a different theory for non-propagating mode contributions based on fracton hopping. Their theory describes the contributions from fractons, which conceptually must include both diffusons and possibly locons, in terms of their lifetime (e.g., scattering). However, their work only examined the contributions at low temperatures 10-100K, where the locons are not even excited. Hence the fractons they studied were really only diffusons in most cases. Furthermore, their perspective is fundamentally different than the GKMA viewpoint, which casts their contributions in terms of correlation, as can be seen from each respective derivation [13,16,113]. The phonon fracton model results in a generalized contribution from fractons that is linear with temperature and has mostly been applied at cryogenic temperatures [113], where the locon contribution is effectively zero, due to their suppressed heat capacity. This result is then general and would suggest that fractons contribute strongly in all amorphous materials. The GKMA formalism, on the other hand, naturally includes the mode character and anharmonic interactions, which are specific to a given material. As a result, GKMA shows excellent agreement with experiments on both a-Si and a-SiO_2, but the locon contributions in a-Si are negligible, while in a-SiO_2 they are not.

In Fig. 4.5, the thermal conductivity contributions vs. temperature without the locon contributions included are shown. Most notably, even after quantum correction, locons are responsible for approximately half of the continual rise in thermal conductivity for a-SiO_2 above room temperature. Without the contributions from locons, the thermal

conductivity begins to deviate from the experiments after 250K. Furthermore, the cross-correlation maps at different temperatures (see Figs. 3.13 in Chapter 3) show that even though the autocorrelation appears dominant at all temperatures, the cross-correlation contribution increases with temperature and comprises the dominant portion of the locon contributions. This behavior suggests that modes interact more strongly with other modes of differing frequency as temperature increases, which is consistent with our intuitive understanding of anharmonicity.

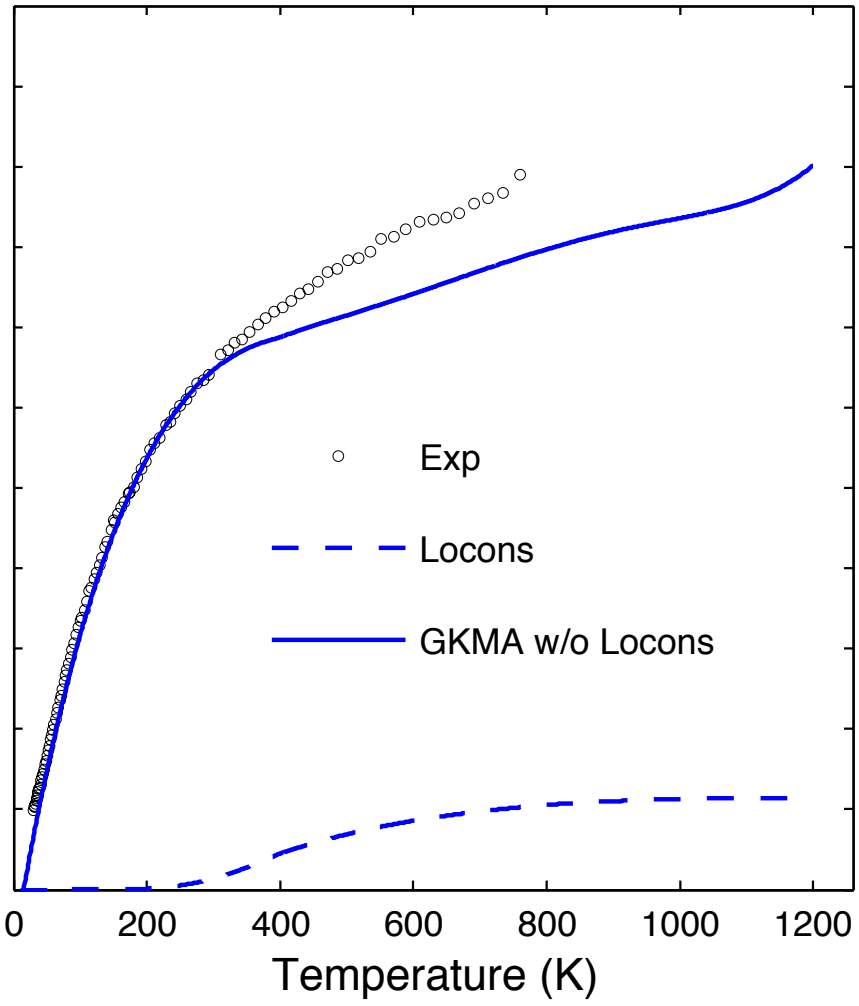

Figure 4.5 Thermal conductivity vs. temperature as compared to other models and experiments. The solid blue curve represents the locon contribution to the thermal conductivity and the dashed blue curve is the sum of all other delocalized mode contributions.

The locon contributions come from both cross-correlations and auto-correlations, but it is not entirely clear how these modes are able to help transfer energy from one location to another. One interpretation, motivated by the fact that the cross-correlation contributions to thermal conductivity for locons, as shown in the Figs. 4.6 and 4.7, is that locons serve as bridges between other modes in regions of the material where atoms are over coordinated and therefore require

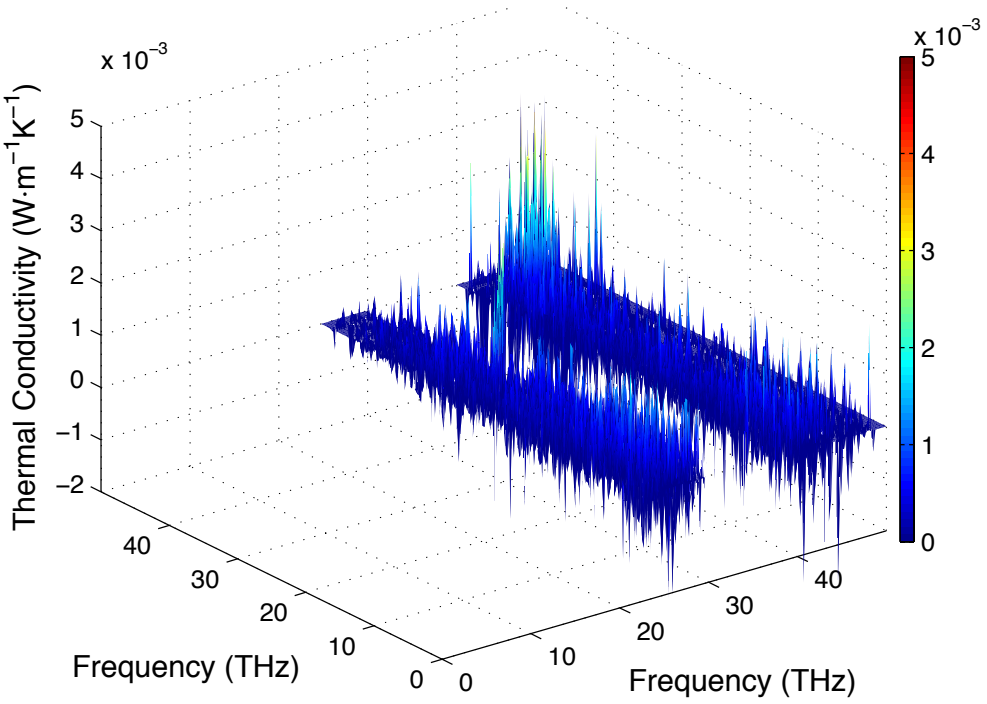

Figure 4.6 The 3D correlation plot for locons at 800K.

localized solutions to the equations of motion. As shown in Fig. 4.6, the correlation between propagons and locons are negligible. However, the correlations between diffusons and locons, and between locons and locons, comprise 55% and 45% of the locon thermal conductivity respectively. The correlations between propagon and locons are negligible because the number of propagons in a-SiO_2 is very small [68,93]. From this perspective, even though locons may not move the energy over a significant distance by

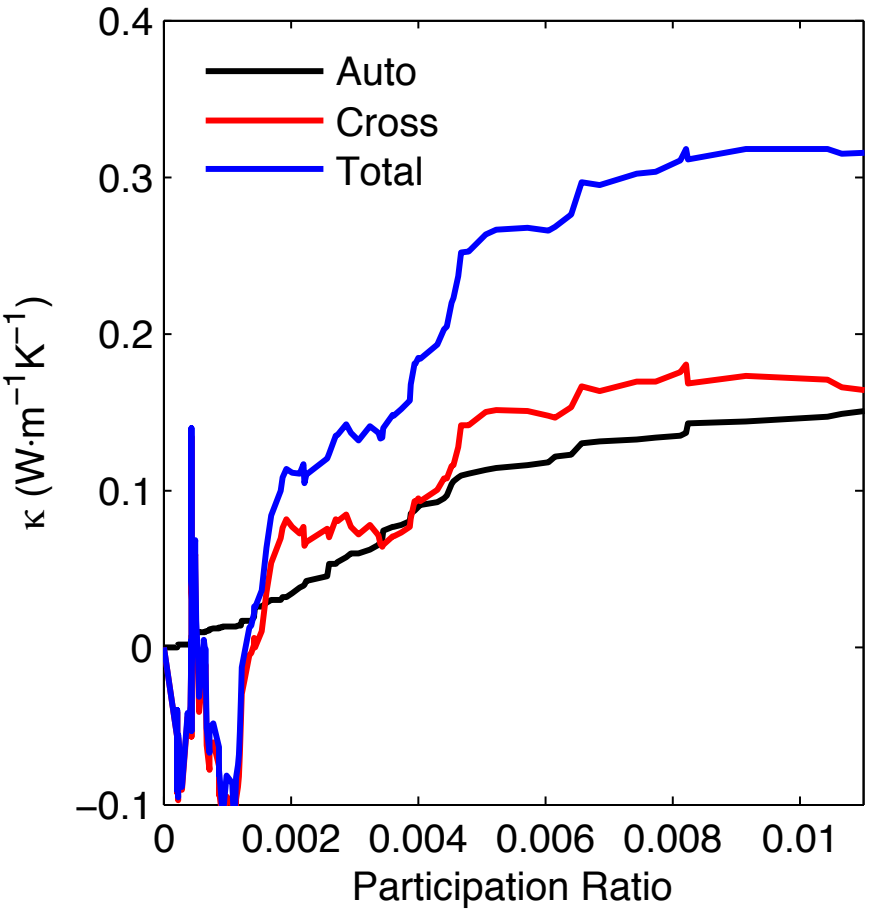

Figure 4.7. Thermal conductivity contributions from locons that are composed of less than 1% of the system's participation, showing the respective contributions from autocorrelations and cross-correlations.

themselves, they may serve as critical bridges between modes that do, suggesting that their contributions to thermal conductivity rely on collaboration with other modes. When these modes are excited at high temperature, they help to bridge the energy transfer between diffusons that have vibrations on surrounding atoms. Given that localization causes the motions of some atoms to be largely described by a smaller subset of modes, we then calculated the normalized harmonic energy [114] associated with locons on each atom in the system. As shown in the Fig. 4.8, more than 2% of the atoms have more than 40% of the total harmonic energy carried by locons. These locons must somehow couple to other modes to participate in the heat conduction, as Fig. 4.7 shows that the

predominant contributions from locons arise from the locons with the larger participation ratios.

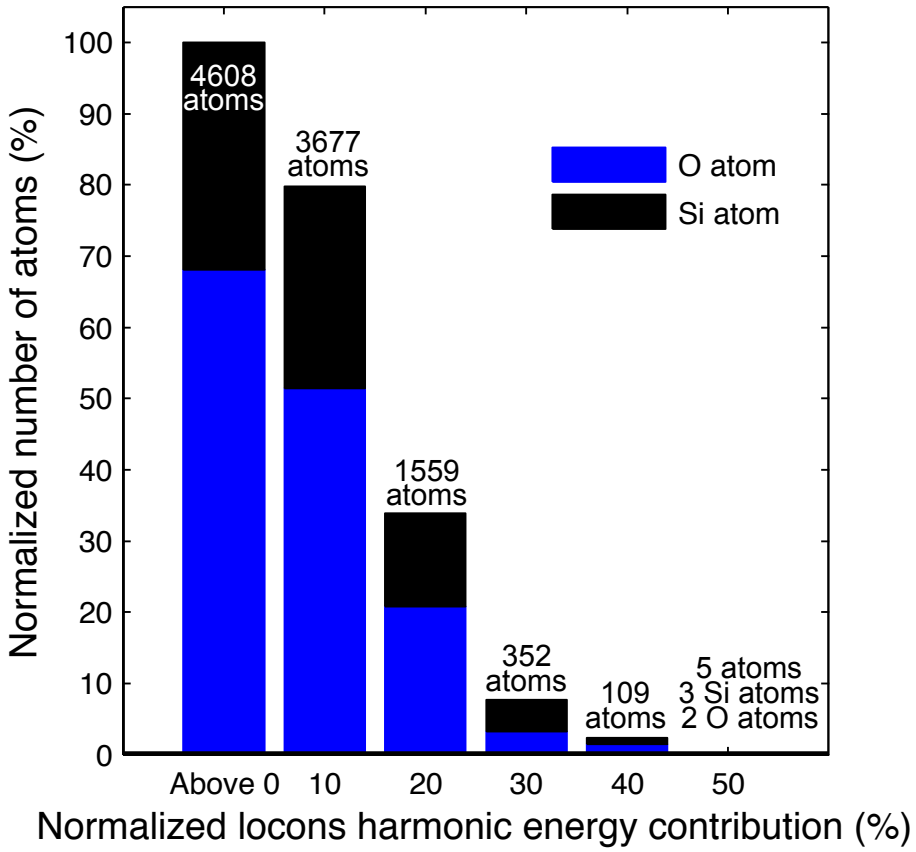

Figure 4.8 The percentage of number of atoms with different normalized locon harmonic energy contributions. The system has total 4608 atoms; 80% of these atoms have more than 10% of their energy attributed to locons; 35% of the atoms have more than 20% of their energy attributed to locons; 8% of the atoms have more than 30% of their energy attributed to locons; 2% of the atoms have more than 40% of their energy attributed to locons; and 5 atoms in the system have more than 50% energy attributed to locons.

The GKMA study on a-Si [16] showed that locons have negligible contribution to the thermal conductivity, consistent with previous intuition and A-F also reached a similar conclusion for a-Si using the harmonic approximation [21]. Based on their work, researchers have generally neglected the locon contributions to the thermal conductivity of amorphous materials [18,23,40]. However, using GKMA for a-SiO_2, we find that locon contributions are non-negligible. We believe this is primarily due to the fact that

locons constitute 18% of the modes in a-SiO_2, which is 6X greater than a-Si (3%). If such a large portion of the spatially localized modes in a material does not interact with other modes, then nanometer scale inhomogeneity in the temperature field during steady state heat conduction can arise, due to the inability to conduct heat in certain locations. Such a phenomenon would be rather unphysical and thus it is much more plausible that locons simply exchange energy with surrounding modes and do in fact substantially participate in heat conduction, once excited.

The localized modes that have the strongest contributions typically occur where atoms are over-coordinated, and therefore, since they have localized solutions to describe their motion, other diffuson solutions to the equations of motion become somewhat suppressed or non-existent in those regions. As a result, when these modes are excited at high temperature, they help to bridge the energy transfer between diffusons that have vibrations on surrounding atoms. Otherwise, if such modes did not participate in the heat conduction, there would be regions in the material that participate in the heat flow to a lesser extent. This would then lead to non-uniform temperature gradients/fields at the nanometer scale, even during steady state heat conduction, which is problematic. This mechanism is further supported by the data in Fig. 4.8, where we see that for 109 atoms, the locons comprise more than 40% of the total energy (we calculated the harmonic portion – which is several orders larger than the anharmonic portion). The harmonic energy attributed to each atom for each mode is proportional to the magnitude of the eigenvector for each mode on each atom. The detailed derivation and formula are discussed in a recent paper by Gordiz and Henry [114]. Fig. 4.9 is the normalized spectral harmonic energy contribution and accumulation for the atom in the supercell that had the

largest locon harmonic energy contribution. For this atom, more than 58% of its energy comes from locons between 25-30 THz and above 35 THz.

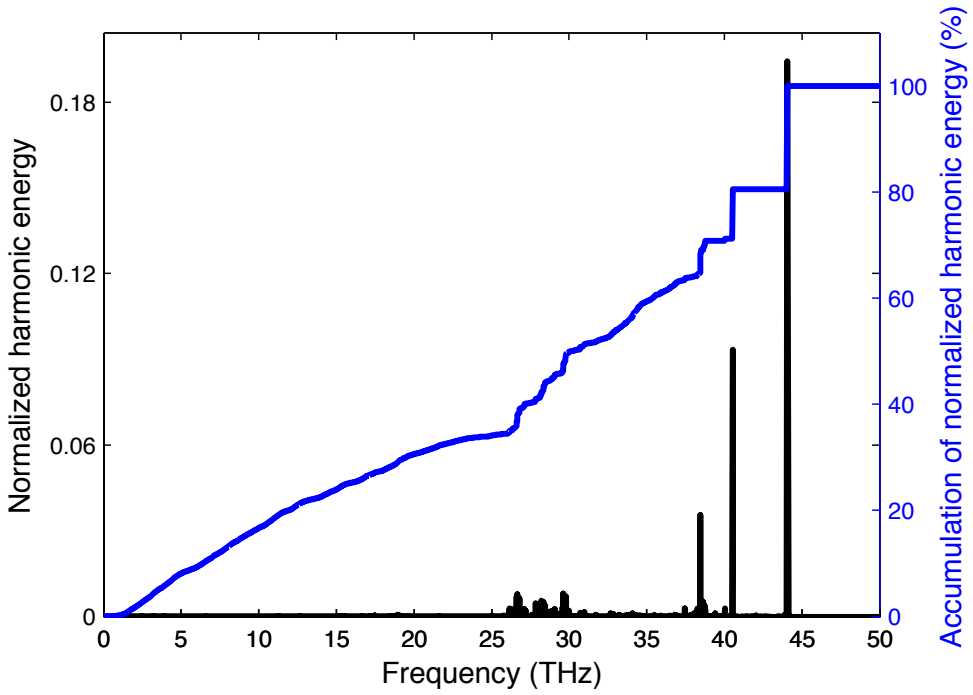

Figure 4.9 The spectral normalized harmonic energy of one atom and the accumulation. This plot shows the spectral distribution of energy associated with the atom that has the most energy associated with locons.

The examination of the contributions from different types of modes revealed quantitative evidence that localized modes (e.g., locons) can contribute significantly to the total thermal conductivity of a material. In a-SiO_2, locons are responsible for approximately half of the rise in thermal conductivity above 400K.

Until now, we have shown that the contributions from different types of modes proves that localized modes (e.g., locons) can contribute significantly to the total thermal conductivity of a material for the first time. In a-SiO_2, locons are responsible for approximately half of the rise in thermal conductivity above 400K. This serves as the second numerical evidence that the PGM fails for the disordered materials. The A-F

method also predicts the locons do not have contribution to the thermal conductivity since the locon eigenvectors have little overlap with other modes [18]. Using GKMA, we find the locons couple with other modes, which is possibly caused by anharmonicity. Because A-F does not include anharmonicity, it fails to detect the locon thermal conductivity contribution.

The anharmonicity plays an important role in amorphous materials by allowing locons to couple to other modes. One would wonder how does anharmonicity influence other modes in amorphous materials. Hence in the next section, we dedicate to discuss the anharmonic effect in amorphous solids using GKMA. The results again contradict the PGM prediction and will be the 3rd evidence that PGM fails on disordered materials.

4.4 Anharmonicity can increase thermal conductivity

Anharmonicity in crystalline materials has previously been extensively studied by others [2,102,115,116] using the PGM. Based on PGM, the increasing of the anharmonicity will result in rising of the scattering rates of phonons. Hence the mode thermal conductivity will reduce. It is the cause of the 1/T trend of the thermal conductivity changing with temperature at high temperature in crystalline materials [1]. However there is no similar trend observed in the experiment for amorphous materials [59].

As discussed in Chapter 2, Allen and Feldman used A-F method to qualitatively describe the trend of thermal conductivity changing with temperature for a-Si [10]. However, researchers have later found out that A-F method failed on several other amorphous materials [23]. And it was due to the harmonic assumption they used. In the

derivation of A-F formula from Hardy derived heat current operator [35], Allen and Feldman neglected the higher order (anharmonic) terms in the Hamiltonian [40].

One effect of neglecting anharmonicity is that using the A-F formula, the localized modes always have zero thermal diffusivity and hence no contribution to the thermal conductivity [36]. However Allen and Feldman have also claimed it is possible that locons contribute to the thermal conductivity once the anharmonicity processes are included in the calculation. In the previous section, we demonstrated that the locons have non-negligible contributions to the thermal conductivity for a-SiO_2 using GKMA [93].

Another effect neglecting anharmonicity has on the A-F formalism is that it introduces a delta function, requiring that only same frequency modes can interact, although in actual calculations, they used a Lorentzian function to broaden the delta function. This brought to the fact that of A-F method only considers the interactions of modes with similar frequencies [40], which neglects interactions of modes with large frequency difference. And A-F method neglects the possibility of multi-phonon scattering events. GKMA method, which is based upon MD, intrinsically includes all types of phonon interactions and all degree of anharmonicity. Using GKMA method, each mode's thermal conductivity comes from two types of heat current correlations, which are mode self-correlations (autocorrelations) and mode-mode correlations (crosscorrelations). From this basic assessment, one would expect that the A-F model should then correspond well with the autocorrelations, while the cross-correlations can be associated with anharmonicity. Here we test this hypothesis, which allows us to assess the affect anharmonicity has explicitly on the thermal conductivity for amorphous solids.

In the previous chapter, we have validated GKMA by examining the contributions in crystalline silicon and found agreement with PGM [16] based on the mode level comparison. We have then used GKMA to predict thermal conductivity of a-Si using Tersoff potential [62] and found excellent agreement with experimental result [59]. In this section, since we want to understand the anharmonicity effect on amorphous solids, we decide to calculate thermal conductivity using different empirical potentials. Different empirical potentials have different anharmonicity due to different mathematical form of the potential energy function. Here we will present the GKMA applications to a-Si using Stillinger-Weber (SW) [18] and Environment-Dependent Interatomic Potential (EDIP) [64] potentials. After we obtain the thermal conductivity from these empirical potentials, we then compute the degree of anharmonicity of them. If the PGM is still valid, the higher anharmonicity, the lower the thermal conductivity. However if it is not the case, then it becomes another evidence that the PGM fails on amorphous solids. The comparison between these three potentials' results and A-F result gives us deeper insights of how does anharmonicity affect the thermal conductivity in a-Si.

The a-Si structure is generated using WWW random walk method [66]. We use Tersoff, SW and EDIP potentials to simulate a-Si and used melt-quenching method using three potentials to relax the a-Si structure. Then apply the LD study on the amorphous structure from MD using GULP [69]. The relaxed structure for the LD study is computed at 0K with constant volume. The final structure contains 4096 atoms, supercell size of 43.44 $\mathring{A}$, with a density of 2330 kg/m^3, which is close to the crystalline silicon. The eigenvectors and harmonic frequencies are calculated using GULP [38,69].

All the MD simulations were performed using LAMMPS with a time step of 0.25 fs. In order to reduce the meta-stability of the structure, all the atomic structures are annealed at high temperature (1100K) for 10 ns [68]. After 100 ps equilibration with NVT , the total heat current, the modal heat current and mode energy were captured for 10 nanoseconds ($2*10^7$ time steps) at equilibrium in the microcanonical ensemble at 300K. The frequency of capturing heat current has been evaluated by calculating the convergence of the total heat current auto-correlation. We chose every 5 femtoseconds to calculate the heat current, modal heat current and kinetic energy of every mode without losing accuracy. We did not observe any difference in total thermal conductivity when using smaller time steps. By computing the mode kinetic energy correlation, which is NMA method [22,23], we then obtained the mode relaxation times. The cut-off of the heat current correlation is set to be 500 ps, much longer than the largest relaxation time calculated in the system, which is less than 100 ps.

Figure 4.10 demonstrates IPR and DOS for three potentials. The a-Si structure generated by three potentials produce similar density of states and are in a good agreement with experiments [117]. The IPR shows how localized a vibrational mode is [16]. The locons have high IPR values. From Fig 4.10 (a), the cut-off between diffusons and locons from three potentials are also close. Based on Fig 4.10, we conclude that similar structures are generated by three potentials.

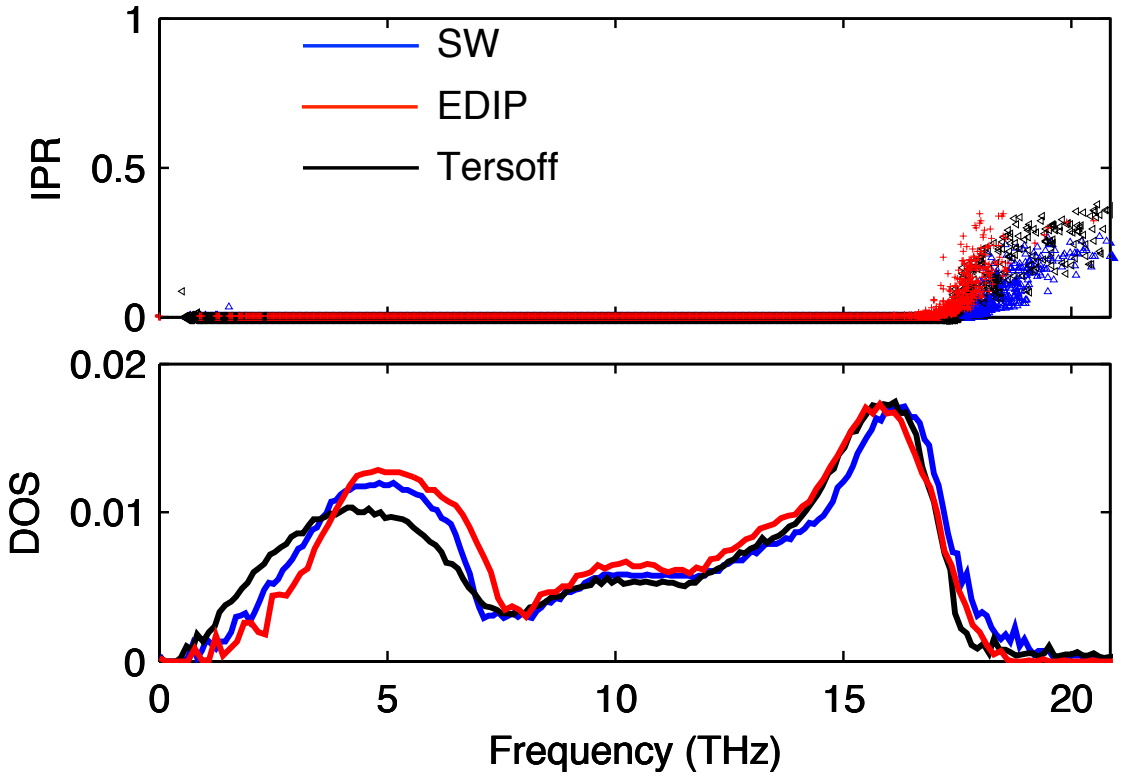

Figure 4.10 (a) Inverse participation ratio of modes in a-Si calculated using SW, EDIP and Tersoff potentials; (b) Phonon density of states of a-Si calculated using SW, EDIP and Tersoff potentials.

Figure 4.11 shows the relaxation times calculated from three different potentials for a-Si at 300K. The relaxation times are calculated NMA [25,94]. The results are consistent with previous results published before using Tersoff [67] and SW [68] respectively. The magnitude of the relaxation times computed by EDIP and SW are similar. We obtained the relaxation times using Tersoff potential, which are close to the results He et al. calculated [67] using the same potential. Although the DOS and IPR of Tersoff are close to the other two potential results, the relaxation times are very different. From Fig. 4.13 (a), we find that the temperature dependent thermal conductivity calculated from GKMA using Tersoff and SW

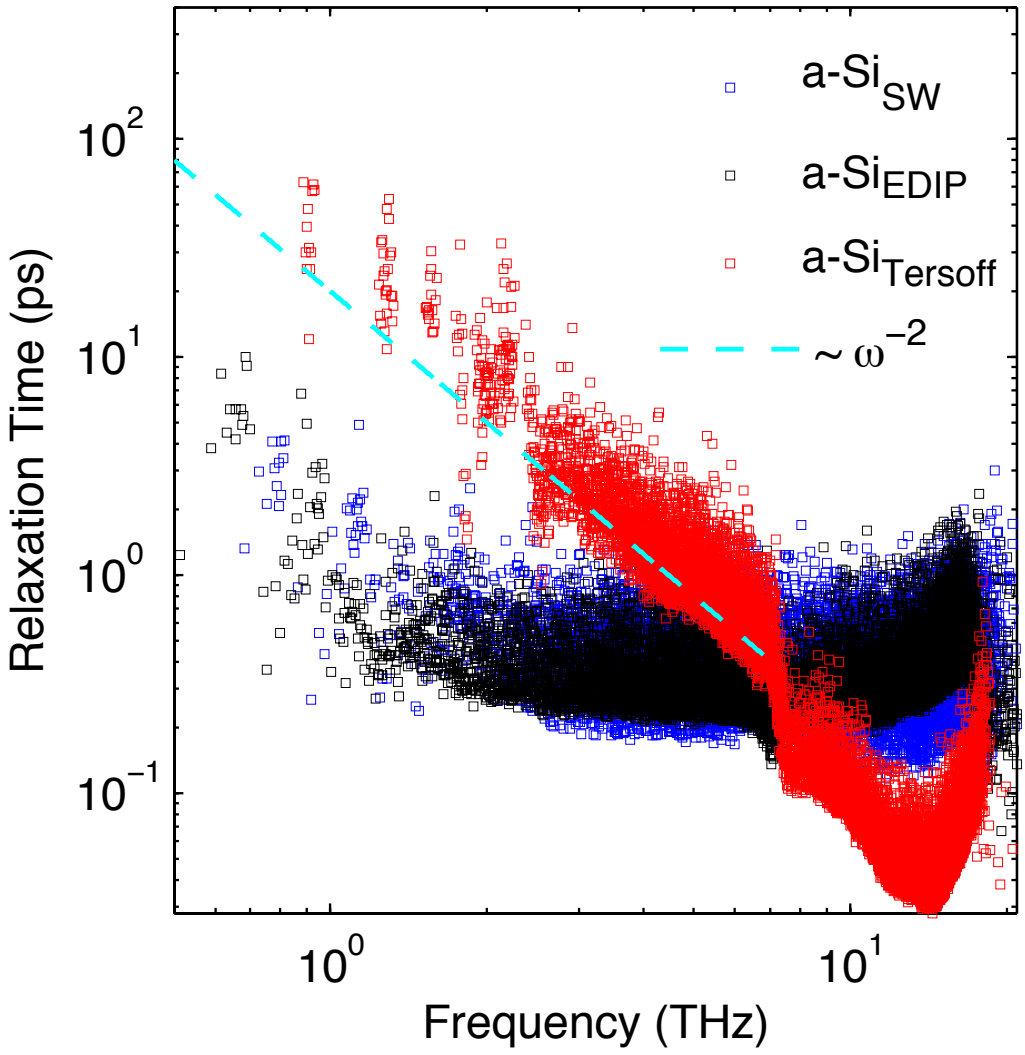

Figure 4.11 Relaxation times calculated from GKMA for amorphous silicon using three potentials (SW, EDIP, Tersoff). The dotted cyan line represents $1/\omega^2$ relation.

are very close, even though the relaxation times from these two potentials are orders of magnitude different. Since the relaxation time is the inverse of the scattering rate, one can relate the relaxation time with the degree of anharmonicity in the system. The higher the anharmonicity, the lower the relaxation time is. Based on PGM, the mode thermal conductivity is proportional to the mode relaxation time. We demonstrate that the thermal conductivity calculated from two potentials for amorphous silicon is not proportional to

the relaxation time respectively, which add another evidence that the relaxation time is not the proper descriptor for calculating the thermal conductivity [95] and question the validity of PGM for amorphous materials [3].

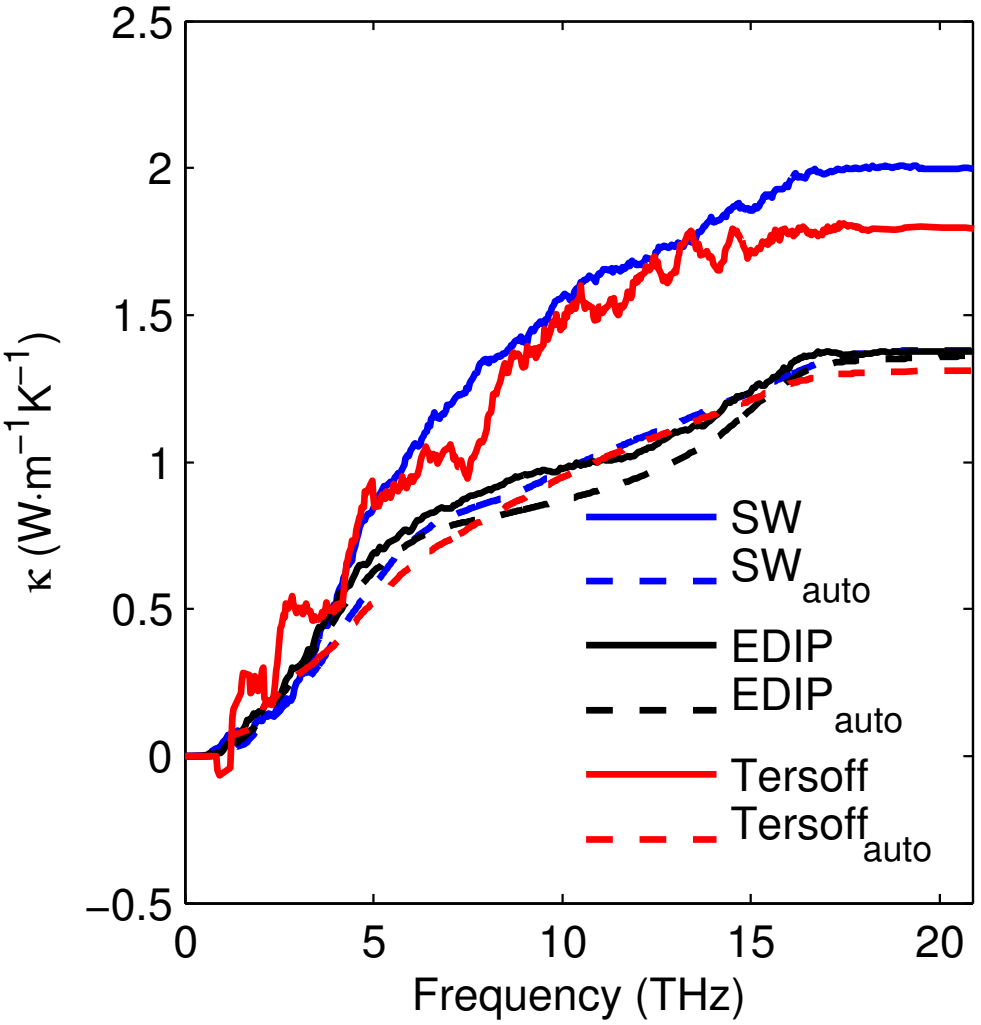

Figure 4.12 Thermal conductivity accumulation with frequency calculated from GKMA of amorphous silicon using three empirical potentials (SW, EDIP, Tersoff). The dotted curves are the auto-correlation accumulations. All the autocorrelation accumulations are close to the A-F result. And for EDIP, the total correlation accumulation is close to its autocorrelation.

We then applied GKMA on a-Si using Tersoff, SW and EDIP potential at room temperature (300K). Figure 4.12 shows the thermal conductivity accumulation with phonon frequencies. The spectral thermal conductivity calculated using GKMA with

Tersoff and SW potential is very close, however EDIP predicts lower thermal conductivity than the other two. On the other hand, the EDIP result is close to the results calculated by Feldman et al. using A-F method [19]. Interestingly, the mode auto-correlations between these three are all similar and close to the A-F results. The difference between GKMA results from two (Tersoff and SW) potentials and A-F results comes from mode cross-correlations. EDIP predicted the thermal conductivity lower than the other two potentials. Because the EDIP result has little contributions from cross-correlations, which makes EDIP result close to the A-F result.

After applying quantum correction, Tersoff and SW predicted temperature dependent thermal conductivity is in good agreement with the experimental results as shown in Fig. 4.13 (a). The EDIP predicted thermal conductivity is close to A-F result. However A-F method is based upon harmonic approximation. In order to understand the discrepancy between EDIP result and Tersoff, SW result, we conduct further analysis to understand the degree of anharmonicity of the three potentials. In order to quantify the magnitude of anharmonicity in the three potentials, we employ the method developed by Gordiz and Henry [114]. Using this method, one first excites an individual mode based on the amplitude of mode at 300K, then calculates each atom's anharmonic energy. The absolute values of the difference between total anharmonic energy and harmonic energy at 300K of each atom in this mode are calculated to represent the magnitude of the mode anharmonicity. The results are shown in Fig. 4.13 (b), one can observe that anharmonic energy of EDIP is lower than the other two potentials, which means the EDIP is the most harmonic potential for a-Si among three empirical potentials. Because the anharmonicity of EDIP is lowest, the cross-correlation hence becomes negligible. It supports the

hypothesis that the anharmonic interactions increase the cross-correlations. Another important observation is that although the degree of anharmonicity between SW and Tersoff are very different, the temperature dependent thermal conductivity result is very similar. Hence we conclude that the accuracy of anharmonicity may not be important and the higher anharmonicity increase the thermal conductivity in amorphous materials.

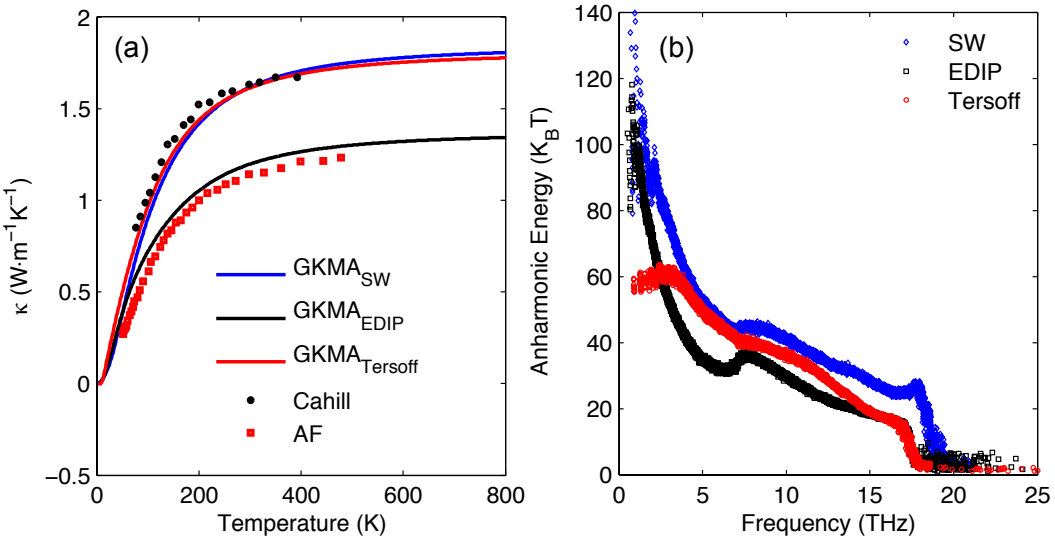

Figure 4.13 (a) Temperature dependent thermal conductivity calculated from GKMA of a-Si using three empirical potentials (SW, EDIP, and Tersoff). Together with the A-F result [4] and experimental result from Cahill et al. [17]; (b) Anharmonic energy per mode for the three empirical potentials on a-Si. Please note that we add the absolute value of anharmonic energy on all atoms for one mode in order to compare the magnitude of anharmonicity in these three potentials.

In crystalline materials, however, the anharmonicity decreases the thermal conductivity [1]. Because the anharmonicity increases, the phonon scattering rates increases, hence the relaxation time, which is the inverse of scattering rate, decreases. In order to verify the anharmonicity calculation, we calculate the magnitude of the anharmonicity of modes using the same three potentials in c-Si. The result is shown in Fig. 4.14 (b) EDIP and SW has similar magnitude of anharmonic energy, and the Tersoff

has much higher anharmonicity. We then demonstrate in Fig. 4.14 that the thermal conductivity calculated using Tersoff potential has much lower thermal conductivity than SW and EDIP results. Note that the Tersoff potential we used here is from Munetoh et al. [65], which is the same empirical potential we used for a-Si. The results in Fig. 4.14 (a) verified the correctness of the anharmonicity calculation. The conclusion is consistent with the PGM that the anharmonicity reduces the thermal conductivity for crystalline materials.

Based on all the calculated results, we believe that the anharmonic interactions contribute to the thermal conductivity of amorphous silicon, and it is necessary to include the anharmonicity to accurately predict the thermal conductivity of amorphous solids.

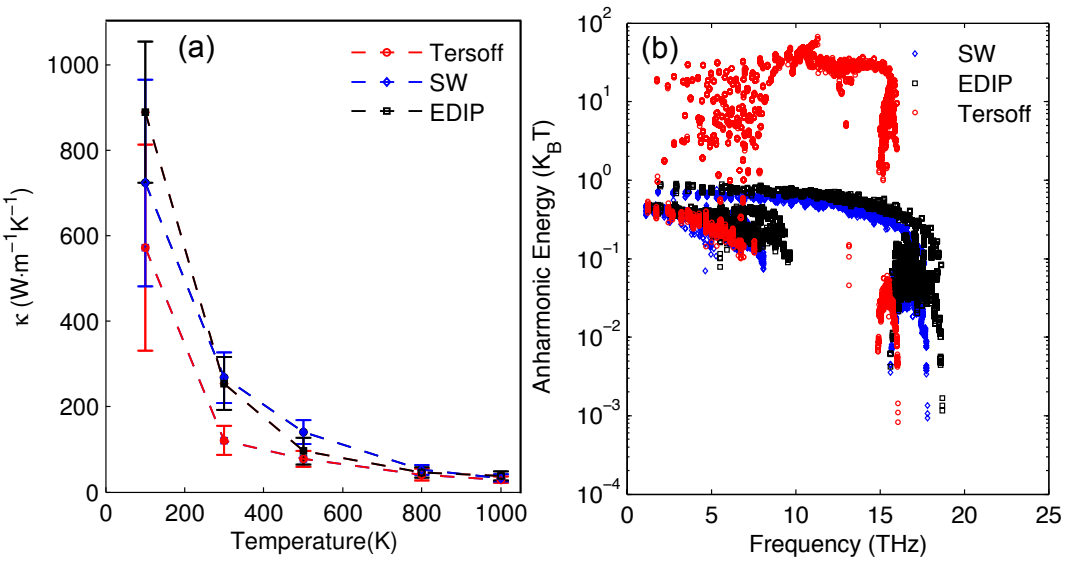

Figure 4.14 (a) Temperature dependent thermal conductivity calculated from Green-Kubo of c-Si using three empirical potentials (SW, EDIP, and Tersoff), each data point is averaged over 10 ensembles; (b) Anharmonic energy per mode for the three empirical potentials on c-Si. Please note that we add the absolute value of anharmonic energy on all atoms for one mode in order to compare the magnitude of anharmonicity in these three potentials.

In this section, we applied GKMA on a-Si using different empirical potentials including Tersoff, SW and EDIP. The spectral thermal conductivity calculated by GKMA using Tersoff and SW are very similar, hence the temperature dependent thermal conductivity calculated from these two potentials is also similar to each other and in good agreement with the experiments. However the relaxation time calculated using Tersoff and SW potentials are significantly different. As for EDIP, the predicted thermal conductivity of a-Si is dominated by the mode auto-correlations. Its spectral thermal conductivity and temperature dependent thermal conductivity is close to the A-F result, which is based on harmonic approximation. We then quantified the magnitude of anharmonicity of these three potentials at room temperature for a-Si [114]. We discover that the magnitude of the anharmonicity from SW and Tersoff are much higher than EDIP for a-Si. The anharmonicity is shown to increase the thermal conductivity of amorphous materials from atomistic level simulations as Payton et al. predicted using one- and two-dimensional lattice models [118]. In GKMA, the anharmonic interactions are represent as the non-diagonal terms or the cross-correlations for amorphous materials. Due to the nature of the vibrational modes of amorphous materials, the anharmonicity plays a different role in the amorphous materials comparing it with crystalline materials. As a result, we find 3rd evidence to disprove the feasibility of PGM on amorphous solids.

Thus far, we find anharmonicity plays an important role in amorphous solids. In section 4.2, we find that the relaxation time is not a proper descriptor for thermal conductivity in amorphous solids. In this section, we discover that the increasing in anharmonicity raises the thermal conductivity. All these phenomena are counterintuitive base on the PGM, which intrigues us to check a related parameter, MFP in amorphous

solids. If the MFP is still applicable in amorphous solids, when anharmonicity increases, MFPs may increase. If this is the case, we will observe a very different size effect in amorphous solids.

However based on PGM, the diffusions should not have any size effect. Because diffusons are not propagating modes, they should not carry the heat longer than the system boundary. On that account, the study on the diffusons' size effect in amorphous materials can be another test of the feasibility of PGM on amorphous solids, hence we will discuss it in the next section.

4.5 Diffusons can exhibit size effects

Diffusons, as discussed in Chapter 2, are extended modes without a well-defined wavevector. Diffusons are the dominant vibrational modes (>90% of the total number of modes) in amorphous solids [16,112]. Due to the lack of the definition of the wavevector, one cannot rigorously calculate their phonon group velocities. Since the diffusons are not propagating, previous researchers claim the diffusons do not travel in the structure [40,59]. Based on the PGM, phonon velocity of diffusons approaches zero, hence the MFP is close to zero. Allen et al. [18] also argued that "diffusive propagation occurs over any meaningful distance, and the concepts of mean free path and wavevector lose usefulness. "

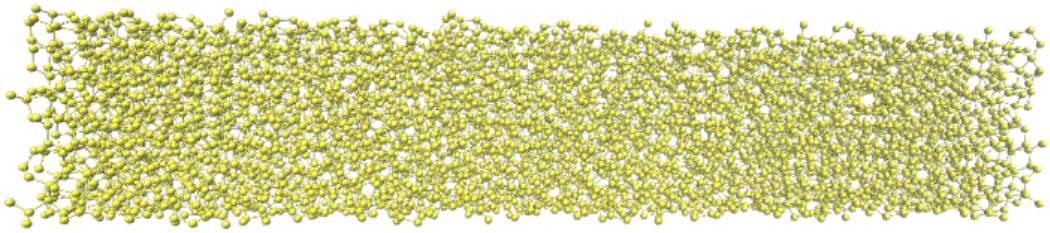

Figure 4.15 a-Si thin film atomistic structure.

GKMA can accurately predict the thermal conductivity of non-crystalline materials. Hence we can quantify the decrease of the mode thermal conductivity when reducing the system dimensions. In order to compute it, we first generate a thin film a-Si structure as shown in Fig. 4.15. The a-Si thin film structure consists 5000 atoms, with about 5 nm * 5 nm * 14 nm dimensions. Similar to bulk amorphous silicon, the initial amorphous structure comes from WWW random walk algorithm [66]. . The initial structures were annealed at 1100K for 10 ns in order to avoid structural meta-stability [68]. In order to form the thin film structure, we add 10 Å vacuum (empty space) between two ends of the structure along 14nm direction. The vacuum causes the atoms on the surface to restructure when relaxed. Then the LD and GKMA are applied on the final thin film structure. The time step of the simulation was 0.25 fs and after 500 ps equilibration with NVT, the modal heat currents were written every 1 fs for 6 ns at equilibrium in the microcanonical ensemble at 300K.

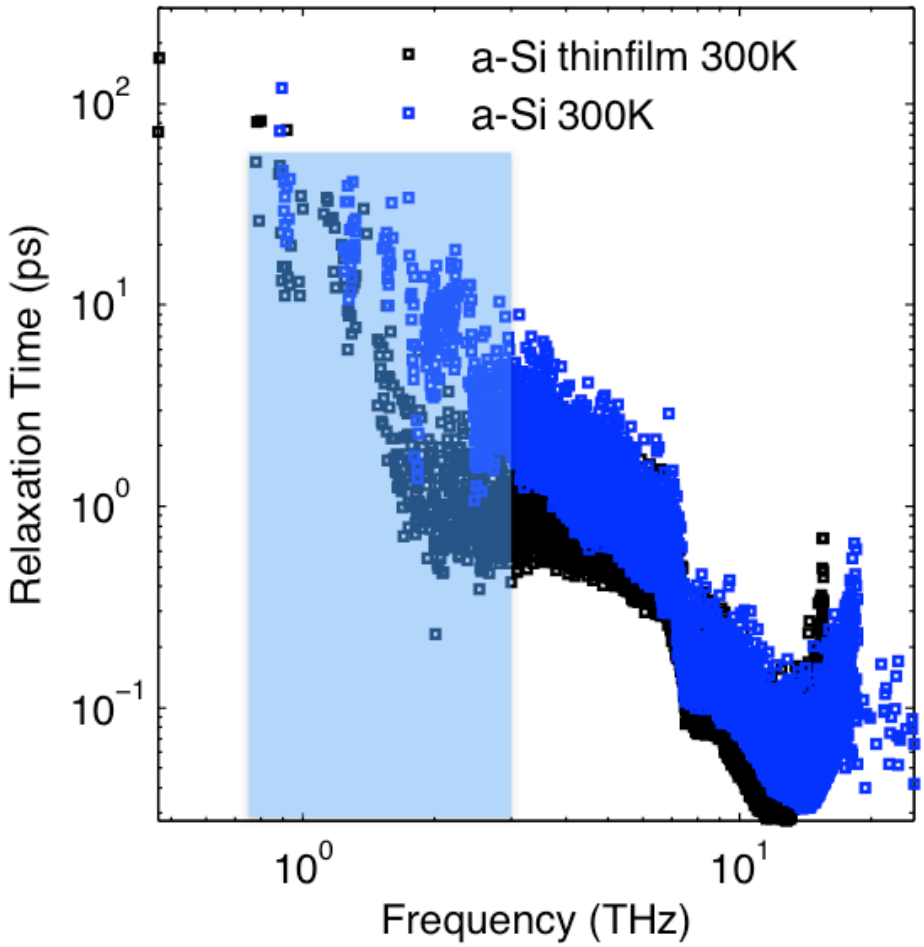

Figure 4.16 Phonon relaxation times from bulk a-Si and a-Si thin film at 300K.

Figure 4.16 shows the relaxation times in the thin film and bulk a-Si at room temperature. The blue shaded zone represents the propagon region. Since the propagons are propagating modes, they typically can travel longer distance before scattering with other phonons, or boundaries. In the thin film case, the propagons hit the boundaries first before they scatter with other phonons. Therefore, the phonon relaxation time of modes in the propagon region decrease significantly. PGM explains the size effect of the propagating modes very well.

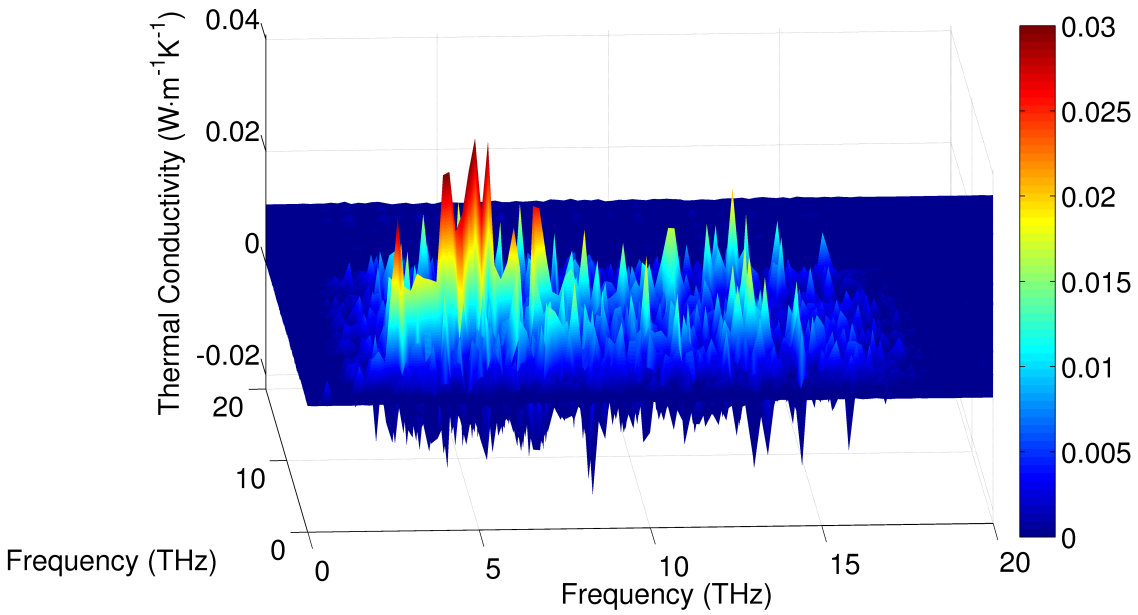

Figure 4.17 Thermal conductivity 3D correlation map of bulk a-Si thin film (cross-plane direction) at 300K.

Figure 4.17 shows the correlation maps of a-Si thin film from GKMA. The peaks represent the mode thermal conductivity contributions from mode-mode correlations. Comparing with the bulk Si 3D correlation map in Fig. 3.4 (a), the magnitude of the low frequency modes reduce a lot on the diagonal directions that are the autocorrelations. However the mid and high frequency modes that are diffusons seem to decease significantly as well.

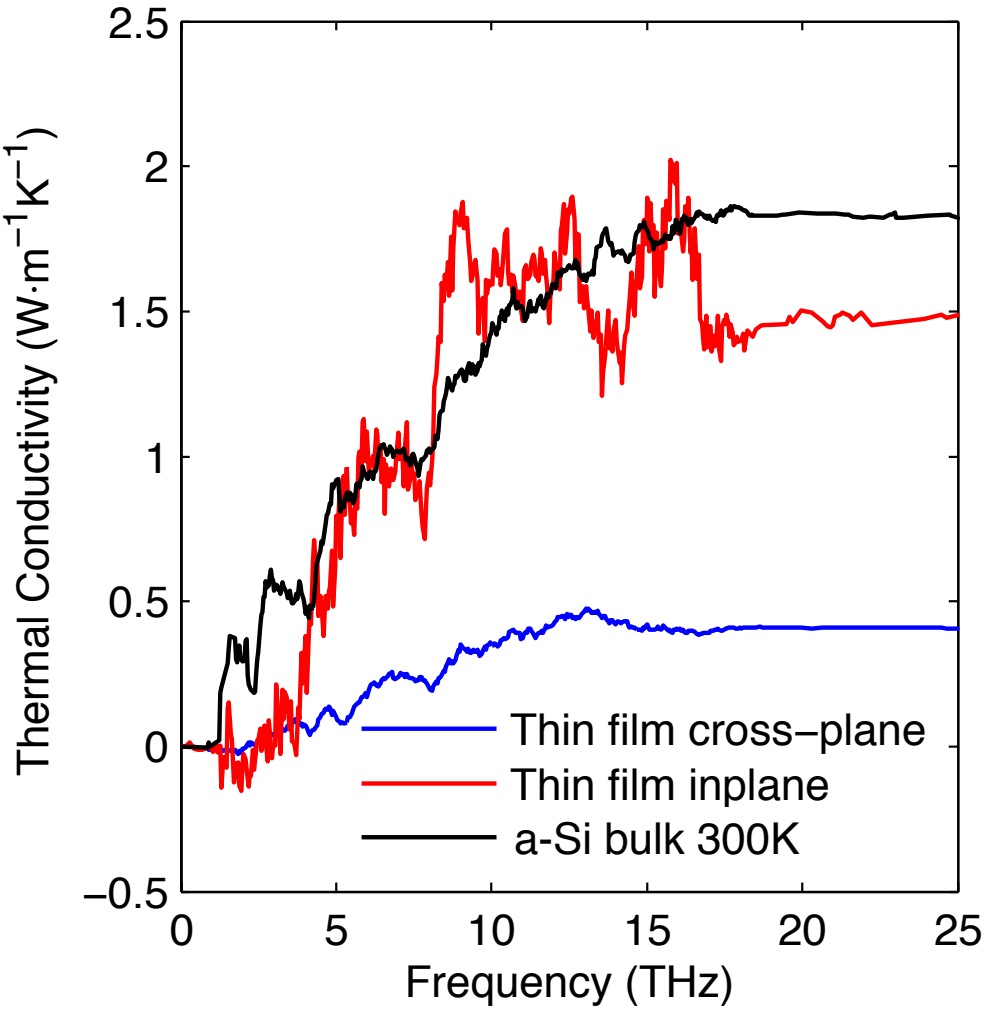

Figure 4.18. Thermal conductivity accumulation of bulk a-Si and a-Si thin film (cross-plane direction) at 300K.

In Fig 4.18, we demonstrate that the thermal conductivity accumulation for the in-plane and cross-plane directions of a-Si thin film and comparing with the bulk a-Si. The red curve shows the thermal conductivity accumulation in the in-plane direction of the thin film a-Si. The size effect is not as dramatic as in the cross-plane direction. However one can still observe the drop of the mode thermal conductivity for propagons and diffusons (frequency above 8 THz). In the cross-plane direction, the size effect is more significant than the in-plane direction as the blue curve shows in Fig. 4.18. More

interestingly, not only the propagons (0~2 THz) thermal conductivity decreases, but also the diffusons' contribution declines substantially comparing with bulk a-Si.

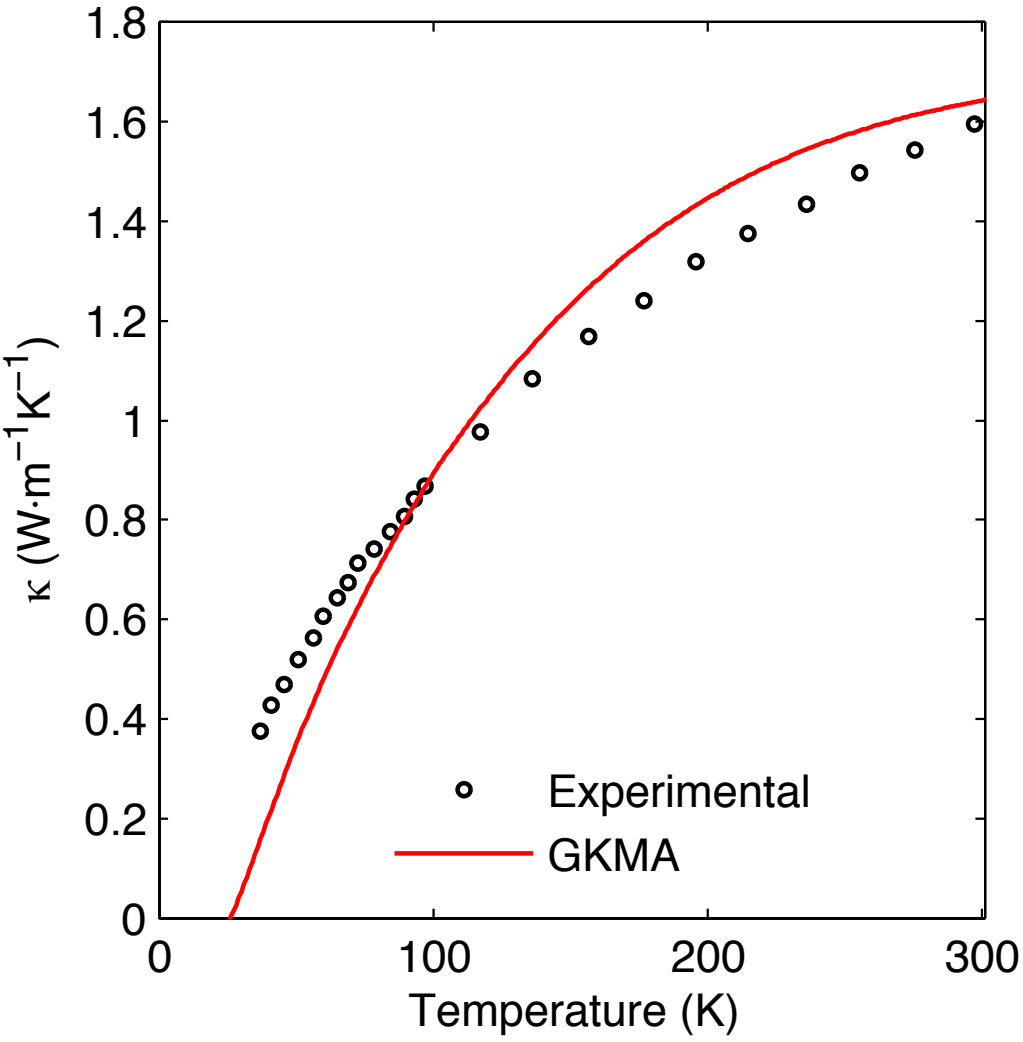

Figure 4.19 Temperature dependent thermal conductivity (in-plane) from GKMA and experimental results of a-Si nanowire [119].

This is the first numerical evidence that the diffusons have size effect. One cannot explain this phenomenon using a PGM based rationale for thermal conductivity, since the diffusons are non-propagating modes without a well-defined group velocity hence they should not have size-effect or boundary scattering effect. Using GKMA, based on the linear response theory, the decline of the mode thermal conductivity owing to the mode

heat current becomes less correlated to the total heat current of the system. At last, we compare the a-Si thin film in-plane thermal conductivity from GKMA (100K and 300K result) with the experiments results, as shown in Fig 4.19. The results from GKMA are again in very good agreement with the experimental results [119].

In this section, we demonstrate that both propagons and diffusons show length scale dependence. So far, we showed four case studies on amorphous solids. All four cases disprove the validity of PGM on disordered materials. And the correlation paradigm and GKMA are able to explain all of them. All four case studies are conducted on the disordered systems. However, as we discussed in section 3.5, even in an ordered single polymer chain, the GK predicted thermal conductivity has significant deviation from the PGM. Since PGM used the stosszahlansatz assumption, it becomes improper to explain the divergent thermal conductivity. If one assumes that it is still somewhat applicable, the only explanation for the anomalous thermal conductivity observed in single polymer chains is that certain phonon modes have infinite relaxation times. However we find out the relaxation time is finite and no significant difference between divergent and convergent cases for the highest thermal conductivity mode. The persistent correlations are the cause of the divergence based on previous study [31]. This problem again needs a new physics picture to understand. The correlation paradigm or GKMA seem to be the best method to explain the divergent thermal conductivity. In the next section, we will continue using GKMA study on the single Pth chain and identify the cause of the divergence.

4.6 Understanding polymer thermal superconductivity through sonification

In the previous sections, we have shown four cases where the PGM fails to describe disordered materials. In the proceeding section, we will demonstrate that even in an ordered polymer chain, the thermal conductivity results deviate from the PGM. Following the PGM, one can predict the maximum thermal conductivity for a finite polymer chain, because the maximum MFP for a phonon in a finite chain is the chain length. However in GKMA, the thermal conductivity is calculated by the HFAC, hence there is no such limitation. In section 3.5, we demonstrated the divergent thermal conductivity in single Pth chains, but based on the PGM, this divergence requires an infinite relaxation time.

To test whether the PGM works for a single polymer chain, we calculate the finite chain thermal conductivity using GK and compare with PGM predictions and also verify if the divergent mode has infinite relaxation time. In section 3.5, we have shown that two transverse acoustic branches are responsible for the divergence. In the proceeding section, we determine which mode on the acoustic branch is responsible for the divergence and discover the cause of the divergence.

We simulated Pth chains without PBC using one unit cell of rigid atoms (i.e., atoms with infinite mass) on each end to mimic a finite chain. This was done to prevent an individual chain from coiling, which is a potential problem for very long chains. Using this modification, phonon propagation is restricted by the chain length. These simulations still used EMD but not PBC, a 0.15 fs time step, and were run for 3 ns at equilibrium in the microcanonical ensemble with 100 ps of equilibration time. Five independent

simulations were run for each chain length for better averaging. Each data point is averaged over 15 ensembles to avoid statistical fluctuations. The results of the finite chain simulations are shown in Fig. 4.20 and indicate that a large deviation from the trend at 90 unit cells (ucs). The GK results are almost always higher than the PGM limit. The PGM limit is calculated by the largest group velocity times the mode specific heat and chain length for all the acoustic modes. The optical modes were neglected in the calculation, because their contribution to the thermal conductivity is negligible, as shown in Fig. 3.22. GK results deviate from the PGM, especially for the 90ucs chain, which has caused us to question the feasibility of the PGM for single polymer chains.

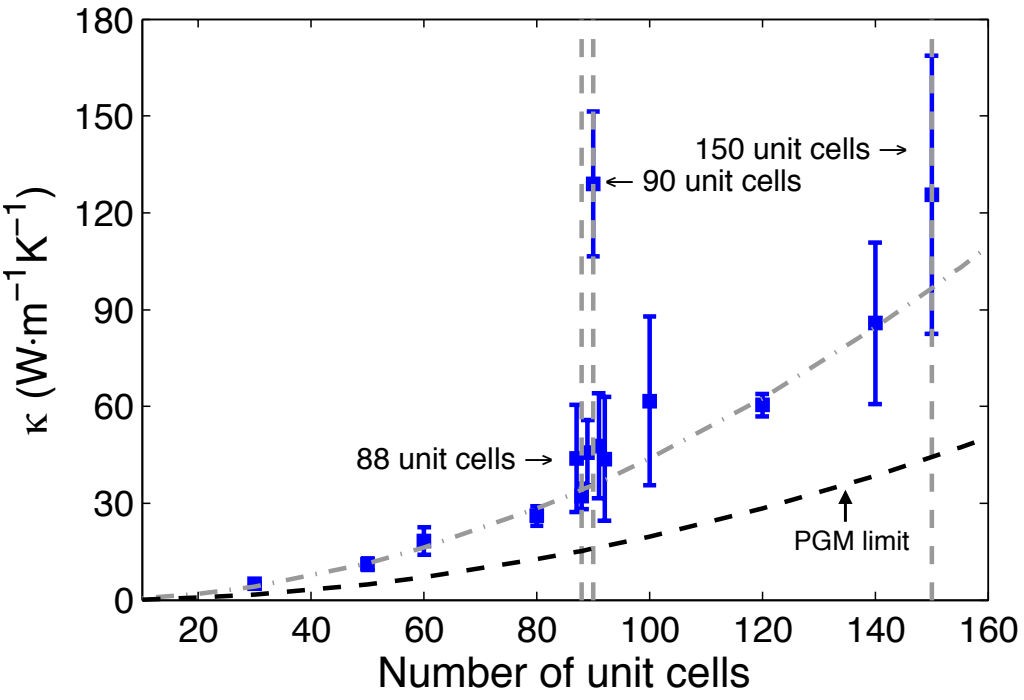

Figure 4.20 Finite Pth Chain thermal conductivity versus chain length. The dash-dot line is a trend line fit to the non-anomalous data. The dash line represents the PGM limit.

In the simulations using PBC, we observed divergence for chain lengths at multiples of 30 ucs and, interestingly, Fig. 4.20 shows that even without PBC, we observe anomalous behavior for chains with multiples of 30 ucs. The short length multi-30 ucs chains (30 ucs and 60 ucs) do not behave differently, presumably because when the system length is too small, the long wavelength phonons are constrained by the boundary scattering. However, what is particularly interesting is the difference between 88 ucs and 90 ucs. The two chain lengths only differ by 1.5 nm, yet the difference in thermal conductivity is a factor of four, which is quite anomalous. This result suggests that the anomalous behavior arises from specific interactions that occur in chains with a very specific length, such as multiples of 30 ucs. From Fig. 4.20, we also observe that the thermal conductivity of 90 ucs and 150 ucs are similar in magnitude. It is likely a very specific relationship and interplay between the mode energies and momenta that gives rise to the anomalous behavior, since slightly shorter or longer chains have modes with very similar wavelengths and frequencies, but not chain lengths that are an exact multiple of 30 ucs. It is also important to note that the phenomenon can become less pronounced for longer chains, whereby the presence of other modes opens up additional channels for phonon interaction sequences. This could be the reason the 150 ucs chain in Fig. 4.20, has almost the same thermal conductivity as the 90 ucs chain and not a much higher value.

Computing the power spectrum of the HFAC, the dominant frequency shifts dramatically between chains with similar lengths and is peaked around 0.1 THz for the anomalous 90 ucs chain. This frequency corresponds to atom vibrations close to 0.05 THz (50 GHz), since Q is proportional to the atom velocities and Q is squared in the

HFAC, such that the mode frequency is half that of the HFAC frequency. Figure 4.21 shows that the heat current for chains with 90 and 150 vibrating unit cells has a dominant frequency at 0.1 THz, while other chains have different peak frequencies. Figure 4.21 (c) shows that the modes near 0.05 THz exist in both 88 and 90 ucs chains, yet the frequency peaks in Fig. 4.21 correspond to significantly different areas of the spectrum.

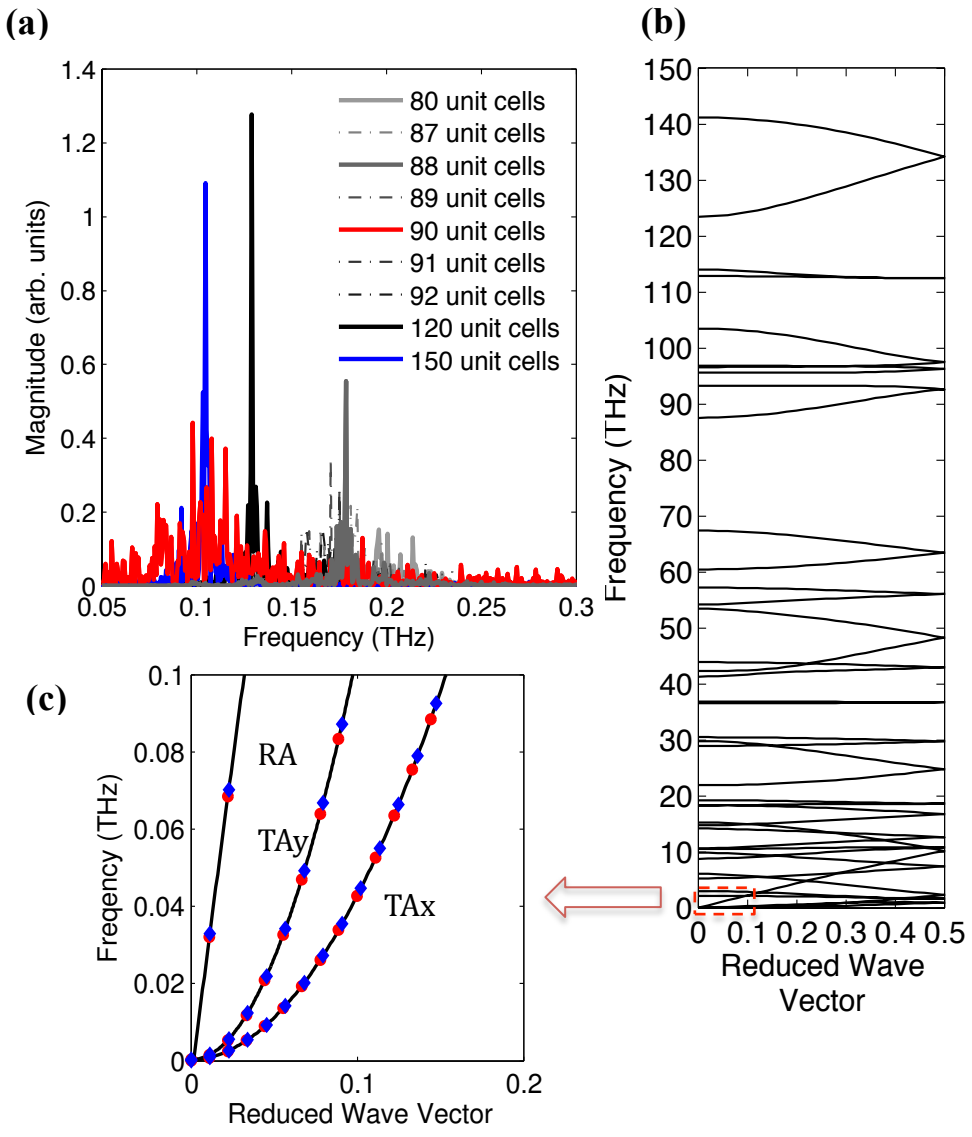

Figure 4.21 (a) Power spectrum of the HFAC of different length Pth chains, from the finite chain simulations. (b) Phonon dispersion curves for a single Pth chain. (c) Zoomed in close up view of the dispersion curves near 0.05 THz, only 3 acoustic branches exist in this range. The discrete

modes that exist in the 90 ucs (red circles) and 88 ucs (blue diamonds) modes indicate that the modes are very similar in both cases, even though the HFAC power spectra differ significantly.

Upon examination of the HFAC for the chains with PBC and the chains without PBC, approximately 0.8 ns of time delay are needed to reach a thermal conductivity of 120 W m^{-1} K^{-1}. This time scale is three orders of magnitude longer than the time necessary for modes with frequencies near 0.05 THz to reach the chain ends and scatter. This discrepancy is important because it suggests that somehow these modes are able to remain correlated even after encountering the chain ends. For comparison, consider the maximum thermal conductivity contribution a mode can have as predicted by the PGM/BTE. For a mode in a 1D system to transfer energy and contribute to the thermal conductivity, it must scatter at the chain ends. The group velocity for the modes near 0.05 THz is ~ 820 m/s, which suggests that if the high thermal conductivity is due to modes in this frequency range, and they remain correlated for 3 ns, they are somehow unperturbed by the chain ends since they must encounter the chain ends every 0.0873 ns. Using the PGM, the thermal conductivity contribution from a mode is given by $\kappa(k,p) = cv_g l$, where c is classical specific heat, k_B / V, v_g is phonon group velocity, and l is the phonon MFP, which at its maximum, is equal to the chain length. Using this model, the thermal conductivity of this mode can only be as large as 0.0443 W m^{-1} K^{-1}, which is in stark contrast to our result of ~ 120 W m^{-1} K^{-1}.

The finite chain analysis also disproves that divergent thermal conductivity is an artifact caused by PBC. The fact that there is correspondence between the chain lengths that exhibit the divergence in the PBC cases and the finite chains without PBC that exhibited anomalously high thermal conductivity suggests that the divergence is not

caused by the PBC, even though it can occur using PBC. Using PBC allows the thermal conductivity to diverge, but the fact that anomalous behavior is also observed at the same chain lengths without PBC indicates that it is not the cause of the divergence. Instead the divergence is most likely associated with the specific modal interactions in chains with multiples of 30 ucs and not the PBC itself. To understand the phenomenon more deeply and find the cause for the divergence, we used the GKMA formalism [16] to study the divergent behavior in more detail.

In examining the divergence in Pth, the first objective was to identify which modes are responsible for the divergence by determining which phonon polarization contributes most to the thermal conductivity. In the section 3.5, we identified two transverse acoustic branches which are most responsible for the divergence. Figure 4.22 (a) shows that the transverse acoustic modes that correspond to vibrations in the plane of the aromatic rings (TA-y) and out of the plane (TA-x) contribute most to the total thermal conductivity in 30 unit cell chains. In Fig. 4.22 (b) we show the divergent and convergent comparison for these two branches. The results are averaged over 35 ensembles (10 divergent cases, 25 convergent cases). If the TA-y and TA-x branches diverge then the total thermal conductivity diverges and vice versa.

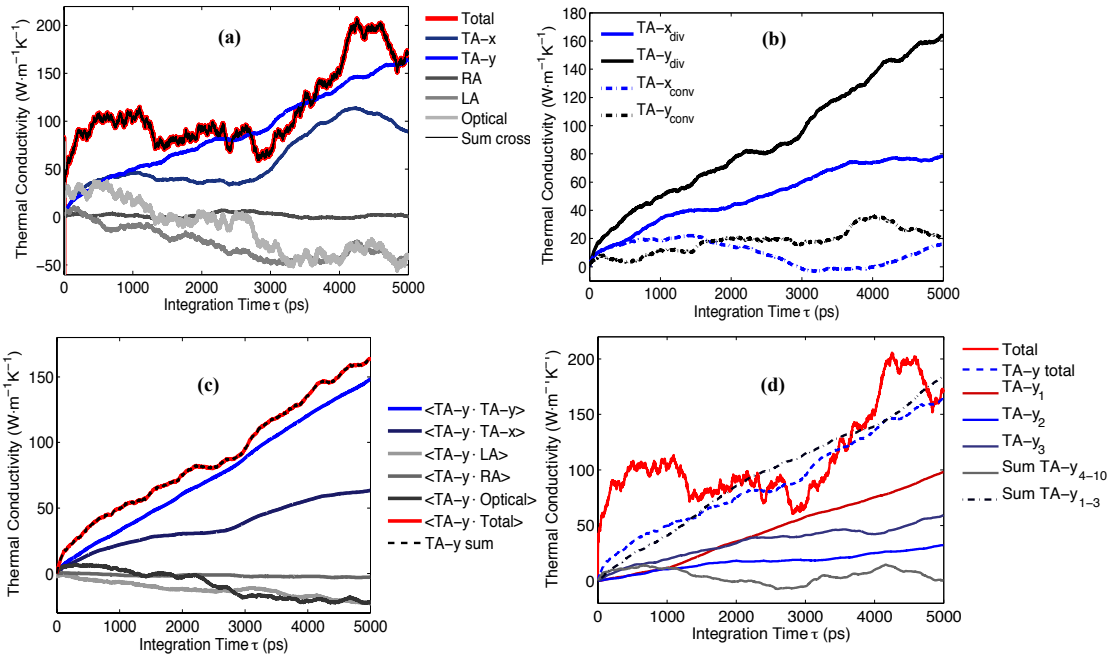

Figure 4.22 Thermal conductivity contributions from different polarizations, TA-y branch and TA-y_1 mode thermal conductivity contributions. (a) Pth thermal conductivity contribution from different branches. (b) TA-x, TA-y branch thermal conductivity contributions in convergent and divergent cases, averaged over 30 ensembles. (c) TA-y cross-correlations with other branches. (d) TA-y thermal conductivity from each mode on the branch.

Using the GKMA approach, we can also study the correlation between individual branches and individual modes. In the following we focused on the TA-y branch since it contributes most to the thermal conductivity. Using Eq. 2.43 we examined the TA-y branch's correlation with other branches, and as shown in Fig. 4.22 (c), the autocorrelation of the TA-y branch is most important. With the focus on TA-y mode-mode interactions, we computed the individual mode contributions to the TA-y branch to determine which of the modes is most responsible for the divergence. Figure 4.22 (d) shows that the lowest frequency mode on the TA-y branch contributes the most and when combined with the other 3 lowest frequency modes on the TA-y branch, the three modes (out of 30 total modes) comprise almost the entire thermal conductivity for the entire branch (Note that this includes the symmetric +k and –k modes, which are identical). The

fact that the divergence is associated with the lowest frequency modes seems consistent with the ideas of mode coupling theory. However, mode-coupling theory suggests that the divergence arises because the long-wavelength modes have very slow energy diffusion, – in other words, long (infinite) relaxation times. If one uses the PGM to explain the divergent thermal conductivity, the velocity is finite and specific heat is constant, hence the infinite relaxation time is also the only possible interpretation.

To determine if infinite relaxation time is the most suitable explanation for the behavior observed in Pth we calculated the relaxation times of these low frequency modes using the NMA method [51]. By comparing the relaxation times for converging and diverging cases, we can determine if the difference in thermal conductivity can be explained by a lack of scattering or a lack of interaction with other modes. The relaxation time of the lowest frequency modes on TA-y branch calculated in divergent and convergent cases are very close (roughly between 100-300 ps). Fig. 4.23 shows the energy autocorrelation functions for a convergent and divergent case. In both cases the autocorrelations decay. Similar to the phenomenon observed before, [28] the autocorrelations for the divergent cases show a significant resurgence in correlation at much later times, but the integration still remains of similar magnitude to the convergent cases. From the relaxation time analysis, there is no major difference between converging and diverging cases, and in both cases the relaxation times are finite. For this reason, the PGM appears insufficient for describing the divergent behavior in Pth, as the only mechanism available in the PGM for attaining infinite thermal conductivity is for a mode to have an infinite relaxation time.

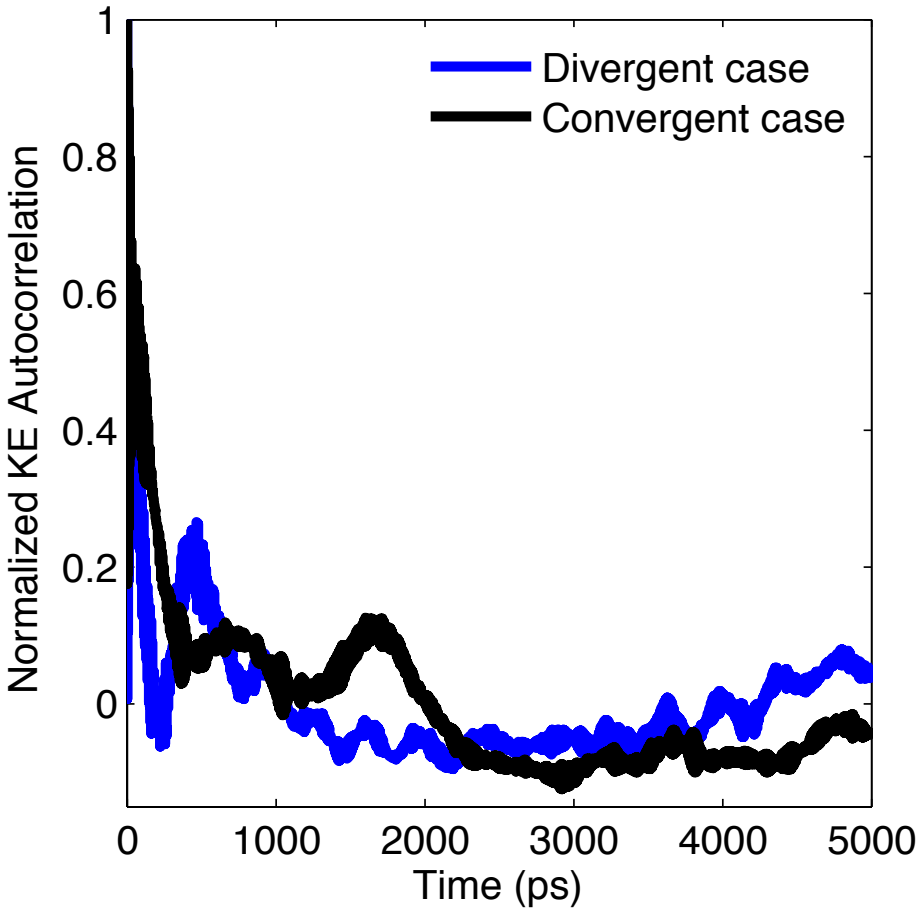

Figure 4.23 Normalized mode TA-y_1 kinetic energy autocorrelation functions in Pth convergent and divergent cases.

From Fig. 4.22 (d) it is clear that over the course of 5 ns, the lowest frequency mode on the TA-y branch (labeled TA-y_1) contributes 100 W m^{-1} K^{-1}. It should be noted here that both the positive and negative k-vector contributions are shown summed together since they are indistinguishable. Such a large contribution from a single mode is anomalous, as 100 W m^{-1} K^{-1} is higher than most elemental metals, which transport heat using many vibrational modes as well as many electrons. However, in Pth, it is remarkable that one single mode is able to transfer so much heat. It is important to emphasize that the contribution of this mode is linearly increasing during the 5 ns of

correlation time computed from Fig 4.22 (d). We have even extended the simulation times by an additional 10 ns (20 ns total, yielding a maximum 10 ns long correlation), and the divergence simply continues along the same path. What is also interesting is that the anomalous conducting mode's frequency is 0.05 THz. This frequency corresponds to the peak in the Fourier transform of Q for the finite chains with lengths that are exact multiples of 30 ucs. For 88 unit cells the peak moves to 0.09 THz, but even on the 88 ucs chain there is a mode on the TA-y branch with a frequency very close to 0.05 THz. It is an anomalous effect of the anharmonicity that two individual chains with such similar lengths (i.e., 88 and 90 ucs) do not exhibit similar modal interactions and thermal conductivity, even though the frequencies and wavelengths in each case are very similar. In addition to the results shown in Fig 4.22, we have used GKMA to study the correlation of the TA-y_1 mode with the other modes on the TA-y branch. The analyses and results show that there are strong cross-correlations/interactions amongst the lowest three modes on the TA-y branch that give rise to the divergence.

Ultimately we seek to understand the behavior of this special anomalous conducting mode (TA-y_1) in more detail. The TA-y_1 mode correlates strongly with the entire TA-y branch as indicated by the <TA-y_1·TA-y> autocorrelation shown in Fig. 4.24. Using GKMA, we calculated mode-mode cross correlations between the TA-y_1 mode and other modes on TA-y branch. By examining the correlation with individual modes we found that the correlation is strongest between the 3 lowest frequency modes (TA-y_1, TA-y_2, TA-y_3), where TA-y_2, TA-y_3 are second and third lowest frequency modes on the TA-y branch. In Fig. 4.25 it is clear that the TA-y_1 autocorrelation and its

cross correlation with TA-y_2, TA-y_3 is very different for the divergent and convergent cases.

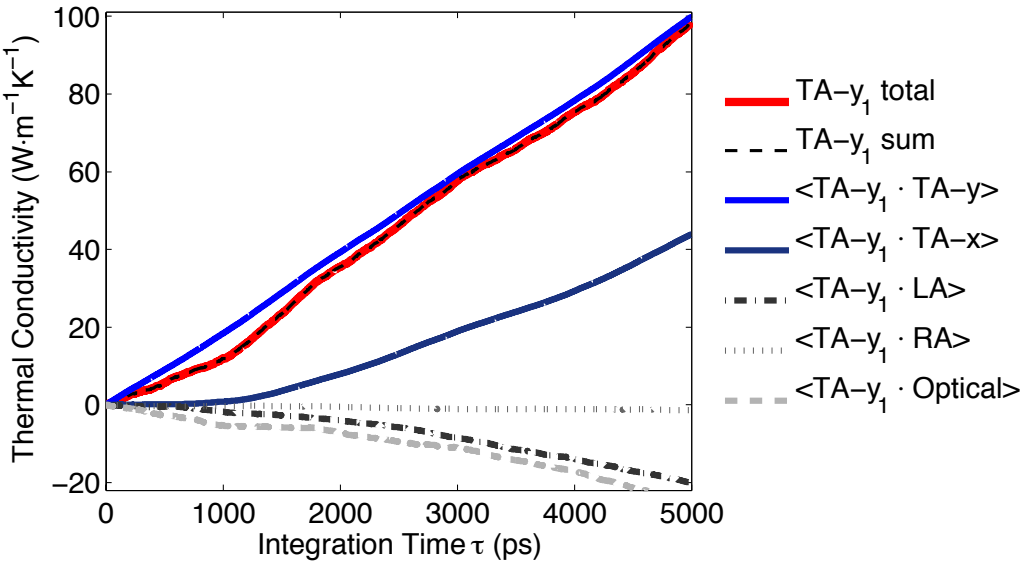

Figure 4.24 TA-y_1 mode thermal conductivity contribution and its correlation with different branches. Note: it includes the contribution of its symmetric mode on the same branch.

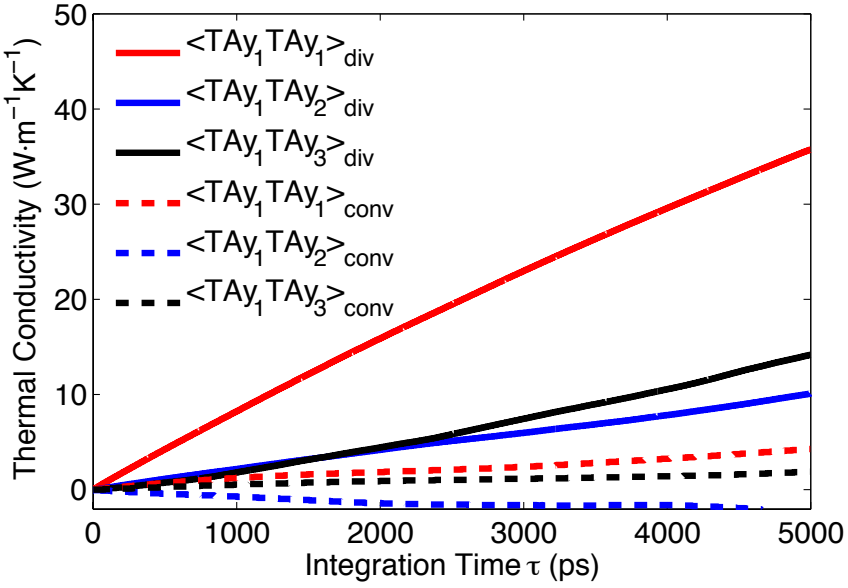

Figure 4.25 TA-y_1 mode thermal conductivity contribution and its correlation with TA-y_2 TA-y_3 in a divergent and convergent case.

With the TA-y_1 mode now identified and the important interactions with other modes now clarified, the last remaining task was to try and develop a better understanding of the underlying mechanism for the divergence. Visual inspection of the heat current for the TA-y_1 modes did not reveal any obvious differences that would indicate what aspects of their heat flows remain correlated and give rise to the divergent thermal conductivity contributions (see Fig. 4.26 (a)). However, the integration of the correlation function clearly indicates that something in the heat currents of these modes is similar and/or repetitious. It should be noted that persistent correlation need not manifests as a periodic pattern occurring on regular intervals. Instead it can merely be some portion of the signal that is recurring, albeit possibly at irregular intervals (i.e., not necessarily rhythmically). Either scenario or any intermediate between these extremes can result in a divergent integral of the correlation functions. Interestingly, we computed the Fourier transform of the total and mode level heat currents for both convergent and divergent cases, as shown in Fig. 4.26 (b). Figure 4.26 (b) shows that there are no major differences in the heat current spectra in the very low frequency regions. Since there was no obvious difference in the frequency content and no obviously significant features obtained from visual inspection, we sonified the mode level heat currents to determine if patterns or any discernable differences would emerge via audible inspection.

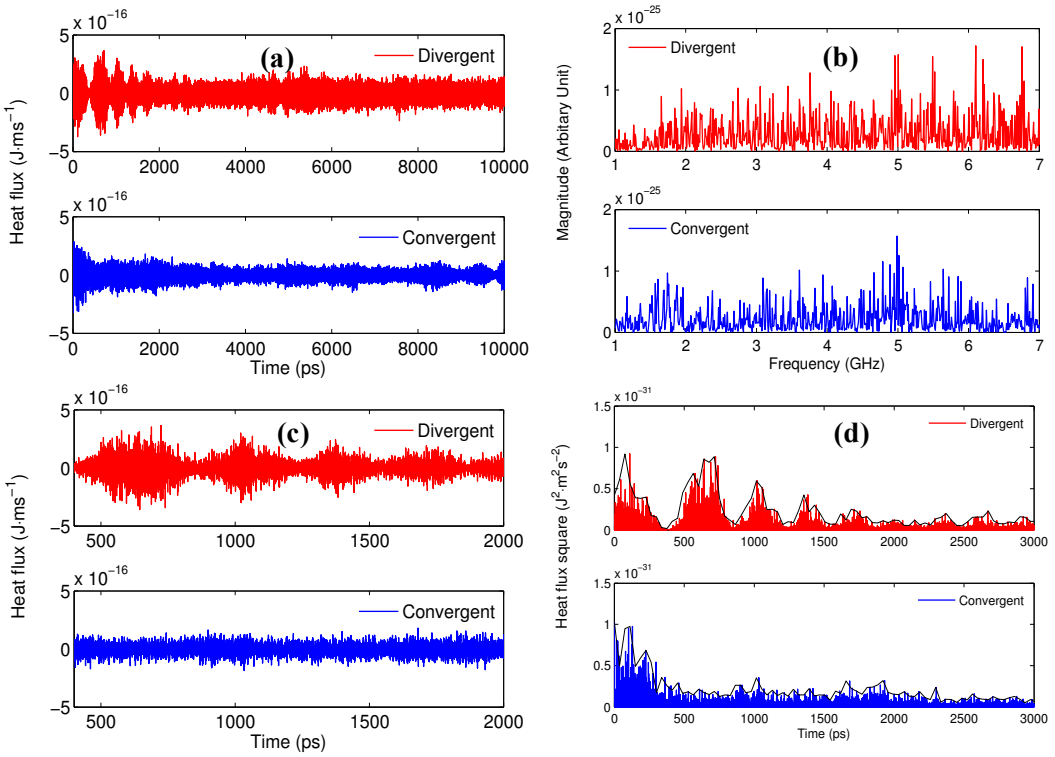

Figure 4.26 (a) TA-y_1 mode heat current for 20 nanoseconds in a divergent and convergent case. (b) TA-y_1 mode heat current power spectra for 20-nanosecond length simulation at low frequency (1-7 GHz) in a divergent and convergent case. (c) TA-y_1 mode heat current zoomed in from 400 ps to 2000 ps in a divergent and convergent case. (d) Square of mode heat current and the envelop function (black curve) in a divergent and convergent case.

Sonification[120] involves slowing down the THz oscillatory data so that it can be studied as an audible sound. The human ear is often much better equipped for identifying oscillating patterns than the human eye; thus sonification can be used to identify features within the data that would go undetected when presented visually. Direct sonification of data has been used in other instances for the same reasons, and in other situations, the data is amended or converted to mimic familiar types of sounds, such as a musical instrument [121,122]. Here, however, we were interested specifically in preserving the original features of the data completely so that the truly distinguishing features between the convergent and divergent cases can be identified and would not be artificially

augmented. The HFAC integral for these two simulations are shown in Fig. 4.27 for reference, which shows that after 5 ns of integration, the convergent case's mode thermal conductivity was 8 W m^{-1} K^{-1}, and the divergent case's mode thermal conductivity was 49 W m^{-1} K^{-1} (6 times larger). In audio files [123], the heat current was slowed down by a factor of 10^{10}, such that the 20 ns of MD data plays as a 200 sec sound, which enables some pattern recognition. For example, if the data were slowed down by a factor of 10^{8}, the entire MD simulation would play for 2 seconds, which is too short to distinguish any features. Slowing the data by a factor of 10^{10} also causes the low 0.05 THz frequencies of the TA-y modes of interest to correspond to 5 Hz, which is below the 20 Hz threshold of the human ear. However, because the heat current contains extremely high frequency components, due to interactions with the much higher frequency optical modes that sound like noise, one can hear each oscillation of the mode as a pulsing sound. In this sense, the high frequency noise imparted by the optical modes, which include the motions of the hydrogen atoms, is the only thing that can be heard, but its volume (e.g., loudness) is modulated by the oscillation of low frequency modes, which are much larger in amplitude. Inspection of the audio in audio files [123] immediately identified a feature that seemed to be much more prevalent in the divergent case than in the convergent case, namely the repeated instances in the divergent case where the signal slowly fades out and then fades back in.

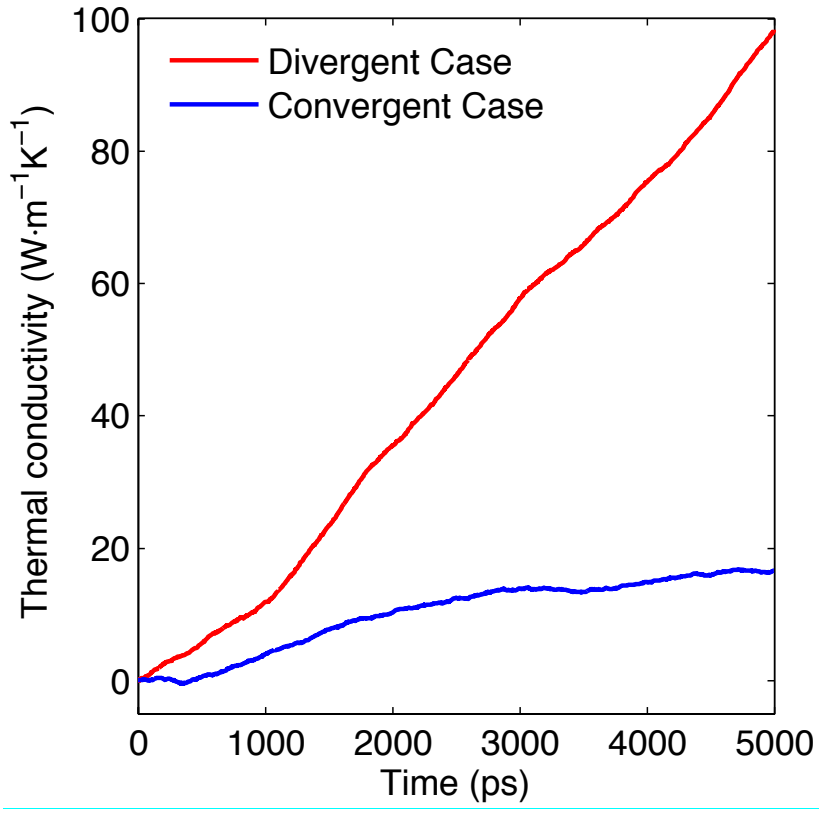

Figure 4.27 TA-y_1 mode thermal conductivity contribution in the divergent and convergent case.

The time scale in between such events is on the order of 15 seconds, which in the MD simulation corresponds to several hundred picoseconds, close to the mode relaxation time. We believe that the fade-in fade-out phenomenon is related to the temporal period between phonon interactions. Conceptually, this relation supports the hypothesis put forth by Henry and Chen that the divergence cannot be attributed to ballistic phonon transport but instead arises from patterned phonon interactions. Individual phonons do in fact experience interactions and scatter, causing the relaxation time to be finite. However, the scattering experience, possibly due to the sequence of energy exchanges, is similar and repeats in a correlated way. In this sense a thermal perturbation excites a mode, which then relaxes, but the mode is later re-excited in a way

the mimics the initial excitation and a repetitious pattern of the same de-excitation-excitation cycle persists. It is therefore confirmatory to note that the cycle/correlated feature time scale is the same as the relaxation time, which represents the time scale between excitation and de-excitation events.

In the divergent case these fade-in and fade-out events occur approximately at the following time marks [15s, 30s, 45s, 58s, 70s]. The difference between the convergent and divergent audio is also easier to hear in the combined audio, which combines separate files into a single stereo file, whereby the convergent audio file is played on the left channel and divergent audio file is played on the right channel. One can then hear the periods near [15s, 30s, 45s, 58s, 70s] where the sound fades out on the right ear channel, while the left ear channel plays almost continuously. The identification of this feature was then inspected audibly for a variety of convergent and divergent cases, which qualitatively confirmed that such events happened more often in the divergent cases than the convergent cases.

The purpose of the sonification was to identify a feature that differs between convergent and divergent results, which would then guide the analysis further. The identification of the fade in and out events then guided their visual identification from a plot of the heat current for the TA-y_1 mode. By properly rescaling the time axis so that regions of 400ps to 2000ps are shown, one can then visually observe the features that were more easily identified in the audio files. Figure 4.23 (c) shows a zoomed in portion of the data in Fig. 4.23 (a), where one can see the oscillatory envelope on the TA-y_1 heat current. We then sought out to quantify these large oscillations in the heat current that generate such large peaks and valleys. The regions of the heat current where these events

occur are similar and repetitious, but occur at irregular intervals. Nonetheless, these features are what repeat throughout the trajectory and they give rise to the persistent correlation. It is not clear if such events are associated with a single scattering event/interaction between modes, as they can also be the result of a series or combination of mode-mode interactions that recur.

To quantify the phenomenon, it was hypothesized that the persistent correlation is a result of these repetitious events, which seemed to be greater in both magnitude and frequency in divergent cases. To test this hypothesis we examined the time history of the TA-y_1 heat current for each individual case and numerically calculated a data series that represents the envelope of the function. This was accomplished by first squaring the mode heat current so that the result is always positive, as shown in Fig. 4.26 (d). The envelope of Q^2 was then determined by taking the numerical derivative at every point, via finite difference, and locating points in the function where the function changed from positive to negative slope (a maximum) and negative to positive slope (a minimum). The resulting maxima and minima were then placed in bins of 0.0375 ps and averaged together, which helped to smear the data set, yielding the overall envelope of the function as shown in Fig. 4.26 (d). Once the envelope function was determined, we calculated each subsequent maximum and minimum in the envelope $f_{\max,i}$, $f_{\min,i}$ and calculated their difference to gauge both the size and frequency (150~190) of the peaks and valleys in the envelope,

$$F_{pv} = \sum_i (f_{\max,i} - f_{\min,i}) \tag{4.2}$$

where the subscript i denotes nearest neighboring maxima or minima. Since there are many cases in between the extremes of clearly convergent vs. divergent cases as shown in Fig. 3.21, we then calculated F_{pv} for 20 different independent MD simulations and compared the value of F_{pv} to the value of the thermal conductivity at the end of the 10 ns of correlation time. The result, which is shown in Fig. 4.28 shows that there is a clear relationship between F_{pv} and thermal conductivity. The greater the magnitude and frequency of the fade-in and fade-out events, the greater the thermal conductivity, which confirms the hypothesis that these events are the root cause of the divergence in Pth.

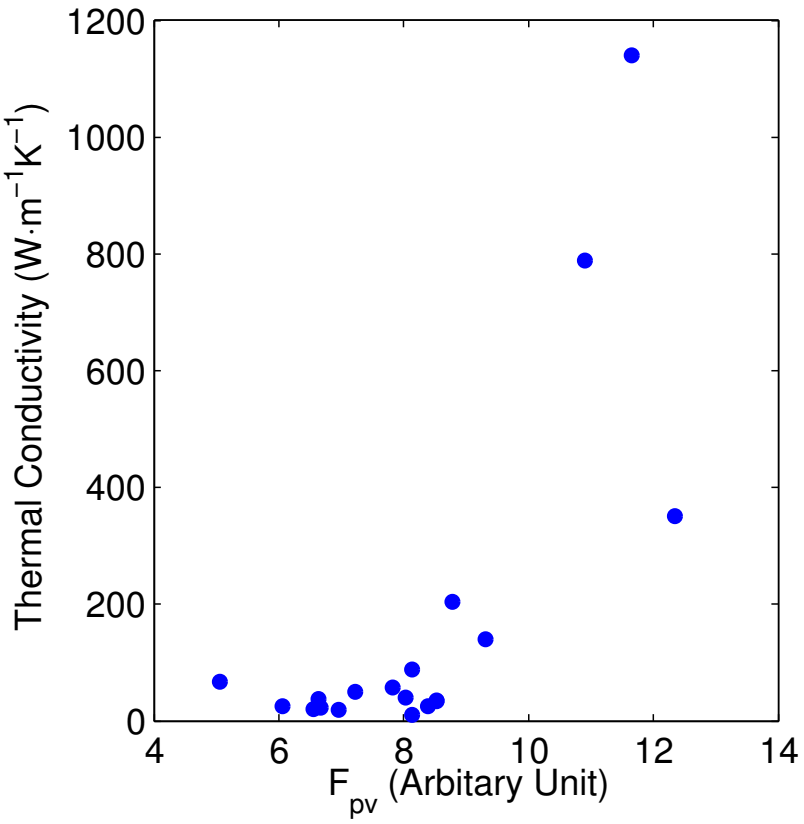

Figure 4.28 Total thermal conductivity vs. sum of the peak height (F_{pv}) as shown in Eq. (4.2).

With the root cause of divergence identified, we must subsequently examine the corresponding physical interpretation of such a phenomenon. First, it is useful to reason through the meaning of the mode level heat current based on the correlation paradigm. If for example, one had a single polymer chain and ran a MD simulation where only one mode is excited, by definition, if one examines all of the mode heat currents, one would see that only the excited mode's heat current is non-zero. This is because the modal contribution to the heat flow is proportional to the mode amplitude. Thus, when only one mode is excited, one would observe the heat current for the excited mode oscillating at the mode frequency. If all of the atomic interactions were harmonic, one would cease to observe mode-mode interactions and the mode heat current would simply oscillate at the excited mode frequency indefinitely. However, as anharmonicity is included and mode-mode interactions take place, the frequency content of the excited mode's heat current will change as it interacts with other modes. Most specifically, as the primary excited mode couples to other modes, one would expect to see some frequency content associated with the interacting modes show up in the primary excited mode's heat current and vice versa – namely the mode interacting with the primary excited mode would also exhibit fluctuations with a frequency component associated with the primary excited mode.

With this framework for interpreting the mode level heat current, it can then be understood that the fade-in and fade-out events correspond to the mode being excited and subsequently de-exited over the course of several hundred picoseconds, which is close to the relaxation time of the mode through a particular sequence of interactions that repeat and remain correlated. It is the fact that each of these events occurs in a similar fashion each time that enables the correlation to persist and leads to divergent thermal

conductivity. In between such periods, there are substantial interactions with lots of other modes, as indicated by the wide range of frequency content, which can both be seen visually in Fig. 4.26 (c) and heard audibly as noise in audio files. These repetitious events are the root cause of the divergence in Pth and they occur to different extents in different independent simulations. To our knowledge the analysis herein serves as one of the most detailed explanations offered to date for understanding the root cause of anomalous heat conduction in polymers.

In this section, we investigated divergent thermal conductivity (anomalous thermal conductivity) in individual Pth chains, using MD simulations, the GKMA method and sonification. We found the divergence was not just a numerical anomaly or aggregated error and was not caused by the usage of PBC, since an anomalous increase in thermal conductivity was observed for a finite chain consisting of the an exact multiple of 30 ucs (e.g., the exact chain length required to observe anomalous thermal conductivity when PBC are applied). We also discovered the divergence arises from the lowest frequency modes on the TA-y branch, which clearly exhibits divergent correlations in every instance where the total thermal conductivity diverges. Furthermore, the results showed that the modes responsible for the divergence do in fact have finite relaxation times and do exhibit significant interactions with other modes i.e., they scatter, which it is not consistent with a ballistic transport interpretation or the PGM. Lastly, the origin of the divergence was determined through sonification of the mode heat current, as the lowest frequency mode (50 GHz) exhibited repeated excitation and de-excitation events that repeated more strongly and more frequently in divergent cases. These findings offer new insight into the root causes and underlying physics at play in polymer chains where

anomalous heat conduction occurs. Thus the analysis herein serves as a significant step forward in our understanding of this intriguing phenomenon of anomalous thermal conductivity.

CHAPTER 5

CONCLUSIONS AND FUTURE DIRECTIONS

This dissertation investigates a correlation based method to understand and calculate the thermal conductivity from atomistic level simulations. The detailed calculations expand our fundamental understanding of the transport processes in non-crystalline materials and provide guidance for practical materials design to meet different needs. The first portion of the thesis focuses on introducing the GKMA formula and its results on several materials while the second portion focuses on a few case studies to illustrate new physics using GKMA.

In Chapter 2, we introduce the Green-Kubo mode analysis method formulation and implementation. We also briefly describe the other modal analysis methods including normal model analysis, first principle BTE method, A-F method. The difference between correlation paradigm and PGM paradigm is discussed.

In Chapter 3, the applications of GKMA on a few materials (including crystalline silicon, amorphous silicon, amorphous silica, amorphous carbon and single polythiophene chains) are shown. The mode level comparison between GKMA and NMA & BTE methods on crystalline silicon manifests the validity of GKMA. Then the excellent agreement with experiments on the GKMA results of a few different amorphous solids further proves the accuracy and correctness. We claim that the GKMA is so far the most accurate atomistic level simulation methods to predict the thermal conductivity of amorphous solids.

In Chapter 4, we aim to find new insights of the thermal transport properties of disordered materials. Meantime we want to test whether the PGM is still applicable on the disordered materials. A series of case studies has been done using accurate mode level information from GKMA. The first test in on the relaxation time. If PGM is right, then the relaxation time is proportional to the mode thermal conductivity. We uncovered that the relaxation time become irrelevant for amorphous materials' mode thermal conductivity above room temperature. It becomes the first evidence that PGM fails. Following the PGM, locons do not contribute to the thermal conductivity. We demonstrated the first numerical evidence that the locons can contribute to the thermal conductivity due to anharmonicity. PGM indicates that anharmonicity decreases thermal conductivity. And we find the anharmonicity can increase thermal conductivity in amorphous materials. PGM predicts the diffusons do not have size effect. However we uncover the diffusons can exhibit size effect. At last but not least, we pinpoint one individual phonon in single polythiophene chain that makes the total thermal conductivity diverging. And find out the relaxation time of the mode is finite, different from PGM prediction. The cause of the divergence is the patterned phonon interactions, which is identified by GKMA and sonification. In sum, we discovered five independent cases that PGM fails. And the GKMA or correlation paradigm are able to explain. All these evidences substantiate the accuracy of the correlation paradigm and disprove the ubiquitous usage of PGM.

The future work will go to understanding the thermal properties in amorphous polymers. Although polymers have been widely applied in industry [124], there is little understanding of its thermal transport properties. The investigation of phonon transport in

amorphous materials is still in its infancy, and there are many unresolved problems, some examples are listed below. How does propagaon transfer heat in amorphous polymers? How do inter-molecule and intra-molecular force influence on the thermal conductivity? How does crystallinity affect the polymer thermal transport properties? How does the chain alignment affect the thermal conductivity of the amorphous polymers? What is the side chain effect on the thermal conductivity of the amorphous polymers? How does the hydrogen atom or hydrogen bond affect the diffusons and locons? Therefore, a deep understanding of the phonon transport properties of the amorpshous polymers is in great need.

Moreover, we observed size effect on the amorphous solids, however there is no existing theory to explain this phenomenon. In the last past decade, there have been lots of advance in understanding and quantifying the size effect in crytalline solids based on PGM. However, PGM is not applicable on the amorphous materials, another analytical function or theory is needed to quantify the size effect with the combination of the GKMA numerical results. Experiments will also be necessary to further understanding phonon transport in amorphous materials. The theory and experiments will not only help to further understand phonon transport in amorphous solids but also pave the way for turning thermal properties in amorphous materials into real-world applications and commercializing the relevant devices.

REFERENCES

[1] Chen, G., 2005, Nanoscale energy transport and conversion: a parallel treatment of electrons, molecules, phonons, and photons, Oxford University Press, USA.

[2] Srivastava, G. ., 1990, The Physics of Phonons, CRC Press.

[3] Sun, T., and Allen, P. B., 2010, "Lattice thermal conductivity: Computations and theory of the high-temperature breakdown of the phonon-gas model," Phys. Rev. B, **82**(22), p. 224305.

[4] Broido, D. A., Malorny, M., Birner, G., Mingo, N., and Stewart, D. A., 2007, "Intrinsic lattice thermal conductivity of semiconductors from first principles," Appl. Phys. Lett., **91**(23), p. 231922.

[5] Esfarjani, K., Chen, G., and Stokes, H. T., 2011, "Heat transport in silicon from first-principles calculations," Phys. Rev. B, **84**(8), p. 85204.

[6] Lindsay, L., Broido, D. A., and Reinecke, T. L., 2013, "Ab initio thermal transport in compound semiconductors," Phys. Rev. B, **87**(16), p. 165201.

[7] Tian, Z., Garg, J., Esfarjani, K., Shiga, T., Shiomi, J., and Chen, G., 2012, "Phonon conduction in PbSe, PbTe, and PbTe 1- x Se x from first-principles calculations," Phys. Rev. B, **85**(18), p. 184303.

[8] Henry, A. S., and Chen, G., 2008, "Spectral Phonon Transport Properties of Silicon Based on Molecular Dynamics Simulations and Lattice Dynamics," J. Comput. Theor. Nanosci., **5**(2), pp. 141–152.

[9] Koh, Y., and Cahill, D., 2007, "Frequency dependence of the thermal conductivity of semiconductor alloys," Phys. Rev. B, **76**(7), p. 75207.

[10] Regner, K. T., Sellan, D. P., Su, Z., Amon, C. H., McGaughey, A. J. H., and Malen, J. A., 2013, "Broadband phonon mean free path contributions to thermal conductivity measured using frequency domain thermoreflectance.," Nat. Commun., **4**, p. 1640.

[11] Einstein, A., 1911, "Elementare Betrachtungen {ü}ber die thermische Molekularbewegung in festen K{ö}rpern," Ann. Phys., **340**(9), pp. 679–694.

[12] Klemens, P. G., 1951, "The thermal conductivity of dielectric solids at low temperatures (theoretical)," Proc. R. Soc. London. Ser. A. Math. Phys. Sci., **208**(1092), pp. 108–133.

[13] Alexander, S., Entin-Wohlman, O., and Orbach, R., 1986, "Phonon-fracton anharmonic interactions: The thermal conductivity of amorphous materials," Phys. Rev. B, **34**(4), pp. 2726–2734.

[14] Cahill, D. G., and Pohl, R. O., 1988, "Lattice vibrations and heat transport in crystals and glasses," Annu. Rev. Phys. Chem., **39**(1), pp. 93–121.

[15] Allen, P. B., and Feldman, J. L., 1989, "Thermal Conductivity of Glasses: Theory and Application to Amorphous Si," Phys. Rev. Lett., **62**(6), pp. 645–648.

[16] Lv, W., and Henry, A., 2016, "Direct calculation of modal contributions to thermal conductivity via Green–Kubo modal analysis," New J. Phys., **18**(1), p. 13028.

[17] Allen, P. B., and Kelner, J., 1998, "Evolution of a vibrational wave packet on a disordered chain," Am. J. Phys., **66**(6), p. 497.

[18] Allen, P. B., Feldman, J. L., Fabian, J., and Wooten, F., 1999, "Diffusons, locons and propagons: Character of atomic vibrations in amorphous Si," Philos. Mag. B,

79(11–12), pp. 1715–1731.
[19] Feldman, J. L., Kluge, M. D., Allen, P. B., and Wooten, F., 1993, "Thermal conductivity and localization in glasses: Numerical study of a model of amorphous silicon," Phys. Rev. B, **48**(17), pp. 12589–12602.
[20] Mott, N. F., and Davis, E. A., 1971, Electronic process in non-crystalline materials, Oxford University Press.
[21] Feldman, J. L., Kluge, M. D., Allen, P. B., and Wooten, F., 1993, "Thermal conductivity and localization in glasses: Numerical study of a model of amorphous silicon," Phys. Rev. B, **48**(17), p. 12589.
[22] Michalski, J., 1992, "Thermal conductivity of amorphous solids above the plateau: molecular-dynamics study," Phys. Rev. B, **45**(13), p. 7054.
[23] Shenogin, S., Bodapati, A., Keblinski, P., and McGaughey, A. J. H., 2009, "Predicting the thermal conductivity of inorganic and polymeric glasses: The role of anharmonicity," J. Appl. Phys., **105**(3), p. 34906.
[24] McGaughey, A., and Kaviany, M., 2006, "Phonon Transport in Molecular Dynamics Simulations: Formulation and Thermal Conductivity Prediction," Adv. Heat Transf., **39**(2), pp. 169–255.
[25] McGaughey, A., and Larkin, J. M. ., 2014, "Predicting phonon properties from equilibrium molecular dynamics simulations," Annu. Rev. Heat Transf., **17**, pp. 49–87.
[26] Schelling, P. K., Phillpot, S. R., and Keblinski, P., 2002, "Comparison of atomic-level simulation methods for computing thermal conductivity," Phys. Rev. B, **65**(14), p. 144306.
[27] He, Y., Savić, I., Donadio, D., and Galli, G., 2012, "Lattice thermal conductivity of semiconducting bulk materials: atomistic simulations," Phys. Chem. Chem. Phys., **14**(47), pp. 16209–16222.
[28] Henry, A., and Chen, G., 2008, "High Thermal Conductivity of Single Polyethylene Chains Using Molecular Dynamics Simulations," Phys. Rev. Lett., **101**(23), p. 235502.
[29] E.Fermi, J.Pasta, S. U., 1955, Studies of the Nonlinear Problems.
[30] Cercignani, C., 1988, The Boltzmann Equation and Its Applications, Springer New York, New York, NY.
[31] Henry, A., and Chen, G., 2009, "Anomalous heat conduction in polyethylene chains: Theory and molecular dynamics simulations," Phys. Rev. B, **79**(14), p. 144305.
[32] Freeman, J. J., Morgan, G. J., and Cullen, C. A., 1987, "Thermal conductivity of a single polymer chain," Phys. Rev. B, **35**(14), pp. 7627–7635.
[33] Luo, T., Esfarjani, K., Shiomi, J., Henry, A., and Chen, G., 2011, "Molecular dynamics simulation of thermal energy transport in polydimethylsiloxane," J. Appl. Phys., **109**(7), p. 74321.
[34] Liu, J., and Yang, R., 2012, "Length-dependent thermal conductivity of single extended polymer chains," Phys. Rev. B, **86**(10), p. 104307.
[35] Hardy, R. J., 1963, "Energy-flux operator for a lattice," Phys. Rev., **132**(1), p. 168.
[36] Allen, M. P., and Tildesley, D. J., 1989, Computer simulation of liquids, Oxford university press.
[37] Teng, K.-L., Hsiao, P.-Y., Hung, S.-W., Chieng, C.-C., Liu, M.-S., and Lu, M.-C.,

"Enhanced Thermal Conductivity of Nanofluids Diagnosis by Molecular Dynamics Simulations," J. Nanosci. Nanotechnol., **8**(7), pp. 3710–3718.
[38] Dove, M. T., 1993, Introduction to Lattice Dynamics, Cambridge University Press.
[39] McGaughey, A. J. H., and Kaviany, M., 2004, "Quantitative validation of the Boltzmann transport equation phonon thermal conductivity model under the single-mode relaxation time approximation," Phys. Rev. B, **69**(9), p. 94303.
[40] Allen, P. B., and Feldman, J. L., 1993, "Thermal conductivity of disordered harmonic solids," Phys. Rev. B, **48**(17), pp. 12581–12588.
[41] Turney, J., McGaughey, A., and Amon, C., 2009, "Assessing the applicability of quantum corrections to classical thermal conductivity predictions," Phys. Rev. B, **79**(22), p. 224305.
[42] Asheghi, M., Leung, Y. K., Wong, S. S., and Goodson, K. E., 1997, "Phonon-boundary scattering in thin silicon layers," Appl. Phys. Lett., **71**(13), pp. 1798–1800.
[43] Holland, M. G., 1964, "Phonon scattering in semiconductors from thermal conductivity studies," Phys. Rev., **134**(2A), p. A471.
[44] Ziman, J. M., 1960, Electrons and phonons: the theory of transport phenomena in solids.
[45] Larkin, J. M., Turney, J. E., Massicotte, A. D., Amon, C. H., and McGaughey, A. J. H., 2014, "Comparison and Evaluation of Spectral Energy Methods for Predicting Phonon Properties," J. Comput. Theor. Nanosci., **11**(1), pp. 249–256.
[46] Tian, Z., Esfarjani, K., Shiomi, J., Henry, A. S., and Chen, G., 2011, "On the importance of optical phonons to thermal conductivity in nanostructures," Appl. Phys. Lett., **99**(5), p. 53122.
[47] Broido, D. A., Ward, A., and Mingo, N., 2005, "Lattice thermal conductivity of silicon from empirical interatomic potentials," Phys. Rev. B, **72**(1), p. 14308.
[48] Garg, J., 2011, "Thermal conductivity from first-principles in bulk, disordered, and nanostructured materials," Massachusetts Institute of Technology.
[49] Li, W., Carrete, J., A. Katcho, N., and Mingo, N., 2014, "ShengBTE: A solver of the Boltzmann transport equation for phonons," Comput. Phys. Commun., **185**(6), pp. 1747–1758.
[50] Togo, A., Chaput, L., Tanaka, I., and Hug, G., 2010, "First-principles phonon calculations of thermal expansion in Ti_3SiC_2, Ti_3AlC_2, and Ti_3GeC_2," Phys. Rev. B, **81**(17), p. 174301.
[51] Ladd, A. J. C., and Moran, B., 1986, "Lattice thermal conductivity: A comparison of molecular dynamics and anharmonic lattice dynamics," Phys. Rev. B, **34**(8), pp. 5058–5064.
[52] Ward, A., Broido, D. A., Stewart, D. A., and Deinzer, G., 2009, "Ab initio theory of the lattice thermal conductivity in diamond," Phys. Rev. B, **80**(12), p. 125203.
[53] Luo, T., Garg, J., Shiomi, J., Esfarjani, K., Chen, G., al, I. A. V. et, Gallego Lluesma E., M. G. . A. C. A. and L. R. C. C., W., P., T., E. K. and S. H., Broido D. A., M. M. . B. G. . M. N. and S. D. A., Esfarjani K., C. G. and S. H. T., J., G., Ward A., B. D. A. . S. D. A. and D. G., Shiomi J., E. K. and C. G., al, S. T. et, al, G. P. et, A., P. J. P. and Z., D., M. H. J. and P. J., Parlinski K., L. Z. Q. and K. Y., Baroni S., de G. S. . D. C. A. and G. P., E., M. A. A. and F. A., G., E. D. J. and K. P., B., S. D. and D., Trommer R., M. H. . C. M. and V. P., Wickboldt P., A. E. . S.

R. and C. M., Buchenauer C. J., C. F. . C. M., G., H. M., G., H. A. S. and C., Dames C., C. G., G., C., al, M. A. J. et, A., D., von der Linde D., K. J. and K. H., C., K. J. A. and T. J., and Bao H., Q. B. . Z. Y. and R. X., 2013, "Gallium arsenide thermal conductivity and optical phonon relaxation times from first-principles calculations," EPL (Europhysics Lett., **101**(1), p. 16001.

[54] Shiomi, J., Esfarjani, K., and Chen, G., 2011, "Thermal conductivity of half-Heusler compounds from first-principles calculations," Phys. Rev. B, **84**(10), p. 104302.

[55] Shiga, T., Shiomi, J., Ma, J., Delaire, O., Radzynski, T., Lusakowski, A., Esfarjani, K., and Chen, G., 2012, "Microscopic mechanism of low thermal conductivity in lead telluride," Phys. Rev. B, **85**(15), p. 155203.

[56] Lindsay, L., Broido, D., and Mingo, N., 2009, "Lattice thermal conductivity of single-walled carbon nanotubes: Beyond the relaxation time approximation and phonon-phonon scattering selection rules," Phys. Rev. B, **80**(12), p. 125407.

[57] Lindsay, L., Broido, D. A., and Mingo, N., 2011, "Flexural phonons and thermal transport in multilayer graphene and graphite," Phys. Rev. B, **83**(23), p. 235428.

[58] Cahill, D. G., and Pohl, R. O., 1988, "Thermal properties of a tetrahedrally bonded amorphous solid: CdGeAs 2," Phys. Rev. B, **37**(15), pp. 8773–8780.

[59] Cahill, D., and Pohl, R., 1987, "Thermal conductivity of amorphous solids above the plateau," Phys. Rev. B, **35**(8), pp. 4067–4073.

[60] Shamsa, M., Liu, W. L., Balandin, A. A., Casiraghi, C., Milne, W. I., and Ferrari, A. C., 2006, "Thermal conductivity of diamond-like carbon films," Appl. Phys. Lett., **89**(16), p. 161921.

[61] Liu, X., Feldman, J. L., Cahill, D. G., Crandall, R. S., Bernstein, N., Photiadis, D. M., Mehl, M. J., and Papaconstantopoulos, D. A., 2009, "High thermal conductivity of a hydrogenated amorphous silicon film," Phys. Rev. Lett., **102**(3), p. 35901.

[62] Tersoff, J., 1988, "New empirical approach for the structure and energy of covalent systems," Phys. Rev. B, **37**(12), p. 6991.

[63] Plimpton, S., 1995, "Fast parallel algorithms for short-range molecular dynamics," J. Comput. Phys., **117**(1), pp. 1–19.

[64] Bazant, M. Z., Kaxiras, E., and Justo, J. F., 1997, "Environment-dependent interatomic potential for bulk silicon," Phys. Rev. B, **56**(14), pp. 8542–8552.

[65] Munetoh, S., Motooka, T., Moriguchi, K., and Shintani, A., 2007, "Interatomic potential for Si--O systems using Tersoff parameterization," Comput. Mater. Sci., **39**(2), pp. 334–339.

[66] Barkema, G. T., and Mousseau, N., 2000, "High-quality continuous random networks," Phys. Rev. B, **62**(8), p. 4985.

[67] He, Y., Donadio, D., and Galli, G., 2011, "Heat transport in amorphous silicon: Interplay between morphology and disorder," Appl. Phys. Lett., **98**(14), p. 144101.

[68] Larkin, J. M., and McGaughey, A. J. H., 2014, "Thermal conductivity accumulation in amorphous silica and amorphous silicon," Phys. Rev. B, **89**(14), p. 144303.

[69] Gale, J. D., 1997, "GULP: A computer program for the symmetry-adapted simulation of solids," J. Chem. Soc. Faraday Trans., **93**(4), pp. 629–637.

[70] Cahill, D. G., Katiyar, M., and Abelson, J. R., 1994, "Thermal conductivity of a-

Si:H thin films," Phys. Rev. B, **50**(9), pp. 6077–6081.
[71] Li, D., Wu, Y., Kim, P., Shi, L., Yang, P., and Majumdar, A., 2003, "Thermal conductivity of individual silicon nanowires," Appl. Phys. Lett., **83**(14), p. 2934.
[72] Volz, S. G., and Chen, G., 1999, "Molecular dynamics simulation of thermal conductivity of silicon nanowires," Appl. Phys. Lett., **75**(14), pp. 2056–2058.
[73] Chen, Y., Li, D., Lukes, J. R., and Majumdar, A., 2005, "Monte Carlo simulation of silicon nanowire thermal conductivity," J. Heat Transfer, **127**(10), pp. 1129–1137.
[74] Callaway, J., 1959, "Model for lattice thermal conductivity at low temperatures," Phys. Rev., **113**(4), p. 1046.
[75] Lee, Y. H., Biswas, R., Soukoulis, C. M., Wang, C. Z., Chan, C. T., and Ho, K. M., 1991, "Molecular-dynamics simulation of thermal conductivity in amorphous silicon," Phys. Rev. B, **43**(8), pp. 6573–6580.
[76] Ong, Z.-Y., and Pop, E., 2010, "Molecular dynamics simulation of thermal boundary conductance between carbon nanotubes and SiO_{2}," Phys. Rev. B, **81**(15), p. 155408.
[77] Carpenter, J., and Price, D., 1985, "Correlated Motions in Glasses Studied by Coherent Inelastic Neutron Scattering," Phys. Rev. Lett., **54**(5), pp. 441–443.
[78] SMYTH, H. T., SKOGEN, H. S., and HARSELL, W. B., 1953, "Thermal Capacity of Vitreous Silica," J. Am. Ceram. Soc., **36**(10), pp. 327–328.
[79] Kaviany, M., 2002, Principles of Heat Transfer, John Wiley & Sons.
[80] McGaughey, A. J. H., and Kaviany, M., 2004, "Thermal conductivity decomposition and analysis using molecular dynamics simulations: Part II. Complex silica structures," Int. J. Heat Mass Transf., **47**(8–9), pp. 1799–1816.
[81] C. Kittel, 1986, Introduction to Solid State Physics, Wiley, New York.
[82] Taraskin, S. N., and Elliott, S. R., 1997, "Nature of vibrational excitations in vitreous silica," Phys. Rev. B, **56**(14), pp. 8605–8622.
[83] van Beest BW, Kramer, G., and van Santen RA, 1990, "Force fields for silicas and aluminophosphates based on ab initio calculations.," Phys. Rev. Lett., **64**(16), pp. 1955–1958.
[84] Kramer, G. J., Farragher, N. P., van Beest, B. W. H., and van Santen, R. A., 1991, "Interatomic force fields for silicas, aluminophosphates, and zeolites: Derivation based on ab initio calculations," Phys. Rev. B, **43**(6), pp. 5068–5080.
[85] Jund, P., and Jullien, R., 1999, "Molecular-dynamics calculation of the thermal conductivity of vitreous silica," Phys. Rev. B, **59**(21), pp. 13707–13711.
[86] Robertson, J., 2001, "Ultrathin carbon coatings for magnetic storage technology," Thin Solid Films, **383**(1–2), pp. 81–88.
[87] Robertson, J., 2002, "Diamond-like amorphous carbon," Mater. Sci. Eng. R Reports, **37**(4–6), pp. 129–281.
[88] Hauert, R., 2004, "An overview on the tribological behavior of diamond-like carbon in technical and medical applications," Tribol. Int., **37**(11–12), pp. 991–1003.
[89] Bullen, A. J., O'Hara, K. E., Cahill, D. G., Monteiro, O., and von Keudell, A., 2000, "Thermal conductivity of amorphous carbon thin films," J. Appl. Phys., **88**(11), p. 6317.
[90] Fabian, J., and Allen, P., 1996, "Anharmonic Decay of Vibrational States in

Amorphous Silicon.," Phys. Rev. Lett., **77**(18), pp. 3839–3842.
[91] Li, L., Xu, M., Song, W., Ovcharenko, A., Zhang, G., and Jia, D., 2013, "The effect of empirical potential functions on modeling of amorphous carbon using molecular dynamics method," Appl. Surf. Sci., **286**, pp. 287–297.
[92] Sha, Z. D., Branicio, P. S., Pei, Q. X., Sorkin, V., and Zhang, Y. W., 2013, "A modified Tersoff potential for pure and hydrogenated diamond-like carbon," Comput. Mater. Sci., **67**, pp. 146–150.
[93] Lv, W., and Henry, A., 2016, "Non-negligible Contributions to Thermal Conductivity From Localized Modes in Amorphous Silicon Dioxide," Sci. Rep., **6**, p. 35720.
[94] Feng, T., and Ruan, X., 2014, "Prediction of Spectral Phonon Mean Free Path and Thermal Conductivity with Applications to Thermoelectrics and Thermal Management: A Review," J. Nanomater., **2014**(206370), p. 206370.
[95] Lv, W., and Henry, A. S., 2016, "Examining the validity of the phonon gas model in amorphous materials," Sci. Rep., **6**, p. 37675.
[96] Volz, S. G., and Chen, G., 2000, "Molecular-dynamics simulation of thermal conductivity of silicon crystals," Phys. Rev. B, **61**(4), pp. 2651–2656.
[97] Mingo, N., and Broido, D. A., 2005, "Length Dependence of Carbon Nanotube Thermal Conductivity and the 'Problem of Long Waves,'" Nano Lett., **5**(7), pp. 1221–1225.
[98] van Duin, A. C. T., Dasgupta, S., Lorant, F., and Goddard, W. A., 2001, "ReaxFF: A Reactive Force Field for Hydrocarbons," J. Phys. Chem. A, **105**(41), pp. 9396–9409.
[99] Singh, V., Bougher, T. L., Weathers, A., Cai, Y., Bi, K., Pettes, M. T., McMenamin, S. A., Lv, W., Resler, D. P., Gattuso, T. R., Altman, D. H., Sandhage, K. H., Shi, L., Henry, A., and Cola, B. A., 2014, "High thermal conductivity of chain-oriented amorphous polythiophene," Nat Nano, **9**(5), pp. 384–390.
[100] Dames, C., and Chen, G., 2004, "Theoretical phonon thermal conductivity of Si/Ge superlattice nanowires," J. Appl. Phys., **95**(2), p. 682.
[101] Seol, J. H., Jo, I., Moore, A. L., Lindsay, L., Aitken, Z. H., Pettes, M. T., Li, X., Yao, Z., Huang, R., Broido, D., Mingo, N., Ruoff, R. S., and Shi, L., 2010, "Two-dimensional phonon transport in supported graphene.," Science, **328**(5975), pp. 213–6.
[102] Garg, J., Bonini, N., Kozinsky, B., and Marzari, N., 2011, "Role of Disorder and Anharmonicity in the Thermal Conductivity of Silicon-Germanium Alloys: A First-Principles Study," Phys. Rev. Lett., **106**(4), p. 45901.
[103] Garg, J., and Chen, G., 2013, "Minimum thermal conductivity in superlattices: A first-principles formalism," Phys. Rev. B, **87**(14), p. 140302.
[104] Callaway, J., 1959, "Model for Lattice Thermal Conductivity at Low Temperatures," Phys. Rev., **113**(4), pp. 1046–1051.
[105] Asen-Palmer, M., Bartkowski, K., Gmelin, E., Cardona, M., Zhernov, A. P., Inyushkin, A. V., Taldenkov, A., Ozhogin, V. I., Itoh, K. M., and Haller, E. E., 1997, "Thermal conductivity of germanium crystals with different isotopic compositions," Phys. Rev. B, **56**(15), pp. 9431–9447.
[106] Amo, A., Lefrère, J., Pigeon, S., Adrados, C., Ciuti, C., Carusotto, I., Houdré, R.,

Giacobino, E., and Bramati, A., 2009, “Superfluidity of polaritons in semiconductor microcavities,” Nat. Phys., **5**(11), pp. 805–810.
[107] Pigeon, S., Carusotto, I., and Ciuti, C., 2011, “Hydrodynamic nucleation of vortices and solitons in a resonantly excited polariton superfluid,” Phys. Rev. B, **83**(14), p. 144513.
[108] de Faoite, D., Browne, D. J., Chang-Díaz, F. R., and Stanton, K. T., 2011, “A review of the processing, composition, and temperature-dependent mechanical and thermal properties of dielectric technical ceramics,” J. Mater. Sci., **47**(10), pp. 4211–4235.
[109] Mathioudakis, C., and Kelires, P. ., 2000, “Softening of elastic moduli of amorphous semiconductors,” J. Non. Cryst. Solids, **266–269**, pp. 161–165.
[110] Marx, J. W., and Sivertsen, J. M., 1953, “Temperature Dependence of the Elastic Moduli and Internal Friction of Silica and Glass,” J. Appl. Phys., **24**(1), p. 81.
[111] Ni, H., Li, X., and Gao, H., 2006, “Elastic modulus of amorphous SiO[sub 2] nanowires,” Appl. Phys. Lett., **88**(4), p. 43108.
[112] Allen, P. B., Feldman, J. L., Fabian, J., and Wooten, F., 1999, “Diffusons, locons and propagons: Character of atomie yibrations in amorphous Si,” Philos. Mag. Part B, **79**(11–12), pp. 1715–1731.
[113] Jagannathan, A., Orbach, R., and Entin-Wohlman, O., 1989, “Thermal conductivity of amorphous materials above the plateau,” Phys. Rev. B, **39**(18), pp. 13465–13477.
[114] Gordiz, K., and Henry, A., 2016, “Phonon Transport at Crystalline Si/Ge Interfaces: The Role of Interfacial Modes of Vibration.,” Sci. Rep., **6**, p. 23139.
[115] Turney, J. E., Landry, E. S., McGaughey, A. J. H., and Amon, C. H., 2009, “Predicting phonon properties and thermal conductivity from anharmonic lattice dynamics calculations and molecular dynamics simulations,” Phys. Rev. B, **79**(6), p. 64301.
[116] Feng, T., Qiu, B., and Ruan, X., 2015, “Anharmonicity and necessity of phonon eigenvectors in the phonon normal mode analysis,” J. Appl. Phys., **117**(19), p. 195102.
[117] Kamitakahara, W. A., Shanks, H. R., McClelland, J. F., Buchenau, U., Gompf, F., and Pintschovius, L., 1984, “Measurement of Phonon Densities of States for Pure and Hydrogenated Amorphous Silicon,” Phys. Rev. Lett., **52**(8), pp. 644–647.
[118] Payton, D. N., Rich, M., and Visscher, W. M., 1967, “Lattice Thermal Conductivity in Disordered Harmonic and Anharmonic Crystal Models,” Phys. Rev., **160**(3), pp. 706–711.
[119] Wingert, M. C., Kwon, S., Hu, M., Poulikakos, D., Xiang, J., and Chen, R., 2015, “Sub-amorphous Thermal Conductivity in Ultrathin Crystalline Silicon Nanotubes,” Nano Lett., **15**(4), pp. 2605–2611.
[120] Walker, B. N., and Nees, M. A., 2011, “Theory of Sonification,” The Sonification Handbook, T. Hermann, A. Hunt, and J.G. Neuhoff, eds., Logos Publishing House, Berlin, Germany.
[121] Hermann, T., and Ritter, H., 1999, “Listen to your data: Model-based sonification for data analysis,” Adv. Intell. Comput. Multimed. Syst., **8**, pp. 189–194.
[122] Pereverzev, S. V., Loshak, A., Backhaus, S., Davis, J. C., and Packard, R. E., 1997, “Quantum oscillations between two weakly coupled reservoirs of superfluid

3He," Nature, **388**(6641), pp. 449–451.
[123] Lv, W., "Pth sonification files" [Online]. Available: http://pwp.gatech.edu/weilv/pth/.
[124] Henry, A., 2013, "Thermal transport in polymers," Annu. Rev. Heat Transf.